UNIVERSITY OF READING
DEPARTMENT OF MATHEMATICS

HIGHER ORDER GODUNOV BLACK-OIL SIMULATIONS FOR COMPRESSIBLE FLOW IN POROUS MEDIA

by

EDWIN MICHAEL DICKS

This thesis is submitted for the degree of
Doctor of Philosophy

MARCH 1993

Abstract

Numerical reservoir simulation is an important area of research within the oil industry. An accurate prediction of the performance of a reservoir under a recovery strategy is needed to assess the optimum oil recovery, and hence to determine the economics of the project.

The industry uses a standard mathematical model to simulate reservoir fluid flow, known as the Black-Oil model. A variant of the Black-Oil model, consisting of a system of three hyperbolic mass conservation laws and a parabolic pressure equation is investigated. The system of conservation laws exhibits local linear degeneracies and eigenvector deficiencies, and is solved using the Higher Order Godunov method which includes modifications to the basic numerical scheme to deal with such degeneracies. This numerical method is Total Variation Diminishing (TVD) ensuring oscillation free solutions and achieves second order accuracy in both space and time.

Analytic solutions of 3-phase incompressible Buckley-Leverett problems are constructed and compared with the numerical results of the scheme. A locally implicit procedure is also used to model source terms for injection and production of fluid.

The particular Black-Oil model used has a 'volume error discrepancy' due to a splitting of the flow equations. The impact of the volume error discrepancy on the numerical results is examined, and two potential techniques of reducing it investigated. The effect of fluid compressibility on the volume error discrepancy is also investigated.

The commercial reservoir simulation code (VIP) uses a flux-limiter TVD scheme to achieve second order accurate numerical solutions. Numerical results from this scheme are compared with those from the Higher Order Godunov scheme, applied to the degenerate system of conservation laws forming the Black-Oil model, both in terms of quality and efficiency.

Acknowledgements

I would like to express many thanks to my supervisor Dr Pete Sweby for his ideas, encouragement and patience during the writing of this thesis.

I also thank Dr Mike Christie of B.P. Research Sunbury for his guidance of the research and much advice.

I would also like to thank the Postgraduates who have been at the Mathematics Department over the last three years for making my stay so enjoyable.

I also thank the members, past and present, of Dr Mike Christies's research team at Sunbury for their help during my visits, especially Dr Mark Mansfield for many hours spent in obtaining the results from the reservoir simulation code VIP.

In addition I acknowledge the Science and Engineering Research Council for the award of a CASE studentship for the period of my studies, and the British Petroleum Company plc for their financial support.

Contents

Chapter 1

Introduction

1.1 Oil Reservoir Engineering

Oil reservoir engineering encompasses the processes of reservoir characterisation, mathematical modelling of the physical processes involved in reservoir fluid flow, and finally the numerical prediction of a given fluid flow scenario. The basic problem associated with oil recovery involves the injection of fluid or combinations of fluids and/or chemicals into the reservoir via injection wells to force as much oil as possible towards and hence out of production wells. Accurate prediction of the performance of a given reservoir under a particular recovery strategy is essential for an estimation of the economics, and hence risk, of the oil recovery project. Therefore a large amount of research, and money, is directed towards the above processes, by the oil industry.

The reservoir characterisation process provides the physical parameters, such as size, resident fluid and rock composition and properties, which are needed by the mathematical model. Given the physical parameters, the mathematical model describes the fluid flow with a set of partial differential equations and other relations, which are derived from physical principles. The resulting set of partial differential equations are too complex, for most realistic reservoir fluid flow models, to be solved by analytic methods. Therefore numerical methods are called upon to perform this task, resulting in the field of numerical reservoir simulation. Design of oil recovery strategies is heavily influenced by numerical simulation, by simulating various injection strategies the optimum recovery technique can

be assessed. Simulation is also useful for aiding understanding of the physical processes involved in reservoir fluid flow.

An oil reservoir can be described as a region of porous rock containing mixtures of oil, gas and water trapped in the rock pores, surrounded above, below, and to the sides by impermeable rock. The available pore volume in the rock, in which the fluid resides, is given by the rock porosity which is defined as the rock pore volume divided by the bulk volume. Another important parameter characterising reservoir rock is the permeability which is a measure of how readily fluid flows through the rock under the influence of the forces causing the flow. Oil reservoirs are located in many parts of the world both inshore and offshore, for example land based reservoirs in the United States and reservoirs under the North Sea. Reservoirs vary in size, usually being very large in area and can be in the region of 200 feet thick, resulting in very large field scale simulation operations. Many different types of rock may exist in the reservoirs, with the porosity of most commercially productive reservoirs being 10-25%, and with rock permeability ranging from 0.5 to 3500 milliDarcy's [14]. In practice reservoirs are not homogeneous in nature, the main reason for this being the variation of the permeability field. Fractures in the rock and shales (impermeable laminates) also add to the complexity of the simulation project.

Three types of oil recovery technique exist and are referred to as primary, secondary and tertiary (also known as enhanced oil recovery EOR). In the primary process, oil is forced out of the reservoir, at a production well, by the naturally prevailing pressure gradients, but is only effective at producing a few percent of the original oil in the reservoir, before the pressure gradients subside. The pressure gradient, which forces the oil towards the production well, may be restored by injection of fluid such as water, known as waterflooding, to help force more oil to the production well. The technique of injecting water (and/or gas) to restore the pressure gradients in the reservoir is known as secondary recovery.

The efficiency of wateflooding may be improved by lowering the water-oil mobility ratio M $(= M_{water}/M_{oil})$. Fluid mobility is defined as $M_p = k_p/\mu_p$, where k_p is the relative permeability of the fluid phase p which quantifies how the presence of other fluid phases hinders its flow and μ_p is the phase viscosity.

A mobility ratio M of greater than unity is referred to as unfavourable since the water is more mobile than the oil and can 'finger' through the oil zone, a process known as viscous fingering. This results in a reduced oil recovery efficiency, but may be improved by decreasing the ratio M by increasing the water viscosity. This can be accomplished by addition of chemicals such as polymers to the water, the displacement of oil by water then occurring in a piston-like way. Application of secondary recovery techniques can result in a 20-50% recovery of oil [14], depending on the oil and reservoir properties.

Tertiary recovery (EOR) involves one of a number of procedures, such as injection of chemicals, miscible displacement processes and thermal recovery methods, which are described in [14]. These methods are designed to increase the recovery from reservoirs previously depleted by secondary recovery techniques. Chemical and miscible displacement processes are used to recover low viscosity oils by controlling the mobility ratio or decreasing the interfacial tension between the oil and the other fluids. The thermal methods of steamflooding and combustion techniques are used to recover high viscosity oils, with the heat transferred to the oil reducing its viscosity causing it to flow more easily. In this thesis we consider injection of water and immiscible gas and therefore consider secondary recovery techniques only.

1.2 Mathematical Modelling of Reservoir Fluid Flow

A number of mathematical models exist for the description of fluid flow in oil reservoirs. These can be divided into categories as to whether the fluid flow is considered to be compressible or incompressible and whether the fluid components are immiscible or miscible. A fluid component is deemed compressible if the volume it occupies is dependent on its pressure. The compressibility associated with the reservoir rock may also be modelled. Fluid components are considered miscible if they are able to mix in all proportions without any interface forming between them. The physical parameters of the resulting fluid mixture, for example viscosity and density, are then obtained from a relation involving the

individual fluid component parameters and are known as mixing laws. This is in contrast to immiscible fluids in which different phases exist which exhibit distinct properties and behaviour. We only consider immiscible flow in this thesis and so describe miscible flow no further.

The mathematical models that describe most isothermal flow situations are derived from four main physical principles. These are: conservation of mass of the fluid components, Darcy's law which describes how the fluid phases flow through the reservoir, thermodynamic equilibrium which determines how the fluid components combine to form phases, and lastly the condition that the fluid fills the rock pore volume. Description of immiscible, incompressible flow of 2 or 3 fluid components is accomplished with the classical Buckley-Leverett models, see Trangenstein [49]. These models consist of a mixed elliptic-hyperbolic system of partial differential equations, with the elliptic equation being for pressure and a system of hyperbolic conservation laws describing conservation of mass of the fluid components.

Addition of compressibility effects (and mass transfer between phases) to the 3-phase Buckley-Leverett model results in the oil industry standard Black-Oil model, which is a mixed parabolic-hyperbolic system of partial differential equations. Similar to the incompressible case, the model consists of a system of hyperbolic conservation laws in component densities, but this time a parabolic pressure equation. In the incompressible case, the fluid pressure and component densities are independent, but this is not the case when compressibility is introduced, due to the condition that the fluid fills the rock pore volume (volume balance condition). This results in the coupling of the pressure field with the conservation laws and hence pressure and component density can not be solved for separately. Therefore the flow equations may be solved, in an unsplit form, with a totally implicit discretisation, otherwise have to be split (or separated out) for solution to be possible.

A number of ways of separating the parabolic and hyperbolic character of the flow equations exist. The industry standard procedure of accomplishing this is use of the IMPES method (IMplicit Pressure Explicit Saturation), see Aziz and Settari [1], and is also outlined in Chapter 7. However, an alternative method

has been presented by Trangenstein and Bell in [46] and is the formulation of the flow equations used in this thesis. This method decouples the parabolic and hyperbolic behaviour by a linearisation of the volume balance equation to form the parabolic equation for pressure, however this introduces a 'volume error discrepancy' which is a consequence of the linearisation and indicates that the volume balance equation is not exactly satisfied.

An alternative compressible fluid flow model exists, called the compositional model, which is used when the modelling capabilities of the Black-Oil model are inadequate. This model uses a more accurate representation of hydrocarbon phase behaviour which is needed to model, for example the EOR technique of miscible gas injection. However, use of this more sophisticated model is more computationally demanding and so its use is limited.

1.3 Numerical Methods for Reservoir Simulation

Both finite difference and finite element methods are used in oil reservoir simulation, although in this thesis we concentrate solely on finite difference methods for solution of the Black-Oil flow equations. The classical finite difference method employed in the industry is known as one-point upstream weighting (or upwind), and achieves first order accuracy in space and time. A second order extension exists, referred to as two-point upstream weighting which uses an extrapolation technique to attain improved spatial accuracy. These methods use information one point (or two points) upstream to calculate numerical fluxes, resulting in first order (or second order) spatial accuracy, whilst both achieving first order time accuracy. However the two-point scheme may introduce oscillations into the results, much akin to the classical second order schemes of Lax Wendroff [29] and Warming and Beam [54]. A 'constrained' version of the two-point scheme exists, in which the results of the extrapolation are constrained to lie between neighbouring cell centred values, but this version can sometimes yield unphysical shocks.

Classical first order accurate numerical methods suffer from large amounts of

numerical diffusion, resulting in the smearing of shock fronts over many grid cells. Whereas the classical second order methods, although increasing the resolution of the shocks suffer from spurious oscillation in their vicinity. Hence work in the oil industry on high resolution (second order accurate), oscillation free Total Variation Diminishing (TVD, see [24]) numerical schemes was undertaken. A number of TVD flux-limiter type methods had been independently proposed, outside the oil industry, by a number of authors, for example Roe [34] and Van Leer [50]. However explicit and implicit TVD flux-limiter schemes have been developed for use in the oil industry by, for example, Blunt and Rubin [7] and Rubin and Edwards [36]. These methods are based on the types of numerical fluxes typically used in the oil industry, rather than using the Lax Wendroff flux, as in [34] and [50]. Originally reservoir simulation codes only achieved first order accuracy in space and time, but with advent of the flux-limiter schemes in [7] and [36] can now achieve second order accuracy whilst being free of numerical oscillations, i.e. TVD. Flux Corrected Transport (FCT), another high resolution non-oscillatory method [8, 9, 56], has also been applied, but to the more restricted circumstances of incompressible miscible flow.

There has also been a recent interest in the application of Godunov type methods to reservoir simulation. These methods, originally developed by Godunov [20], have undergone extensive development and are applied to a wide range of problem areas. Solutions of Riemann problems are central to these types of scheme and the analytic framework of the conservation laws is incorporated into the numerical scheme. In this thesis we apply the Higher Order Godunov method [2, 10] to the system of conservation laws arising from the Black-Oil model [46]. The scheme includes modifications for certain types of degeneracies present in the system of conservation laws, specifically local linear degeneracies and eigenvector deficiencies which the Black-Oil model possesses, and therefore is particularly suited to numerical reservoir simulation. The scheme relies on a knowledge of the characteristic structure of the conservation laws to achieve second order accuracy in space and time, and in the solution of Riemann problems at cell edges to compute numerical fluxes. We use the 1-D and 2-D schemes to perform numerical reservoir simulations in 1 and 2 dimensions.

1.4 Structure and Contents of the Thesis

The thesis can be considered as having two main themes. Firstly, the reduction of numerical errors associated with Black-Oil simulations using the Black-Oil model [46] with the inherent volume error discrepancy. This is achieved through an investigation of the impact of the volume error discrepancy on the numerical results and possible ways of decreasing the volume error discrepancy. The compressibility of the reservoir fluids is also thought to have an effect on the level of volume error discrepancy, see [48], and hence the numerical errors. This is therefore investigated in the context of the Black-Oil model.

Secondly a comparison is made of the TVD flux-limiter scheme [36], present in the commercial reservoir simulation code VIP used by B.P., and the Higher Order Godunov scheme [2], when applied to the system of degenerate conservation laws associated with the Black-Oil model. The performance of the schemes, and their relative efficiency, when applied to the degenerate systems of conservation laws is discussed. Three types of reservoir simulation problem are performed to compare the numerical results from both the schemes.

We now describe the structure and contents of the rest of this thesis, of which the next three chapters are of a review nature. In the next chapter we give an overview of the theory and nomenclature associated with hyperbolic conservation laws that we use throughout this thesis. Both the analytic structure and numerical solution of conservation laws are examined. We also outline some numerical schemes recently developed for use in the oil industry. Chapter 3 contains a description of the Black-Oil model [46] used to model the compressible flow of the reservoir fluid. We outline the physical principles involved and supply all the flow equations. In Chapter 4 we describe the Higher Order Godunov method [2, 10], for degenerate systems of conservation laws, used to solve the hyperbolic system arising from the Black-Oil model.

In Chapter 5 we describe the implementation of the Higher Order Godunov method on the Black-Oil equations, a Fortran code having been written to perform the reservoir simulations in 1 and 2 dimensions. The 1-D code was validated by comparison of numerical results with those given by Trangenstein and

Bell [46], we show results of three of these simulations. We also present results of a 2-D Areal problem, which have not previously been seen in the literature. In this chapter we also investigate the accuracy of the Higher Order Godunov method when applied to degenerate systems, by comparing the numerical results of 3-phase incompressible Buckley-Leverett simulations with the corresponding analytic solutions which we construct. The incorporation of source terms in 1 and 2 dimensions, to model injection of fluid into, and production of fluid from the reservoir, in conjunction with the Black-Oil model and Higher Order Godunov method, is also described. Locally implicit procedures are used to model the source terms, to remove the numerical stability problem associated with their use.

In Chapter 6 we investigate the impact of the volume error discrepancy on the numerical results of 2-component 2-phase reservoir simulations, and describe potential techniques of reducing the volume error discrepancy. The techniques investigated are an iterative solution of the volume balance equation for pressure, which is performed locally in each grid block, and a global second order pressure correction procedure. The effect of fluid compressibility on the volume error discrepancy is also investigated.

Chapter 7 is devoted to a comparison of the TVD flux-limiter scheme used in the reservoir simulation code VIP and the Higher Order Godunov scheme. Numerical results from three types of reservoir simulation problem are used to aid the comparisons, these being a standard 1-D, 2-D Areal, and a 2-D cross-sectional simulation. The results from the latter of the three problems is of particular interest since these problems exhibit counter-current flow and will hence be a good test of the numerical methods, especially the Higher Order Godunov method.

Finally in Chapter 8 we summarise the work undertaken and outline ideas for further work.

Chapter 2

Hyperbolic Conservation Laws

2.1 Introduction

In this chapter we review some of the theory and nomenclature, associated with hyperbolic conservation laws, which we use throughout this thesis. Firstly an indication of how hyperbolic conservation laws are derived and characterised is given. Particular attention is given to systems that exhibit two types of degeneracies which commonly arise in the modelling of flow in porous media. We then concentrate on the analytic solution of systems of conservation laws, in particular weak solutions, which are needed because discontinuities typically arise in reservoir simulation problems. Indeed the majority of problems of interest which are modelled by hyperbolic conservation laws exhibit discontinuous solutions, which either develop with time or result from discontinuities in the initial data. However weak solutions are known to be non-unique, and so a way of ensuring the physically correct solution is needed. This is accomplished by requiring the solution to satisfy an appropriate entropy condition, examples of which are given. The Riemann problem is then outlined along with the types of analytic solution possible.

Since analytic solutions to reservoir engineering problems usually do not exist or are very difficult to construct, we concentrate on numerical solutions. Conservative finite difference approximations are used for reasons described later. Accuracy and stability considerations associated with such schemes are then discussed. Classical first order and second order numerical schemes are described along with

their deficiencies and explanations of how these deficiencies arise. Hence work was prompted by a number of authors on high resolution, non-oscillatory Total Variation Diminishing (TVD) schemes, some of which we review. An example of two types of TVD scheme are given, firstly the flux-limiter type scheme, then a variant of the MUSCL family of schemes which is of Godunov type. Another type of high resolution, non-oscillatory scheme, although not necessarily TVD, namely Flux Corrected Transport (FCT) is also described.

Finally we look at how modern numerical methods for hyperbolic conservation laws have been applied in the oil industry for numerical reservoir simulation. In particular Implicit and Explicit TVD schemes as well as FCT will be discussed.

2.2 Derivation

A conservation law is a relation which holds in a region of space that relates the rate of change with time of a quantity to the flux of that quantity through the boundary of the region. The relation says that in the absence of sources and sinks the quantity being conserved in the region may not be created or destroyed. Hence hyperbolic conservation laws are derived from physical principles and represent conservation of a state variable $\mathbf{U}$ which may be a scalar or vector function of space and time. The state variable may be mass, momentum, energy etc. or a vector of these quantities.

The Gauss divergence theorem may be used on a control volume to derive an integral form of the conservation laws which are valid for non-smooth functions $\mathbf{U}$. If however, $\mathbf{U}$ is a differentiable function, and hence smooth, the integral form may be converted to the more common differential form of the conservation laws, namely

$$\mathbf{U}_t + \mathbf{F}_x = 0, \tag{2.2.1}$$

where $\mathbf{U} = \mathbf{U}(x,t)$ is an K vector and $\mathbf{F}$ is a vector valued function of $\mathbf{U}$, with $K = 1$ corresponding to the scalar case. The vector $\mathbf{U}$ is the conserved variable and the quantity $\mathbf{F}$ is termed the flux function. The differential equation as it stands does not represent a complete description of the problem in hand. An initial condition of the form $\mathbf{U}(x,0)$ is also needed to ensure the problem is well

posed. The differential equation along with the initial condition is said to hold on a region Ω, the boundary of which is denoted by $\partial\Omega$. Boundary conditions on $\partial\Omega$ may be needed depending on the structure of the problem, i.e. whether there is inflow, outflow or reflection from the boundaries.

2.3 Characterisation

The equation (2.2.1) is said to be in conservation form, with the quasi-linear form being given by

$$\frac{\partial \mathbf{U}}{\partial t} + \frac{\partial \mathbf{F}}{\partial \mathbf{U}} \frac{\partial \mathbf{U}}{\partial x} = 0,$$

where $\frac{\partial \mathbf{F}}{\partial \mathbf{U}}$ is an $K \times K$ matrix called the Jacobian matrix. If $\frac{\partial \mathbf{F}}{\partial \mathbf{U}}$ is a function of x and t only then the conservation laws are termed linear, whereas if $\frac{\partial \mathbf{F}}{\partial \mathbf{U}}$ is also a function of $\mathbf{U}$ then we have a non-linear system. The system (2.2.1) is termed hyperbolic if all the eigenvalues of the Jacobian matrix are real. If the eigenvalues are also distinct then the system is referred to as strictly hyperbolic. If this is the case then the eigenvectors and eigenvalues of the Jacobian satisfy

$$\frac{\partial \mathbf{F}}{\partial \mathbf{U}} X = X\Lambda,$$

where Λ is a real diagonal matrix and X a real non-singular matrix. The entries of Λ are termed characteristic wavespeeds and the columns of X, denoted by $\mathbf{x}_k$, the characteristic directions. A loss of strict hyperbolicity occurs when two or more wavespeeds coincide at a point, which is referred to as an umbilic point.

A particular eigenvalue and its corresponding eigenvector define a characteristic field of the system. The characteristic field is said to be genuinely non-linear if

$$\frac{\partial \lambda_k}{\partial \mathbf{U}} \cdot \mathbf{x}_k \neq 0,$$

for all $\mathbf{U}$, where k enumerates the characteristic field. In the scalar case this condition reduces to $f'' \neq 0$, which corresponds to the well known convexity condition $f'' > 0$ or the concave condition $f'' < 0$. Alternatively if

$$\frac{\partial \lambda_k}{\partial \mathbf{U}} \cdot \mathbf{x}_k \equiv 0,$$

for all $\mathbf{U}$ then the k^{th} field is termed linearly degenerate.

In this thesis we consider systems of conservation laws which exhibit certain pathologies in their wave structure as previously mentioned. In particular we consider systems with the following two degeneracies, namely those which exhibit local linear degeneracy and eigenvector deficiencies in the wavefields. A local linear degeneracy occurs at a specific value of $\mathbf{U}$ for which the genuine non-linearity condition fails. An eigenvector deficiency arises when two or more eigenvalues coincide and their corresponding eigenvectors are parallel. Other degeneracies are also possible such as elliptic, parabolic and rotational but we do not consider these.

2.4 Analytic Solutions

2.4.1 The Weak Form

The differential form of the conservation laws preclude discontinuous solutions, however the problems of interest to us, namely the simulation of flow in porous media, typically exhibit discontinuous solutions hence we need to consider the weak form of the conservation laws. The weak form is an integral formulation and hence discontinuous solutions are admitted. It is obtained by multiplying the conservation laws by a smooth test function ϕ which has compact support, i.e. is zero outside of some finite interval, and integrating over the region, resulting in

$$\int_0^\infty \int_{-\infty}^\infty [\phi_t \mathbf{U} + \phi_x \mathbf{F}(\mathbf{U})]\, dx\, dt = -\int_{-\infty}^\infty \phi(x,0)\mathbf{U}(x,0)\, dx.$$

For more details see Smoller [41] or any other standard text on hyperbolic conservation laws. The conservation laws are then satisfied in the sense of distributions and discontinuous solutions are now allowed since the act of integrating by parts moves the derivatives onto the test function. Admission of discontinuous solutions has a consequences in that weak solutions are non-unique, hence a way of selecting the physically correct solution is required.

2.4.2 Entropy Conditions

The way in which a discontinuity is determined as being physically correct is if it satisfies a condition known as an Entropy Condition. The entropy condition

requires that the physically meaningful solution to the conservation laws is the limit of the solution to a modified differential equation, with an infinitesimal amount of diffusion, namely

$$\mathbf{U}_t + \mathbf{F}_x = \epsilon \mathbf{U}_{xx},$$

as the diffusion tends to zero, i.e. $\epsilon \downarrow 0$. This condition is thought, see for example Trangenstein [49], to be reasonable when considering reservoir flow problems, particularly so when diffusive forces such as capillary pressure and mixing are ignored. This is because enforcement of the entropy condition ensures that the solutions to the conservation laws are related to more realistic flow models which do include diffusive forces.

Work by Oleinik [31] and Lax [28] has provided straightforward quantitative versions of the entropy condition. Oleinik showed that the scalar Riemann problem has an admissible shock from u^L to u^R if and only if

$$\frac{f(u) - f(u^L)}{u - u^L} \geq \sigma \geq \frac{f(u) - f(u^R)}{u - u^R},$$

for all u between u^L and u^R and termed this condition E, where σ is the shock speed and is given by

$$\sigma = \frac{f(u^L) - f(u^R)}{u^L - u^R}.$$

Condition E applies to both convex and non-convex scalar conservation laws, whereas Lax showed that the convex problem has an admissible weak shock if the shock speed σ satisfies

$$a(u^L) > \sigma > a(u^R),$$

where $a(u)$ $(= f'(u))$ is the wavespeed of the scalar conservation law. This second condition states that the characteristics should go into the shock as time progresses. For convex f Oleinik's condition reduces to that of Lax. A similar condition for systems is also due to Lax and is expressed by

$$\lambda_k(\mathbf{U}^L) > \sigma > \lambda_k(\mathbf{U}^R),$$

where λ_k denotes one of the characteristic wavespeeds of the system, and is only valid for genuinely non-linear fields. If satisfied for a particular k the discontinuity

is referred to as a k shock. In the case of characteristic fields which are not genuinely non-linear another entropy condition is required. This extended entropy condition is due to Liu [30] and is given by

$$\lambda_k(\mathbf{U}^L) \geq \sigma \geq \lambda_k(\mathbf{U}^R),$$

and is less restrictive than the Lax condition for genuinely non-linear fields by allowing equality of the shock speed with one of the wavespeeds.

2.4.3 The Riemann Problem

The Riemann problem is defined as the initial value problem (2.2.1) with a single discontinuity in the initial data,

$$\mathbf{U}(x,0) = \begin{cases} \mathbf{U}^L & \text{if } x < 0 \\ \mathbf{U}^R & \text{if } x \geq 0 \end{cases},$$

where $\mathbf{U}^L$ and $\mathbf{U}^R$ are constant states to the left and right respectively of the initial discontinuity at $x = 0$. The Riemann problem is very important in the theory of hyperbolic conservation laws since it serves as a component of a number of numerical schemes.

The solution to the Riemann problem is composed of two types of elementary waves, termed shocks and rarefactions, usually connected by constant states. Another type of wave termed a contact discontinuity may also arise. A shock is a discontinuity that satisfies an appropriate entropy condition and travels with the Rankine-Hugoniot shock speed which is given below. An expression for the speed of a propagating shock can be obtained from the weak form of the conservation laws, and is given by the following well known Rankine-Hugoniot jump condition

$$\sigma = \frac{f(u^R) - f(u^L)}{u^R - u^L},$$

for the scalar case where u^L and u^R are the states to the left and right of the shock. For details on its derivation see Smoller [41]. Similarly in the system case the jump condition

$$\mathbf{F}(\mathbf{U}^R) - \mathbf{F}(\mathbf{U}^L) = \sigma(\mathbf{U}^R - \mathbf{U}^L),$$

must hold for the discontinuity with these left and right states to be a valid shock.

The contact discontinuity is not a valid shock, but is a valid discontinuity and may arise if one of the characteristic fields is linearly degenerate. In this case the wavespeeds on both sides of the discontinuity are equal and hence the discontinuity moves with speed equal to the wavespeed.

A rarefaction is a smoothly varying solution which is a function of the similarity variable x/t only. The following characterisation of rarefaction solutions exists, a $k-$rarefaction is defined by

$$\frac{x}{t} = \lambda_k(\mathbf{U}),$$

$$\lambda_k(\mathbf{U}^R) > \lambda_k(\mathbf{U}) > \lambda_k(\mathbf{U}^L),$$

where $\mathbf{U}$ is any state on the rarefaction wave and $\mathbf{U}^L$ and $\mathbf{U}^R$ are states to the left and right of the wave.

Classical hyperbolic theory, see Lax [28], states that for an $K-$system the Riemann problem solution is composed of K distinct waves connecting $\mathbf{U}^L$ to $\mathbf{U}^R$. For a strictly hyperbolic system these waves can only be connected by constant states, but for a system that exhibits local linear degeneracies, rarefaction-shock compound waves become a possibility, see Liu [30]. For example a $1-$rarefaction may be connected to a $1-$shock, in fact the two waves must be of the same family because at the connection point the fastest wavespeed in the rarefaction must be equal to the first characteristic speed to the left of the shock. Shock-rarefaction compound waves are also a possibility. However, some types of compound waves are precluded, depending on the number of components in the system K and the degree of the flux function, for example see Schaeffer and Shearer [38]. Also, at points where strict hyperbolicity fails, transitional waves are possible in which a wave of one family may transition into a wave of another family. For example at an umbilic point where the first and second wavespeeds are equal a 1-wave may transition into a 2-wave at that point.

2.5 Numerical Solutions

2.5.1 Conservative Difference Schemes

We shall consider conservative difference schemes for numerically solving the system (2.2.1), as we want to retain the conservation property of the equations. This is important because not only do we maintain conservation, but an important theorem of Lax and Wendroff [29] will then apply. This theorem states that if the numerical scheme is convergent then it converges to a weak solution of the conservation laws (2.2.1). As a consequence shock wave solutions will satisfy the Rankine-Hugoniot relation for the shock speed, so that shocks will appear in the correct locations. This type of difference scheme may be derived by integrating the conservation laws over a box in x, t space defined by $[x_{j-\frac{1}{2}}, x_{j+\frac{1}{2}}] \times [t^n, t^{n+1}]$ and applying the Gauss divergence theorem, which results in

$$\mathbf{U}_j^{n+1} = \mathbf{U}_j^n - \frac{\Delta t}{\Delta x}(\mathbf{F}_{j+\frac{1}{2}}^{n+\frac{1}{2}} - \mathbf{F}_{j-\frac{1}{2}}^{n+\frac{1}{2}}), \tag{2.5.2}$$

where we have used standard notation and $\Delta x = x_{j+\frac{1}{2}} - x_{j-\frac{1}{2}}$ and $\Delta t = t^{n+1} - t^n$. The quantity $\mathbf{U}_j^n$ is an integral averaged value of $\mathbf{U}$ over the interval, i.e.

$$\mathbf{U}_j^n = \frac{1}{\Delta x} \int_{x_{j-\frac{1}{2}}}^{x_{x+\frac{1}{2}}} \mathbf{U}(j\Delta x, n\Delta t)\, dx.$$

The $\mathbf{F}_{j+\frac{1}{2}}^{n+\frac{1}{2}}$ is termed the numerical flux and is defined by

$$\mathbf{F}_{j+\frac{1}{2}}^{n+\frac{1}{2}} = \frac{1}{\Delta t} \int_{t^n}^{t^{n+1}} \mathbf{F}(\mathbf{U}(x_{j+\frac{1}{2}}, t)) \cdot \underline{\mathbf{n}}\, dt,$$

where $\underline{\mathbf{n}}$ is the unit outward normal to the relevant face of the space-time box.

2.5.2 Explicit and Implicit Schemes

If the fluxes $\mathbf{F}_{j+\frac{1}{2}}^{n+\frac{1}{2}}$ in the finite difference update (2.5.2) are functions of quantities at the current time level then the resulting scheme is termed explicit. In this case all the quantities on the right hand side of (2.5.2) are known and hence the update is straightforward. On the other hand, if the fluxes are functions of the solution at the advanced time level $n+1$ then the scheme is implicit and the resulting update formula needs to be solved by an iterative method since both

sides of (2.5.2) are functions of $\mathbf{U}^{n+1}$. In general implicit methods are more diffusive than corresponding explicit methods. However most implicit methods have no stability restriction on their time step and hence can use larger time steps without sacrificing numerical stability. However increasing the time step will degrade the accuracy of the results, so a balance must be struck between efficiency and accuracy. Often the type of problem being solved influences the choice of using an explicit or implicit method.

2.5.3 Accuracy

A fundamental concern when using a numerical scheme is its order of accuracy. Stability is also a central concern and will be discussed later. Schemes that achieve first order accuracy in space and time are referred to as low resolution and suffer from large amounts of numerical diffusion. This means that shocks will be smeared over a large number of grid cells, and hence a large number of cells are needed to accurately capture sharp features present. Therefore it is more desirable to use a higher (second) order method. However classical second order methods such as the famous Lax-Wendroff [29] and Warming and Beam [54] schemes although increasing the resolution of shocks suffer from spurious oscillations behind and in front of shocks respectively.

The different effect the order of numerical scheme has on the type of deficiency present in the numerical scheme, i.e. diffusion with first order methods and dispersion with second order methods, can be explained in terms of the modified equation. The modified equation is the actual partial differential equation solved when a finite difference approximation is used to solve the original partial differential equation. This modified equation should not be confused with the previously mentioned modified equation, with the inclusion of an infinitesimal viscosity term in the section on entropy conditions, since they are not connected. Warming and Hyett give a description of the modified equation approach to analysing finite difference methods in [55]. The modified equation is derived by expanding each term of the finite difference equation approximating the partial differential equation into a Taylor series and eliminating the time derivatives of order higher than first and the mixed space and time derivatives. This leaves the derivatives that

were present in the original equation together with spatial derivatives only. The elimination method should not use the original partial differential equation as its solution will not satisfy the finite difference equations. Instead the result of the Taylor series expansion of the finite difference approximation should itself be manipulated by applying $\frac{\partial}{\partial t}$ and $\frac{\partial}{\partial x}$ operators and taking linear combinations of these forms with the original expansion to remove the required derivatives. The resulting modified equation will have infinitely many terms but in practice only the lowest order terms need be considered as these describe the dominant behaviour. For example when a first order finite difference method is used to approximate the solution to the linear advection equation analysis shows that the modified equation is actually of the form

$$u_t + a u_x = \mu u_{xx},$$

where the μu_{xx} term is a diffusion term. Hence the reason for first order methods suffering from large doses of numerical diffusion. Similarly with second order methods, the modified equation looks like

$$u_t + a u_x = \eta u_{xxx},$$

with the ηu_{xxx} term being a dispersive term. This term gives rise to the dispersive ripples in the Lax-Wendroff and Warming and Beam schemes.

Two examples of scalar first order schemes are the upwind scheme and the Godunov scheme. In the reservoir simulation community the upwind scheme is referred to as one point upstream weighting, with flux

$$f_{j+\frac{1}{2}}^{n+\frac{1}{2}} = \begin{cases} f_j^n & \text{if } \frac{\partial f}{\partial u} \geq 0 \\ f_{j+1}^n & \text{if } \frac{\partial f}{\partial u} < 0 \end{cases}.$$

Hence the numerical flux is calculated at the grid point from where information is propagating, i.e. the upstream or upwind direction. The Godunov scheme [20] follows a different approach in that it utilises the solutions of Riemann problems at cell edges. The solution is represented by a piecewise constant approximation at the current time level with u_j^n being an average value of u in cell j. The solution to the Riemann problem is denoted by $R(u^L, u^R, \lambda)$ with u^L and u^R the

states to the left and right of the discontinuity at $x = \lambda t$, where λ specifies the speed of the discontinuity. Godunov's method takes the cell edge flux to be

$$f_{j+\frac{1}{2}}^{n+\frac{1}{2}} = f(R(u_j^n, u_{j+1}^n, 0)),$$

i.e. the flux at the state that remains stationary at the original location of the discontinuity.

2.5.4 Stability

When numerical methods are used to solve conservation laws a very important concern is the stability of the scheme being used. A necessary condition on the time step Δt exists for hyperbolic problems and is referred to as the Courant-Friedrichs-Lewy (CFL) condition [13]. This condition was derived through the observation that the domain of dependence of the finite difference scheme must be contained within the domain of dependence of the conservation law. The condition for a 3-point difference scheme can be expressed by

$$\Delta t \leq \frac{\Delta x}{\lambda_{max}}, \tag{2.5.3}$$

where λ_{max} is the largest wavespeed in the problem at the current time level. The stability condition can also be expressed in terms of a Courant (or CFL) number ν which is given by

$$\nu = \frac{\lambda_{max}\Delta t}{\Delta x}. \tag{2.5.4}$$

Therefore the necessary condition for stability of a 3-point difference scheme is that the Courant number is no greater than 1. A local CFL number may also be defined and is the right hand side of (2.5.4) evaluated in a particular cell.

2.5.5 TVD Methods

Numerical methods that accurately capture shocks without any oscillation have been sought for a number of years. One such class of scheme are the so called flux-limiter schemes, to be described later, which possess the very desirable property of being Total Variation Diminishing (TVD). The concept of a TVD scheme was first introduced by Harten [24] and is characterised by

$$TV(u^{n+1}) \leq TV(u^n), \tag{2.5.5}$$

where $TV(u^n)$ is the total variation of the solution at time level n and is defined by

$$TV(u^n) = \sum_k |u^n_{k+1} - u^n_k|.$$

The total variation is an important property of a numerical scheme which can be used to prove convergence of a scheme, and also ensures that oscillations cannot appear in the solution.

The concept of a TVD scheme is essentially one-dimensional although a definition of the total variation of the solution to the two-dimensional conservation laws of the form

$$u_t + f_x + g_y = 0,$$

has been given by Goodman and LeVeque [23]. The total variation is defined by the sum of the variations in both coordinate directions and is given by

$$TV(u^n) = TV_x(u^n) + TV_y(u^n) = \Delta y \sum_{j,k} |u^n_{j+1,k} - u^n_{j,k}| + \Delta x \sum_{j,k} |u^n_{j,k+1} - u^n_{j,k}|.$$

Goodman and LeVeque [23] showed that any scheme in two-dimensions which satisfies the TVD criteria (2.5.5) must be only first order accurate. However, when most 1-D TVD methods are applied in 2-D they usually work well in practice. Second order accuracy is maintained on smooth solutions and no oscillatory behaviour is observed, despite the fact that the scheme is not strictly TVD.

Other types of non-oscillatory scheme, which are not TVD, have been developed for multidimensional linear advection by for example Roe and Sidilkover [35]. Their scheme is termed an Optimum Positive Linear Scheme for linear advection. The coefficients of such schemes are positive quantities, which defines a positive scheme, and are optimum in the sense that the truncation error is minimised. This is accomplished by a particular choice of coefficients, subject to the positivity condition. Extension of numerical schemes to model multidimensional flow is usually made on a dimension by dimension basis, i.e. dimensionally splits schemes, which will be outlined later. However this approach is reported in the literature to give poor results if the flow is unsteady or not aligned with the grid directions, hence the development of the Positive schemes. These schemes are said to be the multidimensional equivalent of simple upwinding and in 2-D have been shown to be about 4 times less dissipative than the dimensionally split

schemes, and permit time steps that can be greater by a factor of 2. Roe and Sidilkover [35] point out that their scheme can be written in conservation form and hence will possess the desirable properties previously described for conservative schemes. First order accuracy only is achieved but a second order generalisation is reported as having been developed using flux-limiters.

2.5.6 Flux-Limiter Schemes

To describe the main ideas behind the flux-limiter type of scheme we first define an antidiffusive flux. This is defined as the difference between the first order flux and second order flux of a particular scheme. Firstly a low order entropy satisfying scheme is used, which is then supplemented by a limited amount of the antidiffusive flux. All of the antidiffusive flux is used where the solution is smooth but only a limited amount is used near steep gradients to ensure the TVD property. The amount of limiting taking place depends on the local gradient of the solution at the current time level, i.e. near shocks the most flux-limiting will take place. For example, consider the linear scalar equation

$$u_t + au_x = 0 \quad a > 0.$$

The second order Lax-Wendroff scheme can be used as the underlying scheme, namely

$$u_j^{n+1} = u_j^n - \nu \Delta u_{j-\frac{1}{2}} - \Delta_-(\frac{1}{2}(1-\nu)\Delta u_{j+\frac{1}{2}}),$$

where

$$\nu = a\frac{\Delta t}{\Delta x},$$

and with the notation

$$\Delta_- u_{j+1} = u_{j+1} - u_j = \Delta u_{j+\frac{1}{2}}.$$

It can be seen that this is the result of using the first order scheme

$$u_j^{n+1} = u_j^n - \nu \Delta u_{j-\frac{1}{2}},$$

together with an extra term which is composed of the antidiffusive flux difference

$$-\Delta_-(\frac{1}{2}(1-\nu)\Delta u_{j+\frac{1}{2}}).$$

It is well known that the Lax-Wendroff scheme is not TVD due to the spurious oscillations it produces near shocks, as previously mentioned. This can be remedied by adding only a limited amount of the antidiffusive flux to the first order scheme by introducing a flux-limiter ϕ_j

$$u_j^{n+1} = u_j^n - \nu\Delta u_{j-\frac{1}{2}} - \Delta_-(\phi_j \frac{1}{2}(1-\nu)\Delta u_{j+\frac{1}{2}}),$$

where ϕ_j is a function ϕ of a parameter r_j which is taken to be a ratio of consecutive gradients, i.e.

$$r_j = \frac{\Delta u_{j-\frac{1}{2}}}{\Delta u_{j+\frac{1}{2}}}.$$

The limiter function ϕ is then chosen such that the limited antidiffusive flux is maximised subject to the TVD constraint. Details of this procedure for the linear and non-linear cases can be found in Sweby [45]. The result of the analysis by Sweby can be shown graphically, i.e. a region in ϕ, r space in which the limiter must lie to give a second order TVD scheme, which is given by the shaded area in Figure 2.1. For example $\phi(r) = 1$ reverts the scheme back to Lax-Wendroff and

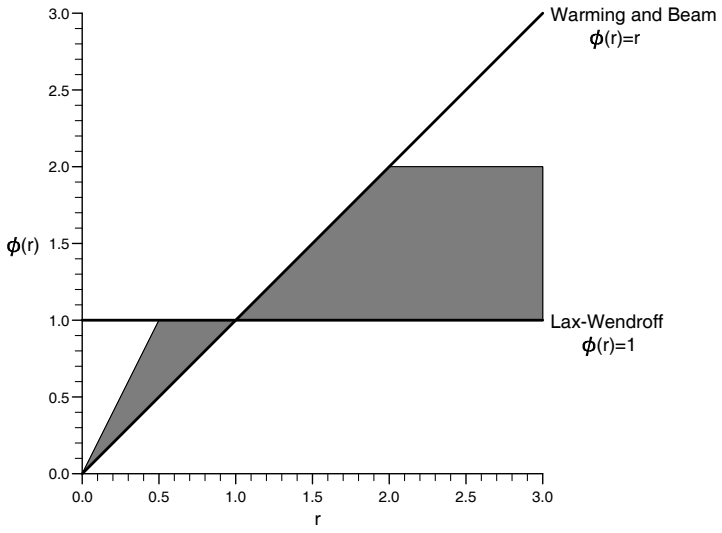

Figure 2.1: The second order TVD region, also indicating the limiter functions ϕ corresponding to the Lax-Wendroff and Warming and Beam schemes.

$\phi(r) = r$ gives the scheme of Warming and Beam. As can be seen from Figure 2.1 these two lines do not lie entirely within the TVD region hence explaining the non TVD property of these two classical schemes. The following conditions also exist on the limiter function, firstly if $r \leq 0$ then $\phi = 0$ so that the sign

of the antidiffusive flux is maintained. This condition means that second order accuracy is lost at extreme points of the solution. Secondly the condition $\phi(1) = 1$ is needed as a general requirement for a second order scheme and ensures Lipschitz continuity of $\phi(r)$. Lastly the condition

$$\frac{\phi(r)}{r} = \phi(\frac{1}{r}),$$

ensures that forward and backward gradients are treated identically.

A number of flux-limiter methods have been presented in the literature by for example Roe [34] and Van Leer [50], each in the authors own notation. For example Roe developed the famous Minmod and Superbee limiters, which correspond to the lower and upper boundaries of the TVD region respectively. The Van Leer limiter is also commonly used and is given by a smooth curve lying within the region. In [45] Sweby translated these limiters into a common formulation (ϕ, r formulation as above) so that it could be seen how the various limiter functions compared both theoretically and numerically.

2.5.7 A MUSCL Type Scheme

We now describe an alternative approach to deriving a second order accurate TVD scheme. We concentrate on a variant of the Monotonised Upstream centred Scheme for Conservation Laws, known as MUSCL, originally due to Van Leer [51], described by Goodman and LeVeque [22]. The derivation of the scheme is geometrically based rather than the algebraic flux-limiter schemes previously outlined. The approach is similar to that of Van Leer's original scheme in that second order accuracy is obtained by using a piecewise linear approximation to the solution at each time step rather than a piecewise constant approximation. Hence the scheme can be viewed as a second order generalisation of Godunov's method. In fact any scheme that constructs states at cell interfaces which are then used to solve the Riemann problem there, is referred to as of Godunov type. The Higher Order Godunov method of Bell et al. [2], to be described in Chapter 4, is related to the MUSCL scheme since it also uses a slope construction to derive left and right states at cell interfaces, which are then used to compute a flux. However the MUSCL scheme solves a linearised Riemann problem at each

cell interface, whereas the Higher Order Godunov scheme uses a fuller description of the Riemann problem.

The general principle is as follows. The piecewise constant approximation, denoted by $w(x,t)$ say, of the solution at the current time level is given in each grid cell $I_j = [x_{j\ \_}, x_{j\ \_}]$ by

$$(\quad ^n) = \ ^n_j \quad \text{for} \qquad _j$$

The piecewise linear approximation ( ) is constructed in each cell by the interpolant of

$$^n_j + \frac{1}{2}\Delta \quad _j \ \text{and} \quad ^n_j \quad \frac{1}{2}\Delta \quad _j \tag{2 5 6}$$

i.e. is given by

$$(\quad ^n) = \ ^n_j + \ _j(\qquad _j) \ \text{for} \qquad _j \tag{2 5 7}$$

The slopes $_j$ must be chosen such that the integral of the piecewise linear approximation over each cell is the same as with $_j = 0$ and the total variation of the resulting profile, is not increased. Hence the piecewise linear representation maintains conservation as cell averages are preserved. The slope $_j$ can be given by a number of formulae, a commonly used form is

$$_j = \begin{cases} \min(\ \frac{u \quad u}{x} \quad \frac{u \quad u}{x}\ )\ \text{sign}(\ _j \qquad _j) & \text{if } (\ _j \qquad _j)(\ _j \quad _j\ ) \quad 0 \\ 0 & \text{otherwise} \end{cases}$$

The two states in (2.5.6) define values of at edge $_j\ \_$ and edge $_j\ \_$ respectively. Using these two states a function ( ) can be defined which interpolates the flux function, i.e. ( ) is approximated as a piecewise linear function. The problem of calculating fluxes at cell edges then reduces to solving a linear problem with piecewise linear data. Hence the problem can now be expressed as

$$_t + \quad (\ )\ _x = 0$$

with initial data (^{n}) given by (2.5.7).

The resulting flux formulae can be found in [22] and are valid for convex away from sonic points $^-$ where $(^-) = 0$. Goodman and LeVeque also quote flux formulae for use when a sonic point is detected. Stability of the scheme is ensured if the time step satisfies the usual CFL condition (2.5.3).

Chapter 3

The Black-Oil Fluid Flow Equations

3.1 Introduction

The Black-Oil model is the industry standard mathematical model most often used in petroleum reservoir simulation. It assumes that the fluid components are immiscible and includes compressibility and the general mass transfer effects between the phases that are needed to model primary (pressure depletion) and secondary (water injection) recovery. The particular form of the model we are using in our reservoir computations was developed by Trangenstein and Bell [46] and is one of a number of formulations of the 'Black-Oil' type which are distinct from another class of model termed the compositional model. A compositional model [47] quite similar to the Black-Oil model [46] has also been developed by Trangenstein and Bell.

The main difference between the two approaches are that Black-Oil models consider general fluid components, i.e. collections of individual chemical species (hydrocarbons) which are then termed either oil or gas, whereas the compositional models consider individual hydrocarbon species such as ethane and butane etc. Therefore a more accurate description of hydrocarbon phase behaviour is provided, but the resulting phase equilibrium problem is very complex. Compositional models are used when the modelling capabilities of Black-Oil models are inadequate, for example in the simulation of miscible gas injection. However the

extra computational expense of the iterative techniques needed to solve phase equilibrium along with the larger systems of conservation laws, because of the consideration of individual species, limits their applicability.

Reservoir fluid flow equations exhibit both hyperbolic and parabolic behaviour, for instance fronts separating different fluid states move at a finite speed of propagation whereas pressure effects are quickly felt throughout the reservoir. Both of these types of behaviour can be treated by a fully implicit discretisation. However, to effectively treat both types of behaviour present in the flow equations, different types of numerical procedure are required for each and so a splitting of the flow equations into a system of hyperbolic conservation laws and a parabolic pressure equation is used. In addition, implicit discretisations of the unsplit equations typically use large amounts of numerical diffusion, providing further reason for use of the sequential (or split) strategy.

In our computations with the Black-Oil model we follow Trangenstein and Bell and use the Higher Order Godunov method to discretise the hyperbolic part of the flow equations. This numerical scheme is able to address the problems associated with eigenvector deficiency and local linear degeneracy which are present in the Black-Oil model. The pressure equation is discretised using a Backward-Euler (implicit) approach.

Sequential methods were first proposed by Sheldon et al. [39] and Stone and Garder [43] around thirty years ago. These early and some subsequent formulations contained certain anomalies, for instance the hyperbolic and parabolic parts were not properly separated. Further developments were made, and in 1986 Bell, Shubin and Trangenstein [5] presented a new sequential method to model two-phase, two-component fluid flow. This formulation is based on conservation of mass of the fluid components and does not have the consequences of a 'volume error discrepancy' which is present in their later work. The volume error discrepancy indicates the extent to which the volume balance equation is not satisfied and is described in Section 3.4. This later work by Trangenstein and Bell [46] models three-phase, three-component fluid flow, and is the formulation we are working with. It should be noted that the form of the Black-Oil model used in this thesis is not currently used in reservoir simulation codes, due to its recent

development. For a description of the formulations that are used, see Aziz and Settari [1].

The fluid flow equations are derived from four main principles which are used to derive most isothermal porous media flow models. These are:

i) Phase equilibrium - determines how the components combine to form phases,

ii) The equation of state - requires that the fluid fills the pore volume,

iii) Darcy's law for the volumetric flow rates,

iv) Mass conservation equations for each component.

The flow equations are formulated sequentially, therefore they cannot be satisfied exactly at each step of the computation, and so some incompatibility is introduced. Phase equilibrium, Darcy's law and the component conservation laws are satisfied exactly but the equation of state is linearised so that it is only satisfied approximately. This splitting of the flow equation is termed a 'volume-discrepancy splitting'.

In the next four sections of this chapter we describe the formulation, and the equations that result, of the four main principles used to derive the mathematical model. Then we summarise the sequential formulation in broad terms and mention the consequences of the splitting of the flow equations and the resulting volume error discrepancy. In the last section we describe the parameters of the model we used for our reservoir computations.

3.2 Thermodynamic Equilibrium

3.2.1 Components and Phases

The fluid in the reservoir is considered to be composed of three components, oil, gas, and water. These are the separations the fluid chooses at surface temperatures and pressures. However to reach phase equilibrium at reservoir conditions these components combine to form at most three phases, liquid, vapour and aqua. At each point in the reservoir the components associate into these phases in order to attain thermodynamic equilibrium. The components flow in phases but

are conserved by mass, thus it is necessary to determine how the mass of each component is apportioned into the phases. This phase equilibrium problem can be expressed as follows: given the pressure p and the vector $\mathbf{n} = [n_o, n_g, n_w]^T$ of mass component densities, find the matrix

$$N = \begin{bmatrix} n_{ol} & n_{ov} & 0 \\ n_{gl} & n_{gv} & n_{ga} \\ 0 & 0 & n_{wa} \end{bmatrix}$$

of component densities in each of the phases, subject to the mass balance condition

$$\mathbf{n} = N\mathbf{e},$$

where $\mathbf{e}$ is a vector of one's of the appropriate length. Thus it can be seen from the definition of N that there is a restriction on the way the components are allowed to mix in the phases, i.e. oil may be allowed in the liquid and vapour phases, gas in all three phases and water in the aqueous phase only. Oil and water do not mix and steam is not treated due to the isothermal nature of the model. At this point there is not enough information to solve the phase equilibrium problem, this extra information is provided in the next two sections.

3.2.2 Mass Transfer and Phase Equilibrium

A principal component is associated with each phase, oil with the liquid phase, gas with the vapour phase and water with the aqueous phase. The amount of each component in each phase is related to the amount of the principal component in that phase by the ratio matrix R. When all three phases are formed R is given by

$$R = \begin{bmatrix} 1 & R_v & 0 \\ R_l & 1 & R_a \\ 0 & 0 & 1 \end{bmatrix} = ND_N^{-1},$$

where D_N is the diagonal part of N. For example the solution gas ratio defined by

$$R_l = n_{gl}/n_{ol},$$

represents the ratio of the amount of gas dissolved in the liquid phase to the amount of oil in the liquid phase. The ratios R_l, R_v, and R_a must be dimensionless non-negative functions of pressure and are supplied as part of the model. In fact the standard Black-Oil model takes both R_v and R_a to be identically zero and thus deals with less general mass transfer effects than considered here. The ratios R_l and R_a are required to be monotonically increasing functions so that as pressure increases more mass is transferred between the phases. The same requirement is not placed on the ratio R_v.

Now we can determine how many phases are present. Firstly the matrix $T = R^{-1}$ is defined, then the vector $T\mathbf{n}$ is formed which represents the amount of the principal component in each phase. If all three entries of $T\mathbf{n}$ are positive then all three phases are formed and the fluid is termed saturated. Hence it can be shown that D_N is given by

$$D_N \mathbf{e} = T\mathbf{n},$$

and the solution to phase equilibrium by

$$N = RD_N.$$

Normally the dimensions of $\mathbf{n}$ and N would be mass per pore volume. However the Black-Oil model is formulated such that the mass of a component is measured in terms of the volume it occupies at surface conditions compared with reservoir conditions, hence the units of $\mathbf{n}$ and N are in standard cubic feet per reservoir cubic foot.

In the next section we examine the effect of mass transfer on the number of fluid phases formed.

3.2.3 Undersaturation

Although three components may be present this does not necessarily mean that three phases are always formed. For example, if gas is allowed to dissolve in liquid ($R_l \neq 0$), then for sufficiently high pressures it is possible for all the gas to dissolve in the liquid phase. Therefore the vapour phase is missing and the liquid phase is said to be undersaturated. Similarly if $R_v \neq 0$, i.e. oil is allowed

to volatilise into vapour, then it is possible that no liquid is formed and the vapour phase is undersaturated. In the present work neither R_l, R_v or R_a are identically equal to zero therefore both types of undersaturation are possible. Analysis of undersaturated flow, see [46], shows that at most one phase can be missing due to undersaturation. Therefore both types of undersaturated flow occurring simultaneously would be impossible. The possibility also exists of a phase being missing due to the principal component associated with that phase being missing. If this is the case the fluid will still be termed saturated as the phase will not be missing due to mass transfer effects. For example if no oil is present then the liquid phase will not be formed.

When the vapour phase is missing the physical meaning of the negative vapour component of $T\mathbf{n}$ is that the fluid pressure is higher than the bubble-point pressure p_b ($p > p_b$) at which the vapour phase forms. The bubble point pressure is implicitly defined by the requirement that the vapour component of $T\mathbf{n}$ is zero, i.e.

$$-R_l(p_b)n_o + n_g - R_a(p_b)n_w = 0.$$

The fact that R_l and R_a are monotone functions of pressure ensure that p_b is unique. When the liquid phase is missing the volatile oil ratio R_v is redefined to make the liquid component of $T\mathbf{n}$ zero, i.e.

$$\overline{R}_v = \frac{n_o}{n_g - R_a(p)n_w}.$$

A dew point pressure could have been defined here, to parallel the previous case of undersaturation, but as R_v is non-monotone this would not necessarily have been unique. Here we have that $\overline{R}_v < R_v(p)$, i.e. not enough oil was present to volatilise into the vapour phase to the extent indicated by $R_v(p)$.

It is possible to derive a combined formulation of undersaturated phase behaviour so that the mathematical structure parallels that of saturated flow. This is achieved by multiplying the relevant flow variables by a constant matrix Q which effectively removes the column corresponding to the missing phase, i.e.

$$\overline{R} = RQ \quad , \quad \overline{D}_N = Q^T D_N Q.$$

A constant vector $\mathbf{q}$ is also defined which will be used later. For example in the

case of the vapour phase being undersaturated, Q and $\mathbf{q}$ are given by

$$Q = \begin{bmatrix} 0 & 0 \\ 1 & 0 \\ 0 & 1 \end{bmatrix} \quad , \quad \mathbf{q} = \begin{bmatrix} 1 \\ 0 \\ 0 \end{bmatrix},$$

and if the liquid phase is undersaturated

$$Q = \begin{bmatrix} 1 & 0 \\ 0 & 0 \\ 0 & 1 \end{bmatrix} \quad , \quad \mathbf{q} = \begin{bmatrix} 0 \\ 1 \\ 0 \end{bmatrix}.$$

Throughout this chapter, quantities denoted with an overbar refer to the reduced matrix or vector in the undersaturated case.

The solution to phase equilibrium is then given by

$$N = \overline{R}\,\overline{D}_N Q^T.$$

In the case of the liquid phase being undersaturated the matrix N is given by

$$N = \begin{bmatrix} n_o & 0 & 0 \\ \overline{R}_l n_o & 0 & \overline{R}_a n_w \\ 0 & 0 & n_w \end{bmatrix},$$

i.e. all the oil is contained in the liquid phase and the gas present is dissolved in both the liquid and aqueous phases. When the vapour phase is undersaturated the matrix N is given by

$$N = \begin{bmatrix} 0 & n_o & 0 \\ 0 & n_g - R_a n_w & R_a n_w \\ 0 & 0 & n_w \end{bmatrix}.$$

Here all the oil has volatilised into the vapour phase and the gas in the vapour phase is equal to the total amount of gas less the gas dissolved in the aqueous phase. In both cases of undersaturation, as well as saturated flow, all of the water must be in the aqueous phase.

In the case of undersaturated flow an undersaturation parameter ω is used to develop the flow equations and becomes one of the dependent variables. In the case of an undersaturated liquid ω becomes the bubble point pressure and in the case of undersaturated vapour ω is the volatile oil ratio.

3.2.4 Compressibility

In this section we examine the compressibility of the reservoir fluids and describe their effect on the phase volumes.

Fluid compressibility is defined by

$$c_f = -\frac{1}{V}\frac{\partial V}{\partial p} = -\frac{1}{\rho}\frac{\partial \rho}{\partial p},$$

where V is the volume of the fluid and ρ is its density. The negative sign is needed since compressibilities are defined as positive numbers. The compressibilities of oil and water are considered constant, typical values would be, for oil $c_o \sim 2.0 \times 10^{-5}\text{psi}^{-1}$ and for water $c_w \sim 3.0 \times 10^{-6}\text{psi}^{-1}$. Gas compressibility is usually considered a function of pressure, and for this work ranges from $c_g \sim 9.0 \times 10^{-4}\text{psi}^{-1}$ at 1000 psi to $c_g \sim 3.0 \times 10^{-4}\text{psi}^{-1}$ at 3000 psi. Here psi refers to the unit of pressure in pounds per square inch.

The small compressibilities of oil and water, along with the relatively high compressibility of gas, and the swelling effects caused by gas dissolving in liquid lead to important volume changes at reservoir pressures. The Black-Oil model incorporates these volume changes by relating the volumes of each of the phases to the amount of the principal component in that phase. To quantify this relationship D_u is defined to be the diagonal matrix of phase volumes per pore volume. The entries of D_N and D_u are related by the phase formation volume factors B_l, B_v and B_a. The matrix of formation volume factors is given by

$$B = \begin{bmatrix} B_l & 0 & 0 \\ 0 & B_v & 0 \\ 0 & 0 & B_a \end{bmatrix} = D_u D_N^{-1},$$

and are functions of pressure and the undersaturation variable ω in the case of undersaturated flow. The formation volume factors would normally have the dimensions of a specific volume but because of the units of **n** they relate the volume of the fluid at reservoir conditions to the volume occupied at standard conditions (pressure and temperature), and therefore compressibility is introduced through matrix B.

The functions B_l, B_v and B_a are quite complicated to describe because of mass transfer and undersaturation effects. For example the liquid phase in the case of

no mass transfer is assumed to have a small compressibility in that as pressure increases the liquid phase volume decreases. If we then allow mass transfer so that gas, which is more compressible than oil, is allowed to dissolve in the oil, then for pressures below the bubble point, increases in pressure cause more gas to dissolve and the phase volume then increases, and to a greater extent than with no mass transfer. Above the bubble point pressure the liquid phase is assumed slightly compressible. These effects can be described by,

$$B_l(p, p_b) = \begin{cases} 1 - c_o\, p & \text{if } R_l = 0 \\ 1 + c_l\, p & \text{if } p < p_b \\ \frac{1 - c_l\, p_b}{1 + c_o\,(p - p_b)} & \text{if } p \geq p_b \end{cases} .$$

Here c_o is the compressibility of the pure oil component and c_l is the compressibility of the liquid phase, i.e. oil containing dissolved gas. Analogous formulas hold for the aqueous phase with c_o replaced by the compressibility of pure water c_w and c_l replaced by the compressibility of water containing dissolved gas c_a. The vapour phase formation volume factor B_v is somewhat harder to describe, so we refrain from describing it here.

We are now in a position to calculate the vector $\mathbf{u}$ of phase volumes per pore volume which is given by

$$\mathbf{u} = BT\mathbf{n}.$$

When the fluid is undersaturated the constant matrix Q is again used to define

$$\overline{B} = Q^T B Q,$$

and then $\mathbf{u}$ is given by

$$\overline{\mathbf{u}} = Q\overline{BT}\mathbf{n}.$$

The vector $\mathbf{u}$ is used in specifying the equation of state as will be seen later.

We also wish to include rock compressibility, which means that the porosity (the ratio of the rock pore volume to the total volume) is an increasing function of pressure,

$$\phi = \phi_0(1 + c_R(p - p_0)),$$

i.e. as the fluid pressure increases the rock pore volume increases. Here ϕ_0 is the porosity at the reference pressure p_0 and c_R is the rock compressibility, which is considered constant and is approximately that of water.

3.3 Darcy's Law

Darcy's law specifies how the phases flow through the reservoir and gives the vector of flow volumes per unit area per unit time, i.e. the phase velocities. For 1-Dimensional flow the law can be written in matrix-vector form as

$$\mathbf{v} = -L(\mathbf{e}\frac{\partial p}{\partial x} - \boldsymbol{\rho} g \frac{\partial d}{\partial x})\kappa, \tag{3.3.1}$$

and hence Darcy's law states that the fluid flow is due to a pressure gradient and a gravitational potential. L is the diagonal matrix of phase mobilities which are phase relative permeabilities divided by phase viscosities

$$L = \mathrm{Diag}(\frac{k_l}{\mu_l}, \frac{k_v}{\mu_v}, \frac{k_a}{\mu_a}),$$

κ is the total rock permeability, $\boldsymbol{\rho}$ is the vector of phase densities and $\frac{\partial d}{\partial x}$ is the depth gradient of the reservoir. Capillary pressure is not considered here so that the pressure in each phase is identical and equal to the fluid pressure p.

The total velocity is defined as the sum of phase velocities and obtained from (3.3.1),

$$v_T = \mathbf{e}^T\mathbf{v} = -\mathbf{e}^T L\mathbf{e}\frac{\partial p}{\partial x}\kappa + \mathbf{e}^T L\boldsymbol{\rho} g\frac{\partial d}{\partial x}\kappa. \tag{3.3.2}$$

Equation (3.3.2) can be used to solve for the pressure gradient and then substitution in (3.3.1) gives

$$\mathbf{v} = \frac{L\mathbf{e}v_T}{\mathbf{e}^T L\mathbf{e}} + [I - \frac{L\mathbf{e}\mathbf{e}^T}{\mathbf{e}^T L\mathbf{e}}]L\boldsymbol{\rho} g\frac{\partial d}{\partial x}\kappa. \tag{3.3.3}$$

This is the form of the Darcy velocities used in the model and is termed a total velocity splitting. The motivation for this step is that for incompressible flow a total velocity splitting correctly decouples the elliptic and hyperbolic character present in the flow equations.

Some of the terms in Darcy's law are now described in more detail.

3.3.1 Saturations

Saturations are the fractions of the total fluid volume occupied by each of the phases and are defined by

$$\mathbf{s} = \frac{\mathbf{u}}{\mathbf{e}^T\mathbf{u}}.$$

With this definition, the saturations sum to one even if the volume balance equation is not satisfied. It should be noted that $\mathbf{s}$ must be considered distinct from $\mathbf{u}$ because of the volume error discrepancy associated with this formulation of the flow equations. However in the case of no volume error discrepancy when $\mathbf{e}^T\mathbf{u} = 1$ the vectors $\mathbf{s}$ and $\mathbf{u}$ are identical.

3.3.2 Relative Permeability

Relative permeability describes how the presence of each phase adversely affects the flow of the other phases and are non-negative functions of the saturations $\mathbf{s}$. Due to the complex interaction of the phases with the rock pore space the dependence of the relative permeabilities on the rock and fluid properties is not fully understood. However it is known that as the saturation of a phase approaches zero, its mobility must tend to zero implying its relative permeability must vanish. In reality a phase will become immobile before its saturation reaches zero, the saturation at which this occurs being termed a 'residual saturation'. In our Black-Oil computations we use fairly simple experimentally determined relative permeability functions, see Stone [42].

3.3.3 Viscosity

The phase viscosity μ is the property of a phase that represents it's resistance to flow under the influence of the forces causing the flow. In the saturated flow case the phase viscosities are positive functions of pressure. When the vapour phase is missing the liquid and aqueous phase viscosities are functions of pressure and bubble point pressure p_b.

3.3.4 Phase Density

The vector of phase densities $\boldsymbol{\rho}$ is needed in order to determine the effects of gravity on the flow, and is defined by

$$\boldsymbol{\rho} = B^{-1}R^T\boldsymbol{\rho}_{stp}.$$

Where $\boldsymbol{\rho}_{stp}$ is the vector of densities of the components (oil, gas and water) at standard temperature and pressure (surface conditions).

3.4 Equation of State

When satisfied exactly, the equation of state (or volume balance equation) states that the fluid fills the rock pore volume, i.e.

$$\mathbf{e}^T\mathbf{u} = 1, \tag{3.4.4}$$

where as usual $\mathbf{e}$ is the vector of one's. The extent to which this equation is not satisfied, i.e. the sum of the phase volumes is not equal to the pore volume, is termed the volume error discrepancy and is given by

$$\mathbf{e}^T\mathbf{u} - 1.$$

In the sequential formulation it is not possible to satisfy all of the fluid flow constraints simultaneously and so equation (3.4.4) is linearised to form an equation for pressure. Performing a Taylor's series linearisation about time level t gives

$$\mathbf{e}^T\mathbf{u}\Big|_{t+\Delta t} \approx \mathbf{e}^T\mathbf{u}\Big|_t + \Delta t\mathbf{e}^T\frac{\partial\mathbf{u}}{\partial t}\Big|_t. \tag{3.4.5}$$

It is assumed that we have a volume error discrepancy at time level t, i.e. $\mathbf{e}^T\mathbf{u}\Big|_t \neq 1$, and we wish to calculate pressure at the advanced time $t+\Delta t$ such that there is no volume error, i.e. $\mathbf{e}^T\mathbf{u}\Big|_{t+\Delta t} = 1$. Applying these assumptions and since $\mathbf{u}$ is a function of $\mathbf{n}$ and p, equation (3.4.5) becomes

$$\frac{1-\mathbf{e}^T\mathbf{u}}{\Delta t} \approx \mathbf{e}^T\frac{\partial\mathbf{u}}{\partial p}\frac{\partial p}{\partial t} + \mathbf{e}^T\frac{\partial\mathbf{u}}{\partial\mathbf{n}}\frac{\partial\mathbf{n}}{\partial t}.$$

Multiplication by the porosity ϕ and use of the mass conservation laws to replace the time derivative of $\mathbf{n}$ results in the following equation for pressure

$$\frac{(\mathbf{e}^T\mathbf{u}-1)\phi}{\Delta t} \approx (\phi\mathbf{e}^T\frac{\partial\mathbf{u}}{\partial p} + \mathbf{e}^T\frac{\partial\mathbf{u}}{\partial\mathbf{n}}\mathbf{n}\frac{\partial\phi}{\partial p})\frac{\partial p}{\partial t} - \mathbf{e}^T\frac{\partial\mathbf{u}}{\partial\mathbf{n}}\frac{\partial}{\partial x}(ND_u^{-1}v).$$

First degree homogeneity properties of the phases are now used to simplify the term multiplying $\frac{\partial p}{\partial t}$. Firstly the matrix of partial phase volumes is computed, which in the saturated case is

$$\frac{\partial\mathbf{u}}{\partial\mathbf{n}} = BT.$$

Post multiplying this by N gives

$$\frac{\partial\mathbf{u}}{\partial\mathbf{n}}N = BTN = BR^{-1}RD_N = D_u.$$

This implies that

$$\frac{\partial \mathbf{u}}{\partial \mathbf{n}}\mathbf{n} = \mathbf{u},$$

which says that each phase volume $\mathbf{u}$ is a homogeneous function of the first degree in the fluid composition $\mathbf{n}$. An identical result also holds in the undersaturated case.

The pressure equation can now be written in the general form

$$c\frac{\partial p}{\partial t} + \mathbf{w}^T \frac{\partial}{\partial x}(\mathbf{f}v_T + \mathbf{g}\tau) = q, \tag{3.4.6}$$

with the total velocity v_T being given by

$$v_T = [-\frac{\partial p}{\partial x} + \gamma]\tau, \tag{3.4.7}$$

where the coefficients c, $\mathbf{w}$, $\mathbf{f}$, $\mathbf{g}$, γ, q and τ depend on the pressure p and component density $\mathbf{n}$. For completeness we define them here

$$c = \phi \mathbf{e}^T \frac{\partial \mathbf{u}}{\partial p} - \mathbf{e}^T \mathbf{u} \frac{\partial \phi}{\partial p},$$

$$\tau = \mathbf{e}^T L \mathbf{e} \kappa \quad , \quad \gamma = \frac{\mathbf{e}^T L \boldsymbol{\rho}}{\mathbf{e}^T L \mathbf{e}} g \frac{\partial d}{\partial x}$$

$$\mathbf{f} = N D_u^{-1} L \mathbf{e} \frac{1}{\mathbf{e}^T L \mathbf{e}}$$

$$\mathbf{g} = N D_u^{-1} L \boldsymbol{\rho} g \frac{\partial d}{\partial x} \frac{1}{\mathbf{e}^T L \mathbf{e}} - \mathbf{f}\gamma$$

$$\mathbf{w}^T = \mathbf{e}^T \frac{\partial \mathbf{u}}{\partial \mathbf{n}} \quad , \quad q = \frac{(\mathbf{e}^T \mathbf{u} - 1)\phi}{\Delta t}.$$

For a more detailed discussion on the pressure equation, including its numerical solution, see Section 3 of [49].

3.4.1 Analysis of the Pressure Equation

To examine the character of (3.4.6) we need to examine the coefficient c of $\frac{\partial p}{\partial t}$ and the coefficient of $\frac{\partial^2 p}{\partial x^2}$ which is obtained after substitution of (3.4.7) into (3.4.6) and is given by

$$-\mathbf{w}^T \mathbf{f} \tau = -\mathbf{e}^T L \mathbf{e} \kappa,$$

since $\mathbf{w}$ and $\mathbf{f}$ satisfy $\mathbf{w}^T \mathbf{f} = 1$. It is known that pressure effects within the reservoir are of parabolic nature for compressible fluid flow, so we need to ensure

that the differential equation (3.4.6) is of parabolic type. The transmissibility τ is positive, hence the coefficient of $\frac{\partial^2 p}{\partial x^2}$ is negative, and therefore for (3.4.6) to be parabolic c is required to be negative. Now, as pressure increases the rock occupies a smaller volume hence porosity ϕ is a non-decreasing function of pressure, $\frac{\partial \phi}{\partial p} \geq 0$. Therefore for c to be negative the inequality $\mathbf{e}^T \frac{\partial \mathbf{u}}{\partial p} < 0$ is required which is the condition of negative total fluid compressibility. This is guaranteed by placing restrictions on the formation volume factors B and ratios R, namely

$$\mathbf{e}^T \frac{\partial}{\partial p} \left(BR^{-1} \right) RB^{-1} < 0,$$

with a more complicated condition in the undersaturated case, see [46].

3.5 Conservation of Mass

The mass of each fluid component is required to be conserved. The matrix ND_u^{-1} represents the density of each fluid component in each phase, hence the conservation of mass equations are

$$\frac{\partial}{\partial t}(\mathbf{n}\phi) + \frac{\partial}{\partial x}(ND_u^{-1}\mathbf{v}) = 0. \tag{3.5.8}$$

The flux function $\mathbf{h} = ND_u^{-1}\mathbf{v}$ can also be expressed as $\mathbf{h} = RB^{-1}\mathbf{v}$, which is the form that will be used in the characteristic analysis. Here the vector of Darcy phase velocities is written in terms of the total velocity v_T, i.e. in the form (3.3.3). The flux is therefore a function of $\mathbf{n}$, p and v_T, hence in quasi-linear form we have

$$\phi \frac{\partial \mathbf{n}}{\partial t} + \frac{\partial \mathbf{h}}{\partial \mathbf{n}} \frac{\partial \mathbf{n}}{\partial x} = -\mathbf{n} \frac{\partial \phi}{\partial p} \frac{\partial p}{\partial t} - \frac{\partial \mathbf{h}}{\partial p} \frac{\partial p}{\partial x} - \frac{\partial \mathbf{h}}{\partial v_T} \frac{\partial v_T}{\partial x} - \frac{\partial \mathbf{h}}{\partial \delta} \frac{\partial \delta}{\partial x}, \tag{3.5.9}$$

where δ is a gravitational term, namely

$$\delta = g \frac{\partial d}{\partial x} \kappa.$$

The term $\frac{\partial \delta}{\partial x}$ is only nonzero if the porous medium is heterogeneous, i.e. we have spatial variation in κ, and if the depth gradient $\frac{\partial d}{\partial x}$ is constant. The system is hyperbolic if and only if the Jacobian matrix

$$H = \frac{\partial \mathbf{h}}{\partial \mathbf{n}}$$

has real eigenvalues for all values of $\mathbf{n}$. We also need to compute the eigenvalues and right eigenvectors of H to provide information about the structure of the wave fields, which will be needed by the numerical method that we use to solve the conservation laws. Both p and v_T are considered to be independent of $\mathbf{n}$ for the purpose of the characteristic analysis since the volume balance equation (3.4.4) is not enforced in the sequential formulation. To calculate the hyperbolic wavespeeds we must divide the eigenvalues by the porosity ϕ since it multiplies the time derivative of $\mathbf{n}$ in the quasi-linear form of the conservation laws.

3.5.1 Characteristic Analysis

For saturated flow a similarity transformation and eigenvector deflation is used to derive the matrix of eigenvectors X, of H. The component derivative of the flux vector $\mathbf{h}$ is given by

$$\frac{\partial \mathbf{h}}{\partial \mathbf{n}} = RB^{-1}\frac{\partial \mathbf{v}}{\partial \mathbf{n}},$$

since only $\mathbf{v}$ is a function of $\mathbf{n}$. Expansion of $\frac{\partial \mathbf{v}}{\partial \mathbf{n}}$ using the chain rule and further manipulation yields

$$H\mathbf{e}^T\mathbf{u} = RB^{-1}\frac{\partial \mathbf{v}}{\partial \mathbf{s}}[I - \mathbf{s}\mathbf{e}^T]BR^{-1}.$$

Therefore it can be seen that $H\mathbf{e}^T\mathbf{u}$ is similar to the matrix

$$V = \frac{\partial \mathbf{v}}{\partial \mathbf{s}}[I - \mathbf{s}\mathbf{e}^T],$$

which is the same matrix that appears in the characteristic analysis of the 3 phase incompressible Buckley-Leverett model [49]. Therefore the similarity transformation defined by

$$H\mathbf{e}^T\mathbf{u} = M_1 V M_1^{-1}, \quad \text{where} \quad M_1 = RB^{-1},$$

can be considered to map from component densities to saturations. The matrix V can now used to deduce one of the eigenvalues of the system because of the relation

$$\mathbf{e}^T V = 0,$$

which arises because the total fluid velocity is independent of $\mathbf{s}$. Thus $\mathbf{e}$ is a left eigenvector of V with eigenvalue zero. This eigenvector is then used to deflate V

as follows:

$$M_2 V M_2^{-1} = \begin{bmatrix} 0 & 0 \\ \mathbf{c} & C \end{bmatrix},$$

where

$$M_2 = \begin{bmatrix} 1 & \mathbf{e}^T \\ 0 & I \end{bmatrix},$$

C is a 2×2 matrix given by

$$C = [\ 0 \quad I\ ] \frac{\partial \mathbf{v}}{\partial \mathbf{s}} \begin{bmatrix} -\mathbf{e}^T \\ I \end{bmatrix},$$

and $\mathbf{c}$ is a 2 vector defined by

$$\mathbf{c} = -C[\ 0 \quad I\ ]\,\mathbf{s}.$$

We therefore now have a block-eigenproblem to solve with the remaining 2 eigenvalues of $H\mathbf{e}^T\mathbf{u}$ being eigenvalues of matrix C, i.e.

$$\begin{bmatrix} 0 & 0 \\ \mathbf{c} & C \end{bmatrix} \begin{bmatrix} 1 & 0 \\ \mathbf{z} & X_c \end{bmatrix} = \begin{bmatrix} 1 & 0 \\ \mathbf{z} & X_c \end{bmatrix} \begin{bmatrix} 0 & 0 \\ 0 & \Lambda_c \end{bmatrix}.$$

This block-eigenproblem yields four equations which are $0 = 0$ twice, $CX_c = X_c\Lambda_c$ and the relation $\mathbf{c} + C\mathbf{z} = 0$ which we need to solve for vector $\mathbf{z}$. If we put $\mathbf{z} = -\mathbf{a}X_c$ then this last relation can be re-expressed, so that we need to solve for $\mathbf{a}$ where

$$X_c\Lambda_c\mathbf{a} = \mathbf{c}. \tag{3.5.10}$$

It is assumed that a real, non-singular matrix X_c and a real diagonal matrix Λ_c can be found so that

$$CX_c = X_c\Lambda_c.$$

The right eigenvectors of H are then given by the columns of

$$X = RB^{-1} \begin{bmatrix} 1 & -\mathbf{e}^T \\ 0 & I \end{bmatrix} \begin{bmatrix} 1 & 0 \\ 0 & X_c \end{bmatrix} \begin{bmatrix} 1 & 0 \\ -\mathbf{a} & I \end{bmatrix},$$

and the corresponding full matrix of eigenvalues is then

$$\Lambda = \begin{bmatrix} 0 & 0 \\ 0 & (\frac{1}{\mathbf{e}^T\mathbf{u}})\Lambda_c \end{bmatrix}.$$

To summarise we have $HX = X\Lambda$ where X and Λ are given above.

When one of the fluid components and hence phases is missing in saturated flow, the corresponding row and column of the Jacobian matrix $\frac{\partial \mathbf{h}}{\partial \mathbf{n}}$, and hence the matrix $\frac{\partial \mathbf{v}}{\partial \mathbf{s}}$, are both zero. This means that the similarity transformation defined by the matrix M_1 cannot be used because $(RB^{-1})(BR^{-1}) \neq I$, hence the analysis must be reformulated. The remedy is straightforward because we can work with the Jacobian matrix H directly, since it has a zero row, instead of deflating matrix V. We still have the zero eigenvalue, and can proceed with the block-eigenproblem as before.

The two non-trivial eigenvalues obtained from matrix C, i.e. the entries of Λ_c, are the same as the eigenvalues from the 3 phase Buckley-Leverett problem. This shows that the hyperbolicity of the system is inherited from the relative permeability model and not the compressibility and mass transfer effects which complicate the Black-Oil model.

In the case of undersaturated flow a similarity transformation of H is also used to find the eigenvectors and eigenvalues, with the eigenvectors given by

$$X = \begin{bmatrix} \overline{R}\,\overline{B}^{-1} & \mathbf{q} \end{bmatrix} \begin{bmatrix} X_{\overline{v}} & 0 \\ 0 & 1 \end{bmatrix} \begin{bmatrix} I & -\mathbf{a} \\ 0 & 1 \end{bmatrix}.$$

The analysis proceeds as before, again reducing to a block-eigenproblem. Here $\mathbf{q}$ is a constant vector dependent on which phase is missing, and the vector $\mathbf{a}$ solves

$$X_{\overline{v}}\,((\frac{1}{\mathbf{e}^T\mathbf{u}})\Lambda_{\overline{v}}\mathbf{a} - \mathbf{a}\lambda) = \overline{B}\,\overline{T}H\mathbf{q}.$$

This auxiliary equation, which we need to solve for $\mathbf{a}$, corresponds to (3.5.10) in the saturated flow analysis. $X_{\overline{v}}$ and $\Lambda_{\overline{v}}$ are given by

$$X_{\overline{v}} = \begin{bmatrix} \mathbf{s}_* & -1 \\ \mathbf{s}_a & 1 \end{bmatrix} \quad , \quad \Lambda_{\overline{v}} = \begin{bmatrix} 0 & 0 \\ 0 & \frac{\partial v_a}{\partial s_a} - \frac{\partial v_a}{\partial s_*} \end{bmatrix},$$

where s_* is the saturation of the other existing phase. The full matrix of eigenvalues is then given by

$$\Lambda = \begin{bmatrix} (\frac{1}{\mathbf{e}^T\mathbf{u}})\Lambda_{\overline{v}} & 0 \\ 0 & \lambda \end{bmatrix},$$

the eigenvalue λ corresponding to a weighted sum of particle velocities and is given in the liquid undersaturated and the vapour undersaturated cases respectively by

$$\frac{R_l n_o \frac{v_l}{u_l} + R_a n_w \frac{v_a}{u_a}}{R_l n_o + R_a n_w} \quad \text{and} \quad \frac{v_v}{u_v}.$$

In fact the two non-zero eigenvalues obtained from the undersaturated characteristic analysis are similar to the eigenvalues obtained from the Polymer Flood Model [49]. Further details of this characteristic analysis can be found in [46]. For more general details on similarity transformations and eigenvector deflation see Golub and Van Loan [21].

3.5.2 Remarks on the Characteristic Structure

The characteristic analysis above has shown that for both saturated and undersaturated flow an eigenvalue exists which is identically zero and hence is linearly degenerate. This linear advection mode carries no information and has an effect on the type of results expected in that we now only expect two wave families in the results rather than three as would be expected from a system of three hyperbolic conservation laws.

The remaining two eigenvalues in saturated flow and the second eigenvalue in undersaturated flow are termed Buckley-Leverett modes because of their similarity to the eigenvalues of the 3-Phase Buckley-Leverett model [49]. These Buckley-Leverett modes have the possibility of local linear degeneracies somewhere in the saturation range and thus we would expect to see shock-rarefaction compound waves in the results. The third eigenvalue in undersaturated flow is the weighted sum of particle velocities and is linearly degenerate, hence giving only contact discontinuities.

As long as the flow remains saturated throughout the reservoir or wholly undersaturated then the eigenstructure will be continuous provided that the functions describing the model are continuously differentiable. If the flow should exhibit a phase change, i.e. a saturated/undersaturated fluid boundary arises then the eigenstructure will no longer remain continuous. This is because of the different functional forms for the formation volume factors and ratios for saturated and undersaturated flow.

3.6 Sequential Formulation

The idea behind the splitting of the equations into a pressure equation and a system of conservation laws is that, over some time interval, we first solve for pressure with the composition fixed and compute a total velocity. We then solve for the new composition with pressure and total velocity fixed, i.e. with the latest values of p and v_T. Thus the sequential method is based on alternately freezing some of the coefficients over the time step Δt. Given the sequential formulation described, it is therefore accepted that mass is conserved at the expense of developing a volume error discrepancy.

Ideally time step control should be based on the overall temporal activity of the flow variables together with some kind of criteria to control the errors due to the splitting of the flow equations. However, there is no such mathematical theory to guide time step selection for such splittings of flow equations. Instead time step control is based solely on Courant-Friedrichs-Lewy (CFL) [13] considerations for the component conservation laws. It is argued in [5] that such a time step is suitable for correctly capturing the transient behaviour in the parabolic pressure equation. We will discuss time step control in more detail later on.

The most evident consequence of the sequential formulation and the resulting volume error discrepancy is that the pressure field is only approximate. Hence the total fluid velocity and corresponding phase velocities are only approximate. Another notable consequence is that the wavespeeds and characteristic directions of the hyperbolic equations are not derived with the effect of the coupling of the pressure and component density, i.e through the term $\frac{\partial p}{\partial \mathbf{n}}$. Hence they are not the true characteristic quantities of the hyperbolic part. For the characteristic analysis p is considered independent of $\mathbf{n}$, hence $\frac{\partial p}{\partial \mathbf{n}} = 0$, in reality this is not the case due to the coupling of p and $\mathbf{n}$ through the volume balance equation (3.4.4). Therefore we have to accept that the use of the split methodology gives only an approximation to the true flow behaviour of the unsplit equations.

Now we have a system of hyperbolic mass conservation laws and a parabolic pressure equation, a computational strategy must be decided upon, i.e. whether to use explicit or implicit numerical methods. Parabolic equations have quite

a severe restriction on their time step due to stability considerations, i.e. Δt should be of the order $(\Delta x)^2$. For this reason the reservoir simulation community have used implicit discretisations of the pressure equation so that this restrictive stability condition does not apply, as most implicit methods are unconditionally stable. This motivation for use of an implicit method does not carry over to the solution of the conservation laws. This is because the stability condition for hyperbolic conservation laws is less restrictive, i.e. Δt should be of the order Δx. Also implicit discretisations of conservation laws typically are more diffusive than explicit methods. For these reasons an explicit method has usually been used to discretise the hyperbolic conservation laws arising in the sequential formulation of the Black-Oil model. However there are cases when an implicit method is desirable, for instance, when the fronts in the problem travel at much slower speeds than the fluid.

3.7 2-Component 2-Phase Black-Oil Model

A 2-component 2-phase Black-Oil model exists [5] which was developed by Bell Shubin and Trangenstein and is the forerunner of the more general 3-phase Black-Oil model described in this chapter. This model considers the fluid components of oil and gas and has a solution gas ratio R_l only so that the only mass transfer effect modelled is gas dissolving in oil. The less general mass transfer effects and the one fewer fluid components leads to a volume balance equation (3.4.4) that is much simpler than that of the 3-phase Black-Oil model. In fact the volume balance equation amounts to a quadratic in pressure and hence can be solved exactly. For this reason the pressure obtained from the parabolic pressure equation is only used to compute a total velocity, pressure is calculated by solving the volume balance equation given the component density vector. Volume error discrepancies do not enter the problem because of the simple nature of the volume balance equation and its ability to be solved directly for pressure. This mass conserving and zero volume error discrepancy formulation of the split equations is thought by Trangenstein and Bell to be the better of the two types in terms of analytic considerations. Addition of an extra component (water) and general

mass transfer (inclusion of R_v and R_a) to this model considerably complicates the formulation. For instance the volume balance equation can now not be solved exactly for pressure, it would have to be iteratively solved. Also the characteristic analysis would be further complicated by the effect of $\frac{\partial p}{\partial \mathbf{n}}$ but a more accurate representation of the characteristic structure is provided compared to the formulation with the inherent volume error discrepancy. Later on we compare some numerical results of the formulation of the flow equations with zero volume error discrepancy from [5] with the corresponding volume error discrepancy formulation to asses the impact of the volume error discrepancy.

3.8 Extension To Multidimensions

Extension of the model to multi-dimensions is fairly straightforward. In terms of notation, all that is needed is to replace derivatives with respect to x with gradients and to replace the vector of phase velocities v with an array of phase velocities in each coordinate direction.

In 2-D the pressure equation becomes

$$c\frac{\partial p}{\partial t} + \mathbf{w}^T \frac{\partial}{\partial x}(\mathbf{f} v_T^x + \mathbf{g}^x \tau^x) + \mathbf{w}^T \frac{\partial}{\partial y}(\mathbf{f} v_T^y + \mathbf{g}^y \tau^y) = q.$$

The superscripts x and y refer to the directionality of the quantities. The same analysis can be used to show the equation has parabolic character, since the arguments involve thermodynamic principles which are independent of the number of coordinate directions. The conservation laws become

$$\frac{\partial}{\partial t}(\mathbf{n}\phi) + \frac{\partial}{\partial x}(N D_u^{-1} \mathbf{v}^x) + \frac{\partial}{\partial y}(N D_u^{-1} \mathbf{v}^y) = 0,$$

which are hyperbolic if and only if the partial derivatives of the flux with respect to the conserved quantity, $\mathbf{n}$, in any particular direction, has only real eigenvalues for all $\mathbf{n}$.

3.9 Black-Oil Model Parameters

In this section we provide the functional forms which specify the Black-Oil model parameters which we use in our Black-Oil computations. Actually these are the

same model parameters as given in [46], so we could try to reproduce the results therein.

The units in use in the reservoir simulations throughout this thesis are as follows. The spatial coordinates x, y and z are measured in feet and time is measured in days. Fluid pressure p is measured in pounds per square inch (psi) and viscosity is measured in centipoise (cp). As a result the units of the total rock permeability κ, appearing in Darcy's law, must have the units of ft^2 cp/psi days. This results in the need to multiply the rock permeability in milliDarcy's (mD) by a factor of 0.006328 to ensure consistency of units.

The relative permeability functions are given by,

$$k_l = s_l(1 - s_v)(1 - s_a),$$

$$k_v = s_v^2,$$

$$k_a = s_a^2.$$

The vapour and aqueous relative permeability functions are the standard square saturation functions, the liquid relative permeability is the result of using the same model in conjunction with Stone's model [42].

The rock porosity is given by

$$\phi = 0.2(1 + 1 \times 10^{-5} p),$$

and hence the rock has a compressibility of $(c_R) = 1.0 \times 10^{-5}\text{psi}^{-1}$. The ratio functions describing mass transfer effects are given by

$$R_l(p) = 0.05p,$$

$$R_v(p) = 9 \times 10^{-5} - 6 \times 10^{-8} p + 1.6 \times 10^{-11} p^2,$$

$$R_a(p) = 0.005p,$$

and the viscosity functions are given by

$$\mu_l = \begin{cases} 0.8 - 1 \times 10^{-4} p & \text{if liquid is saturated} \\ (0.8 - 1 \times 10^{-4} p_b)(1 + 6.78 \times 10^{-5}(p - p_b)) & \text{if liquid is undersaturated} \end{cases}$$

$$\mu_v = 0.012 + 3 \times 10^{-5} p$$

$$\mu_a = \begin{cases} 0.35 & \text{if aqua is saturated} \\ 0.35(1 + 6.78 \times 10^{-5}(p - p_b)) & \text{if aqua is undersaturated.} \end{cases}$$

We recall the component density vector $\mathbf{n}$ has the units of standard cubic feet per reservoir cubic foot. This results in the formation volume factors having the units of reservoir cubic feet per standard cubic foot, and these functions are given by

$$B_l(p, p_b) = \begin{cases} 1 - 2.31 \times 10^{-5}\ p & \text{if } R_l(p) = 0 \\ 1 + 1.5 \times 10^{-4}\ p & \text{if liquid is saturated } (p < p_b) \\ \frac{1+1.5\times10^{-4}\ p_b}{1+2.31\times10^{-5}\ (p-p_b)} & \text{if liquid is undersaturated } (p \geq p_b) \end{cases}$$

$$B_v(p, \overline{R}_v) = \begin{cases} \frac{1}{(6+0.06p)} & \text{if vapour is saturated} \\ \frac{1}{(7+0.06p)} + \frac{\overline{R}_v}{R_v}[\frac{1}{(6+0.06p)} - \frac{1}{(7+0.06p)}] & \text{if vapour is undersaturated} \end{cases}$$

$$B_a(p, p_b) = \begin{cases} 1 - 6.78 \times 10^{-5}\ p & \text{if } R_a(p) = 0 \\ 1 - 3.0 \times 10^{-6}\ p & \text{if aqua is saturated } (p < p_b) \\ \frac{1-3.0\times10^{-6}\ p_b}{1+6.78\times10^{-5}\ (p-p_b)} & \text{if aqua is undersaturated } (p \geq p_b). \end{cases}$$

The definitions of B_l and B_a when R_l and R_a are zero respectively are provided, even though we have $R_l, R_a \neq 0$, because R_l and R_a may be forced to zero when the relevant fluid component is missing.

From the definition of the aqueous formation volume factor B_a above, it can be seen that the compressibility of water (c_w) is $6.78 \times 10^{-5}\text{psi}^{-1}$. The value of c_w that is given by Trangenstein and Bell in [46] is $1.8 \times 10^{-5}\text{psi}^{-1}$. The reason for this discrepancy is thought to be a misprint in [46], Trangenstein having indicated a revised value for c_w in a private communication.

Care must be taken with relation to the units of the parameters needed to specify gravitational effects due to the units used in the other Black-Oil parameters. For instance the gravitational acceleration g used in Darcy's law (3.3.1) must be removed because it is incorporated through the factor of 0.006328 multiplying the rock permeability. Also a factor of 1/144 must be included in the gravitational term to ensure consistency of units. The vector of phase densities

used in the computations, unless otherwise stated, were

$$\boldsymbol{\rho} = \begin{bmatrix} 52.787 \\ 0.05154 \\ 62.3967 \end{bmatrix},$$

with the units of lb ft^{-3}, and are only needed when gravitational effects are included.

Chapter 4

The Higher Order Godunov Scheme

4.1 Introduction

The Black-Oil model described in the previous chapter exhibits both lack of strict hyperbolicity and points of local linear degeneracy. Therefore to effectively treat such a system of conservation laws requires a numerical method that can handle these properties, by making appropriate modifications to the basic scheme where necessary. It is expected that such a scheme would make use of the characteristic information associated with the conservation laws. Porous media flow is also characterised by solutions developing sharp fronts which need to be accurately captured with minimal diffusion, we therefore require a higher (second) order oscillation free (TVD) method. The Higher Order Godunov method is therefore particularly suited to porous media flow because it includes modifications for systems with loss of strict hyperbolicity and local linear degeneracies in the wavefields whilst also being a second order accurate TVD method. Hence we use this method to solve the system of conservation laws arising in the Black-Oil model, paying particular attention to the work by Collela [10] and Bell, Collela and Trangenstein [2].

There has been considerable effort over the last 20 years to develop Godunov type methods for computing discontinuous solutions to systems of hyperbolic conservation laws. These methods, first introduced by Godunov [20], are thought to

be as close as any, of the currently available numerical techniques, to analytic solutions of the conservation laws because they incorporate the nonlinear wave propagation properties of the equations through the solution of Riemann problems. The main aim of this effort has been to develop viable numerical algorithms for areas of application such as compressible fluid flow, plasma physics, and combustion. As a result a set of design criteria has emerged for the construction of high resolution methods for hyperbolic conservation laws, which are summarised by Bell et al. in [2]. A review of some of these developments can be found in Harten et al. [25].

Much of the development of Godunov type schemes has assumed two properties of the hyperbolic system. Firstly that the system should be strictly hyperbolic with the Jacobian matrix possessing a complete set of smooth right eigenvectors and secondly that the system should satisfy the Lax conditions, namely that each mode of wave propagation should either be genuinely non-linear or linearly degenerate, [28]. However the extension of numerical algorithms to such systems that are not strictly hyperbolic or violate the Lax conditions by having local linear degeneracies in the wavefields, has also been undertaken, even though the analytic information on which the formulation depends is unclear for such systems.

A Higher Order Godunov method for strictly hyperbolic systems that obey the Lax conditions has been presented by Collela [10] including extensions to multidimensions. Bell, Collela and Trangenstein [2] have presented the necessary modifications to Collela's original scheme in order that degenerate systems of hyperbolic conservation laws may be considered. Here and throughout this thesis when we refer to degenerate systems of conservation laws, we mean systems with specifically local linear degeneracies and a lack of strict hyperbolicity. However in most of the literature, such systems are referred to as general systems which would seem too wide ranging. The extension to degenerate systems is achieved by adding extra dissipation (diffusion) at such points in order to stabilise the scheme and ensure satisfaction of the appropriate entropy conditions. The Godunov methodology would seem a natural choice for degenerate systems since the same characteristic information used to construct the scheme can be used to detect loss of strict hyperbolicity and local linear degeneracies.

We now review the Higher Order Godunov method [2, 10] for degenerate systems of 1-dimensional conservation laws. In multi-dimensions a central concern is the choice of the unsplit versus split methodology, this will be discussed later in the chapter. The extension of the 1-D scheme to higher dimensions as given by Collela [10], is also described.

4.2 Details of the Scheme

We firstly consider the problem and describe the notation we will use throughout the rest of the chapter. We want to numerically solve the systems of hyperbolic conservation laws

$$\frac{\partial \mathbf{U}}{\partial t} + \frac{\partial \mathbf{F}}{\partial x} = 0,$$

where $\mathbf{U} = \mathbf{U}(x,t)$, with initial data

$$\mathbf{U}(x,0) = \mathbf{U}_0(x),$$

such that the problem is well posed. Here $\mathbf{U}$ is a vector of length K and $\mathbf{F}$ is a vector valued function of $\mathbf{U}$. The system of conservation laws in quasi-linear form is

$$\frac{\partial \mathbf{U}}{\partial t} + \frac{\partial \mathbf{F}}{\partial \mathbf{U}}\frac{\partial \mathbf{U}}{\partial x} = 0,$$

where the matrix $\frac{\partial \mathbf{F}}{\partial \mathbf{U}}$ is the Jacobian matrix which we will call H. (We denote the Jacobian matrix by H rather than the more usual A so as to be consistent with the Jacobian matrix present in the Black-Oil equations, described in the previous chapter.) We perform a characteristic decomposition of H as follows

$$H = R\Lambda R^{-1},$$

where R is the matrix of right eigenvectors of H and Λ is the matrix of eigenvalues. The right eigenvectors (columns of R) are denoted by r_k.

The Higher Order Godunov scheme proceeds by computing a monotonised central difference approximation to the slope in the conserved variables, in order to suppress oscillations at discontinuities and hence ensure the method is TVD. A left and right state is then calculated at each cell interface using characteristic information and the monotonised slope. The idea is used that if these left and

right states, that are used to compute a numerical flux, are second order approximations at the half time level and the cell edge then the overall scheme will be second order accurate. Of course this is only in regions of smooth flow, the monotonisation process lowers the order of accuracy at discontinuities. The numerical flux at the cell edge is computed by solving a local Riemann problem there. Even in problems for which the Riemann problems are well understood analytically, it is usually more computationally efficient to introduce approximations, for example see Roe [33]. In any case there is not much point in solving the Riemann problem to a greater accuracy than that of the underlying discretisation. This idea is central to the approximate Riemann problem solution given in [2], which proceeds by computing a generalisation of the Engquist-Osher numerical flux for systems.

The Higher Order Godunov scheme, in the 1-dimensional case, can be considered as a 5-step procedure:

1. Beginning with the piecewise constant approximation $\mathbf{U}_j^n$, compute 'centred', 'left' and 'right' slopes, whilst maintaining conservation.
2. 'Limit' the slopes using monotonicity criteria, again whilst maintaining conservation. This provides a piecewise linear discontinuous approximation to the solution at time t.
3. Trace along characteristics, using a Taylor series extrapolation, to derive left and right states at grid cell interfaces at time $t + \frac{1}{2}\Delta t$. It is possible that the traced states are unphysical, if this is the case the physical cell centred value is used instead.
4. Solve the Riemann problem with these left and right states.
5. Use a conservative difference approximation to (3.5.8) to produce a piecewise constant approximation to $\mathbf{U}_j^{n+1}$.

We now describe these main steps of the method in more detail including the necessary modifications for the treatment of points of non-strict hyperbolicity and local linear degeneracies.

4.2.1 Monotonised Slope Computation

We begin with a piecewise constant approximation $\mathbf{U}_j^n$ to the solution in each grid block at the current time level, for example see Figure 4.1. Using this piecewise

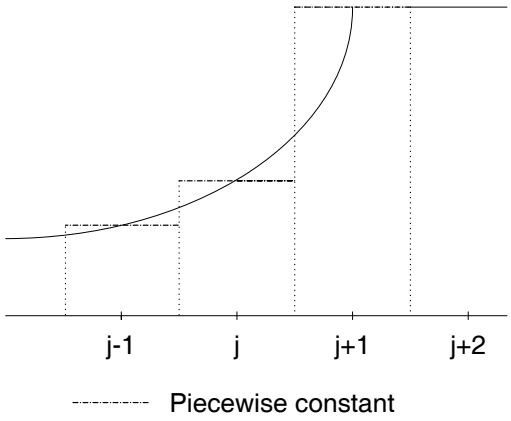

Figure 4.1: An example piecewise constant representation of the solution.

constant approximation in the algorithm would only enable the construction of a first order method. More information about the structure of the solution is needed for a second order method. For this reason we need to calculate an approximation to the slope $\frac{\partial \mathbf{U}}{\partial x}$ so that we may express the data as a piecewise linear profile, which is monotonised to prevent the creation of any new extrema. The monotonised representation will hence be discontinuous piecewise linear, see Figure 4.2, and will ultimately prevent the formation of oscillations near discontinuities in the solution at the advanced time level. Use of an unlimited linear representation

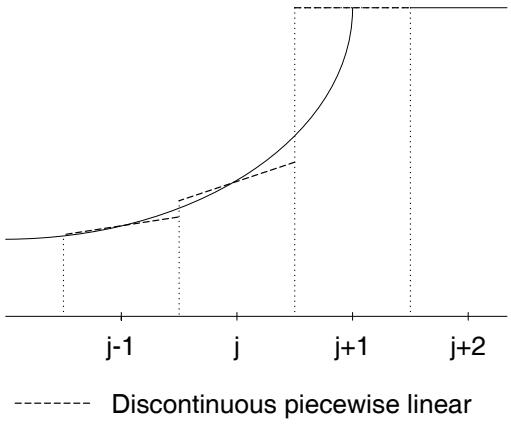

Figure 4.2: An example discontinuous piecewise linear representation of the solution.

would result in oscillations occurring near discontinuities, much akin to those

which occur with the Lax-Wendroff method [29]. We note that this approximation maintains conservation of the conserved variable $\mathbf{U}$ as it preserves cell averages.

A monotonised centred-difference approximation is defined by,

$$\left.\frac{\partial \mathbf{U}}{\partial x}\right|_{x=x_j} \approx \frac{\Delta \mathbf{U}_j}{\Delta x}, \tag{4.2.1}$$

where in order to calculate $\Delta \mathbf{U}_j$ we compute undivided centered, right and left differences in $\mathbf{U}$ and expand these differences in the right eigenvectors $\mathbf{r}_k$ of the system Jacobian matrix $\frac{\partial \mathbf{F}}{\partial \mathbf{U}}$, i.e.

$$\begin{aligned} \frac{1}{2}(\mathbf{U}_{j+1} - \mathbf{U}_{j-1}) &= \sum_{k=1}^{K} \alpha_k^c \mathbf{r}_k, \\ \mathbf{U}_{j+1} - \mathbf{U}_j &= \sum_{k=1}^{K} \alpha_k^r \mathbf{r}_k, \\ \mathbf{U}_j - \mathbf{U}_{j-1} &= \sum_{k=1}^{K} \alpha_k^l \mathbf{r}_k, \end{aligned} \tag{4.2.2}$$

the $\alpha_k^{c,r,l}$ being expansion coefficients. This is an analogous procedure to the scalar case since pre-multiplication of the cell differences by R^{-1} approximately decouples the system. Hence we have three $K \times K$ linear systems to solve for the $\alpha_k^{c,r,l}$, where K is the length of the system.

The monotonised slope is then defined by

$$\Delta \mathbf{U} = \sum_{k=1}^{K} \alpha_k \mathbf{r}_k \tag{4.2.3}$$

where the expansion coefficients from (4.2.2) are 'limited' to give

$$\alpha_k = \begin{cases} \min(|\alpha_k^c|, \gamma|\alpha_k^l|, \gamma|\alpha_k^r|)\ \ \mathrm{sign}(\alpha_k^c) & \text{if } \alpha_k^r \alpha_k^l > 0 \\ 0 & \text{otherwise} \end{cases}, \tag{4.2.4}$$

and where γ is a constant parameter. In regions of smooth flow $\Delta \mathbf{U}$ will be given by central differences whereas near extreme points, $\Delta \mathbf{U}$ will be set to zero. This form of 'limiting' is described by Van Leer [51], and is usually carried out with $\gamma = 2$ which is adequate for systems that are strictly hyperbolic and genuinely nonlinear. The parameter $\gamma = 2$ is the maximum value possible such that the least amount of slope limiting occurs to ensure the resulting piecewise linear profile will not create any new extremum in the data. The smaller the value of

γ, the more numerical diffusion added into the scheme, with $\gamma = 0$ reducing the scheme to first order. There are three important criteria which the above slope limiting formula obeys, these are

1. If the cell average is a local extremum then the slope is set to zero,
2. If the sign of a slope is different to that of either of its neighbours then it is set to zero, i.e. the local trend in slope signs is maintained,
3. The linear profile should not take values beyond those of the neighbouring cell averages.

However, additional limiting is required when local linear degeneracies and eigenvector deficiencies are detected amongst the $\mathbf{r}_k$. A sufficient modification given by Trangenstein [49], when a local linear degeneracy is detected would be to set $\gamma = 1.5$ for that particular wavemode. Local linear degeneracies are associated with shock-rarefaction compound waves and are detected by testing for a change in sign of spatial differences of the wavespeeds, i.e.

$$(\lambda_{k,j+1} - \lambda_{k,j})(\lambda_{k,j} - \lambda_{k,j-1}) < 0.$$

If this test is satisfied at grid point j and for wavemode k then γ is reduced to 1.5 for that wavemode. The effect of reducing γ is to add extra diffusion at that point, this reduction of γ is the least reduction possible such that local instabilities are not introduced due to the prescence of the local linear degeneracy and such that second order accuracy is maintained. After all we do not want to reduce γ too much and excessively smear the discontinuity. We have also seen a value of $\gamma = 1.0$ quoted by Bell et al. [2] for use at such points of local linear degeneracy, $\gamma = 1.5$ is a revised value based on numerical experimentation, reported by Bell and Shubin [4], and in any case is preferential as it introduces less dissipation. Thus extra dissipation is added in the vicinity of the shock to ensure it satisfies the entropy condition.

Near an eigenvector deficiency the right eigenvectors used in (4.2.2) become nearly parallel, which results in unreliable expansion coefficients because the matrix of eigenvectors is nearly singular. In such cases it is assumed that the portion

of the jump

$$\frac{1}{2}(\mathbf{U}_{j+1} - \mathbf{U}_{j-1}),$$

corresponding to

$$\alpha_l^c \mathbf{r}_l + \alpha_m^c \mathbf{r}_m, \tag{4.2.5}$$

involves an eigenvector deficiency, i.e. $\mathbf{r}_l$ and $\mathbf{r}_m$ are nearly parallel. To detect for such an eigenvector deficiency the following test given in [2] may be used

$$|\lambda_l - \lambda_m| < 0.1 \sum_{k=1}^{K} \alpha_k^c |\kappa_{lk} - \kappa_{mk}|.$$

This test estimates whether it is possible for both of the wavespeeds to coincide in a neighbourhood of the state at which the eigenvectors $\mathbf{r}_k$ are evaluated. The κ are called structural coefficients and represent the gradient of the eigenvalue with respect to the conserved variables in the direction of a particular eigenvector, and are defined by

$$\kappa_{kl} = (\nabla_U \lambda_k) \cdot \mathbf{r}_l.$$

If this test is satisfied then the wavemodes l and m are assumed to involve an eigenvector deficiency. To ensure the slope limiting process does not introduce instabilities it is necessary to treat the entire jump corresponding to (4.2.5) as one wave because individual components of the jump are badly behaved. This means that we want to reduce α_l^c and α_m^c by the same amount and force the two components to travel at the same speed. If $\lambda_l \lambda_m < 0$ then both α_l^c and α_m^c are set to zero. If the wavespeeds are of the same sign an effective wavespeed is defined

$$\overline{\lambda}_l = \overline{\lambda}_m = \frac{1}{2}(\lambda_l + \lambda_m),$$

and each component limited by the same amount by using the parameters ω_l and ω_m defined by

$$\omega_l = \alpha_l / \alpha_l^c, \quad \omega_m = \alpha_m / \alpha_m^c.$$

The limited slopes are then redefined by setting

$$\alpha_l = \min(\omega_l, \omega_m) \ \ \alpha_l^c.$$

with a similar definition for α_m, and these modified coefficients are then used in (4.2.2).

4.2.2 Characteristic Tracing

We now focus on the calculation of the traced left and right states used to determine the numerical flux. The monotonised slopes defined by (4.2.3) are used to construct time-centred left and right states at the cell edges. Values in cell j are used to compute $\mathbf{U}_{j+\frac{1}{2}}^{n+\frac{1}{2},L}$ and $\mathbf{U}_{j-\frac{1}{2}}^{n+\frac{1}{2},R}$, the computation being based on a Taylor series expansion about the cell centre, with the quasi-linear form of the hyperbolic equations used to replace the temporal derivatives of $\mathbf{U}$. The left state to second order accuracy in both space and time is given by

$$\begin{aligned} \mathbf{U}_{j+\frac{1}{2}}^{n+\frac{1}{2},L} &= \mathbf{U}_j^n + \frac{\Delta x}{2}\mathbf{U}_{x,j} + \frac{\Delta t}{2}\mathbf{U}_{t,j} \\ &= \mathbf{U}_j^n + \frac{\Delta x}{2}\mathbf{U}_{x,j} - \frac{\Delta t}{2}\mathbf{F}_{x,j} \\ &= \mathbf{U}_j^n + (\frac{\Delta x}{2}I - \frac{\Delta t}{2}H_j)\,\mathbf{U}_{x,j}, \end{aligned} \tag{4.2.6}$$

where H is the Jacobian matrix $\frac{\partial \mathbf{F}}{\partial \mathbf{U}}$.

For linear problems (4.2.6) can be used to compute a left traced state by replacing $\mathbf{U}_x$ with the monotonised slope approximation (4.2.1). A right traced state is calculated with a similarly derived formula. For nonlinear problems however, (4.2.6) must be modified to disregard components of $\mathbf{U}_x$ corresponding to waves that do not propagate towards the correct cell edge, i.e. for nonlinear problems different characteristics may propagate towards both cell edges, but we only want to use information traveling to the left to calculate the left state and information traveling to the right to calculate the right state, due to the upwind nature of the scheme. This subtraction of unwanted information is accomplished by multiplication of the second order terms in (4.2.6) by the characteristic projection operators defined by

$$P^{\pm} = R\Lambda^{\pm}R^{-1},$$

where R is a matrix with columns $\mathbf{r}_k$ and $\Lambda^{\pm}$ is a diagonal matrix with

$$\Lambda_{kk}^{\pm} = \frac{1}{2}(1 \pm \mathrm{sign}(\lambda_k)),$$

where if we have $\lambda_k = 0$ then we take $\Lambda_{kk}^{\pm} = 1$. This procedure is redundant in the linear case but has been reported by Collela [10] to lead to a more robust algorithm for strongly nonlinear problems.

Formally the left and right states at cell edge $j+\frac{1}{2}$ are then given by

$$\mathbf{U}_{j+\frac{1}{2}}^{n+\frac{1}{2},L} = \mathbf{U}_j^n + \frac{1}{2}P_j^+ \left(I - \frac{\Delta t}{\Delta x}H_j\right)\Delta\mathbf{U}_j,$$

$$\mathbf{U}_{j+\frac{1}{2}}^{n+\frac{1}{2},R} = \mathbf{U}_{j+1}^n - \frac{1}{2}P_{j+1}^- \left(I + \frac{\Delta t}{\Delta x}H_{j+1}\right)\Delta\mathbf{U}_{j+1}.$$

(We note The first order Godunov scheme may be recovered by setting the $\Delta\mathbf{U}$'s to zero, i.e. just using the cell centred quantities.) Simplification of these expressions yields,

$$\mathbf{U}_{j+\frac{1}{2}}^{n+\frac{1}{2},L} = \mathbf{U}_j^n + \frac{1}{2}R_j \left(I - \frac{\Delta t}{\Delta x}\Lambda_j\right)\boldsymbol{\alpha}_j,$$

$$\mathbf{U}_{j+\frac{1}{2}}^{n+\frac{1}{2},R} = \mathbf{U}_{j+1}^n - \frac{1}{2}R_{j+1} \left(I + \frac{\Delta t}{\Delta x}\Lambda_{j+1}\right)\boldsymbol{\alpha}_{j+1},$$

where Λ is the matrix of eigenvalues of H and $\boldsymbol{\alpha}$ is the vector of expansion coefficients used in the monotonised slope computation. Use of these simplified expressions means that we do not have to calculate the Jacobian matrix H for saturated flow with the Black-Oil model. The effect of the projection operators $P^{\pm}$, which do not appear in these simplified expressions, is accomplished by setting to zero components of $\boldsymbol{\alpha}$ for which the corresponding wavespeeds are of the wrong sign.

If the quasi-linear form of the hyperbolic equations should contain source terms, as with the Black-Oil model then extra terms will appear in the traced states. These extra terms modify the traced states as below

$$\mathbf{U}_{j+\frac{1}{2}}^{n+\frac{1}{2},L} \rightarrow \mathbf{U}_{j+\frac{1}{2}}^{n+\frac{1}{2},L} + \frac{\Delta t}{2}\mathbf{S}_j,$$

$$\mathbf{U}_{j+\frac{1}{2}}^{n+\frac{1}{2},R} \rightarrow \mathbf{U}_{j+\frac{1}{2}}^{n+\frac{1}{2},R} + \frac{\Delta t}{2}\mathbf{S}_{j+1},$$

where $\mathbf{S}_j$ is the total source term vector associated with cell j.

Since the characteristic tracing step is derived using a Taylor's series expansion with removal of information for which the associated wavespeeds have the wrong sign, it is possible that the traced states could be unphysical. Therefore tests are included in the algorithm to take account of this. If a particular traced state is found to be unphysical then the second order tracing terms are set to zero, leaving the cell centred value and possibly any source term that were present in the quasi-linear form. If source terms were present we perform the test again and if this state is still unphysical we then use the physical cell centred value of $\mathbf{U}$.

4.2.3 Approximate Flux Computation

We now need to solve the Riemann problem at the cell interface with the left and right states derived from the characteristic tracing step. This is done approximately by using a generalisation of the Engquist-Osher numerical flux for systems (see Osher and Solomon [32] and Engquist-Osher [18] [19] for details). Firstly a path is constructed from $\mathbf{U}^L$ to $\mathbf{U}^R$ that approximates the phase space solution to the Riemann problem, then a numerical flux is computed. Both the phase space solution and the numerical flux formulae are constructed so as to be correct to second order in the jump $(\mathbf{U}^R - \mathbf{U}^L)$, which preserves second order accuracy of the method.

For a strictly hyperbolic system the solution of the Riemann problem consists of up to K distinct waves progressing from $\mathbf{U}^L$ to $\mathbf{U}^R$ separated by $K-1$ intermediate states. Thus the solution in phase $(\mathbf{U})$ space is a collection of state transitions

$$\mathbf{U}^L = \mathbf{U}_0 \rightarrow \mathbf{U}_1 \rightarrow \cdots \rightarrow \mathbf{U}_{K-1} \rightarrow \mathbf{U}_K = \mathbf{U}^R$$

where the transition from $\mathbf{U}_{K-1}$ to $\mathbf{U}_K$ occurs along some arc Γ_K of the Kth wave curve. For a more detailed description of the structure of the Riemann problem see Lax [28] and Liu [30].

In the limit of small amplitude jumps the following holds

$$\mathbf{U}_K - \mathbf{U}_{K-1} = \alpha_k \mathbf{r}_k + O(|\mathbf{U}^R - \mathbf{U}^L|^2),$$

i.e. the right eigenvectors approximate the wave curves in phase space to second order in the jump between the left and right states. Here, as is usual it is assumed the system has been ordered such that the wavespeeds are in nondecreasing order, i.e.

$$\lambda_1 < \lambda_2 < \cdots < \lambda_K.$$

This ordering is due to analytic considerations and is needed to ensure single valued solutions. Hence the path in state space between the left and right states can be expressed by

$$\mathbf{U}^R - \mathbf{U}^L = \sum_{k=1}^{K} \alpha_k \mathbf{r}_k + O(|\mathbf{U}^R - \mathbf{U}^L|^2).$$

In the general case of finite amplitude jumps, the phase space solution of the Riemann problem takes the form

$$\mathbf{U}^R - \mathbf{U}^L = \sum_{k=1}^{K} \alpha_k \mathbf{R}_k,$$

where $\mathbf{R}_k$ is a generalised eigenvector that represents the net change along Γ_k, and which is normalised to be of unit length.

The approximate phase space solution is therefore a decomposition of the jump from $\mathbf{U}^L$ to $\mathbf{U}^R$ into K jumps corresponding to each of the wave modes. To approximate this decomposition a simple phase space solution is used, as was recommended in [2] for problems involving flow in porous media. We calculate an expansion state as the average of the left and right states

$$\overline{\mathbf{U}} = \frac{1}{2}(\mathbf{U}^L + \mathbf{U}^R),$$

and then evaluate the generalised eigenvectors at this expansion state

$$\overline{\mathbf{R}}_k = \mathbf{r}_k(\overline{\mathbf{U}}),$$

so that $\overline{\mathbf{R}}_k$ becomes an approximation to $\mathbf{R}_k$. If we expand $\mathbf{U}^R - \mathbf{U}^L$ in terms of the $\overline{\mathbf{R}}_k$ we have,

$$\mathbf{U}^R - \mathbf{U}^L = \sum_{k=1}^{K} \overline{\alpha}_k \overline{\mathbf{R}}_k, \tag{4.2.7}$$

so that $\overline{\alpha}_k$ approximates α_k. It is also assumed that the $\overline{\mathbf{R}}_k$ are orientated so that the $\overline{\alpha}_k$ are positive. The approximate path in phase space, for example a 2-system is shown in Figure 4.3.

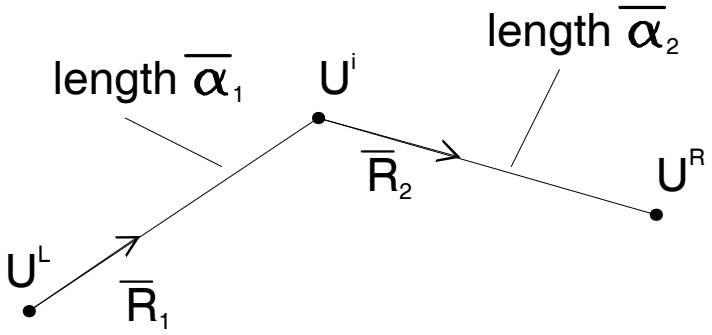

Figure 4.3: The path in phase space, taken by the Riemann problem solution, connecting the left and right states at the cell interface.

The intermediate state $\mathbf{U}^i$ shown in Figure 4.3 given by

$$\mathbf{U}^i = \mathbf{U}^L + \overline{\alpha}_1 \overline{\mathbf{R}}_1.$$

The numerical flux is then written as a flux at a reference state plus integral correction terms which were constructed to be of dissipative form. Firstly to determine this reference state a mean speed

$$\sigma = \frac{(\mathbf{F}(\mathbf{U}^L) - \mathbf{F}(\mathbf{U}^R)) \cdot (\mathbf{U}^L - \mathbf{U}^R)}{||\mathbf{U}^L - \mathbf{U}^R||^2}, \tag{4.2.8}$$

is calculated and the reference state is then defined by

$$\begin{aligned} \mathbf{U}^{ref} &= \mathbf{U}^L \quad \text{if } \sigma \geq 0 \\ &= \mathbf{U}^R \quad \text{otherwise.} \end{aligned}$$

If we assume the Jacobian matrix H has a Roe type decomposition [33] i.e. $\Delta\mathbf{F} = H\Delta\mathbf{U}$, where the Δ refers to the difference between the left and right states, then the mean speed may be re-expressed as,

$$\sigma = \frac{\Delta\mathbf{U}^T \, H \, \Delta\mathbf{U}}{||\Delta\mathbf{U}||^2}.$$

Therefore it can be seen that when H is positive definite i.e. $\Delta\mathbf{U}^T H \Delta\mathbf{U} \geq 0$, and will therefore possess non-negative eigenvalues then the reference state will be the left. This rewriting of the equation for σ enables the relation of the wavespeeds to the determination of the upwind reference state to be seen more clearly.

We now give the approximate Engquist-Osher flux formulae at both reference states

$$\mathbf{F}^{EO}(\mathbf{U}^L, \mathbf{U}^R) = \mathbf{F}(\mathbf{U}^L) + \sum_{k=1}^{K} \left(\int_0^{\overline{\alpha}_k} \min(\overline{\lambda}_k, 0) \, d\alpha \right) \overline{\mathbf{R}}_k, \tag{4.2.9}$$

$$\mathbf{F}^{EO}(\mathbf{U}^L, \mathbf{U}^R) = \mathbf{F}(\mathbf{U}^R) - \sum_{k=1}^{K} \left(\int_0^{\overline{\alpha}_k} \max(\overline{\lambda}_k, 0) \, d\alpha \right) \overline{\mathbf{R}}_k.$$

The $\overline{\lambda}_k$ is an approximation to the wavespeed along the line segments $\overline{\Gamma}_k$ (which approximate the Γ_k) from $\mathbf{U}_{k-1}$ to $\mathbf{U}_k$, i.e. along $\overline{\mathbf{R}}_k$. We now describe the wavespeed approximation process given in [2], which is illustrated in Figure 4.4. Firstly we calculate the wavespeeds and the structural coefficients at the two ends of the path $\overline{\Gamma}_k$ on which we are approximating the wavespeed λ_k. The structural coefficients in this case are defined by

$$\kappa_{kl} = (\nabla_U \lambda_k) \cdot \overline{\mathbf{R}}_l, \tag{4.2.10}$$

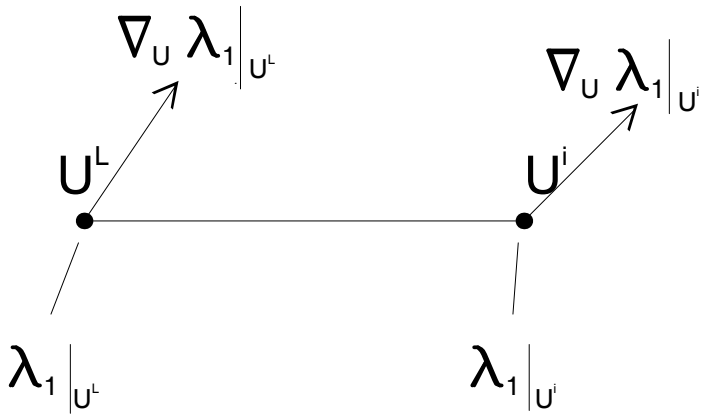

Figure 4.4: The parameters needed in the wavespeed approximation process on path $\overline{\Gamma}_1$

and provide the second derivative information that is needed to compute a cubic approximation of the wavespeed λ_k along $\overline{\Gamma}_k$. A cubic approximation is used so that inflexion points in the flux can be represented. An additional simplifying procedure can also be introduced by replacing the cubic by its piecewise linear approximation in order to avoid finding zeroes of a cubic in the algorithm. Hence we need to compute the extrema of the cubic and then the piecewise linear approximation $\overline{\lambda}_k$ is defined to be the piecewise linear interpolant of the wavespeed at the two ends of the path and the extremum states. We note that analytic expressions for the gradients of the wavespeeds in (4.2.10) may be difficult to obtain, as with the Black-Oil model. In this case an alternative approach may be used, described by Trangenstein [48], which amounts to sampling the wavespeeds at two interior points along the path $\overline{\Gamma}_k$ and then again forming a piecewise linear approximation.

We now turn to the possibility of encountering a point where strict hyperbolicity fails. In a neighbourhood of the eigenvector deficiency two of the eigenvectors become nearly parallel, which leads to large expansion coefficients in (4.2.7). The phase space approximation is not reasonable and its use with the flux computation (4.2.9) can introduce instabilities into the method. The test for eigenvector deficiency described in [2] uses the structural coefficients, for implementation with the Black-Oil model these are not available therefore the approximate tests described in [48] may be used. When we detect that two wavespeeds may coalesce,

say λ_l and λ_m, we only modify the treatment of the two wave families involved, the remaining families are treated as before. Hence we assume that $\overline{\mathbf{R}}_l$ and $\overline{\mathbf{R}}_m$ are nearly parallel and hence the associated expansion coefficients are unreliable. When more than two wavespeeds are involved the changes are a natural extension to the two-mode case.

The modifications needed depend on whether the eigenvector deficiency is associated with a change in sign of the wavespeed during the transition from $\mathbf{U}^L$ to $\mathbf{U}^R$. To test for this the following are defined

$$\lambda_{lm}^{min} = \min(\lambda_l^L, \lambda_l^R, \lambda_m^L, \lambda_m^R),$$

$$\lambda_{lm}^{max} = \max(\lambda_l^L, \lambda_l^R, \lambda_m^L, \lambda_m^R).$$

If λ_{lm}^{min} and λ_{lm}^{max} are of the same sign it is assumed the deficiency is not associated with a transonic wave. In this case the portion of the jump

$$\overline{\alpha}_l \overline{\mathbf{R}}_k + \overline{\alpha}_m \overline{\mathbf{R}}_m,$$

is collapsed into a single jump which is denoted by $\overline{\mathbf{R}}_{lm}$ and is of length $\overline{\alpha}_{lm}$. A modified flux is then defined, which in the case of the reference state being the left is

$$\mathbf{F}^{EO} = \mathbf{F}(\mathbf{U}^L) + \sum_{k \neq l,m} \left(\int_0^{\overline{\alpha}_k} \min(\overline{\lambda}_k, 0)\, d\alpha \right) \overline{\mathbf{R}}_k + \left(\int_0^{\overline{\alpha}_{lm}} \min(\overline{\lambda}_{lm}, 0)\, d\alpha \right) \overline{\mathbf{R}}_{lm},$$

where $\overline{\lambda}_{lm}$ is a linear function which satisfies

$$\overline{\lambda}_{lm}(0) = \max(\lambda_l^L, \lambda_m^L),$$

$$\overline{\lambda}_{lm}(\overline{\alpha}_{lm}) = \min(\lambda_l^R, \lambda_m^R).$$

When λ_{lm}^{min} and λ_{lm}^{max} are of opposite signs the integral correction terms are replaced by a dissipative term similar to that which is incorporated into Rusanov's scheme [37], the modified flux is then given by

$$\mathbf{F}^{EO} = \mathbf{F}(\mathbf{U}^L) + \sum_{k \neq l,m} \left(\int_0^{\overline{\alpha}_k} \min(\overline{\lambda}_k, 0)\, d\alpha \right) \overline{\mathbf{R}}_k - \frac{1}{2} \nu \overline{\alpha}_{lm} \overline{\mathbf{R}}_{lm},$$

where

$$\nu = \max(|\lambda_l^L|, |\lambda_m^L|, |\lambda_l^R|, |\lambda_m^R|).$$

The modified flux formulae for the cases when the reference state is the right state are easy to deduce by comparing with (4.2.9).

The Engquist-Osher flux is known to diminish the total variation of the solution to scalar conservation laws. However for the system case the approximate paths in state phase, between the left and right traced states, may not be a good representation of the true paths in state space. This is because at certain points the system may exhibit a lack of strict hyperbolicity and genuine nonlinearity. Therefore the calculated flux could possibly introduce some oscillation into the results. This is then damped out by addition of an artificial viscosity term which also ensures satisfaction of the entropy conditions and is described in the next subsection.

4.2.4 Entropy Satisfaction

We need to ensure the numerical solution converges to the correct physical solution satisfying appropriate entropy conditions. This is ensured by the addition of a small amount of numerical diffusion. The amount of which must be carefully selected otherwise fronts may become excessively smeared. Therefore in the case of the second order scheme the flux in (4.2.9) is modified by addition of a quadratic artificial viscosity term

$$\mathbf{F}^{n+\frac{1}{2}}_{j+\frac{1}{2}} = \mathbf{F}^{EO}(\mathbf{U}^{n+\frac{1}{2},L}_{j+\frac{1}{2}}, \mathbf{U}^{n+\frac{1}{2},R}_{j+\frac{1}{2}}) - \nu_{j+\frac{1}{2}}(\mathbf{U}^R - \mathbf{U}^L), \tag{4.2.11}$$

where

$$\nu_{j+\frac{1}{2}} = 0.1 \max_k(\lambda^R_k - \lambda^L_k, 0).$$

This form of viscosity is suggested in the introduction of [2] by Bell et al. but is not the form that is actually quoted later in the paper. However Collela et al. [12] describe this form of viscosity for use with their Godunov method. The viscosity term is only added when the eigenvalue at the right state is greater than the eigenvalue at the left state, i.e. a compressing wave is present. It can be seen the artificial viscosity is quadratic in the jump $(\mathbf{U}^R - \mathbf{U}^L)$ which maintains second order accuracy of the method.

The form of artificial viscosity term quoted by Bell et al. in [2] was also used

by Collela and Woodward [11] and is of the form

$$-0.1 \max_k(\lambda_{k,j+1} - \lambda_{k,j}, 0)(\mathbf{U}^n_{j+1} - \mathbf{U}^n_j).$$

This is of $O(\Delta x^2)$ and hence also maintains the accuracy of the method. Collela and Woodward [11], also used the parameter of 0.1. This parameter of 0.1 has been used successively with a number of Godunov type methods. Some schemes are reported in [11] to require more viscosity, and hence have a parameter greater than 0.1.

No artificial viscosity is added for the first order scheme as an ample amount of diffusion will already be present due to the discretisation. The numerical fluxes in (4.2.11) are then used in the conservative difference formula to update the cell averages.

$$\mathbf{U}^{n+1}_j = \mathbf{U}^n_j - \frac{\Delta t}{\Delta x}(\mathbf{F}^{n+\frac{1}{2}}_{j+\frac{1}{2}} - \mathbf{F}^{n+\frac{1}{2}}_{j-\frac{1}{2}}). \tag{4.2.12}$$

4.3 Extension to Higher Dimensions

4.3.1 Introduction

In multi-dimensions a central concern is the choice of the unsplit versus split methodology, which can have an effect on the overall computational efficiency of the scheme. An operator split algorithm would involve applying 1-dimensional operators in their particular coordinate direction separately, in order to advance the solution to the next time level. There being a rule by which the separate advancements of the solution in each coordinate direction are combined to achieve the correct order of accuracy. For a description of these rules and more details of operator splitting techniques see Strang [44]. Operator split schemes have been successful for multi-dimensional problems, in particular their robustness, resolution properties and computational efficiency, compared to the corresponding unsplit scheme, are usually cited. However situations exist for which their use is inappropriate, for example when conservation is required in the coupling of a front tracking algorithm to a conservative difference scheme. Another example is the advection by an incompressible velocity field, as occurs in some models of multiphase flow in porous media. It is therefore felt to be more appropriate

to consider an unsplit scheme, and again follow the work of Collela [10] when describing a multi-dimensional Higher Order Godunov method. We restrict ourselves here to the 2-Dimensional scheme since higher dimensional schemes follow on naturally from this description.

We note that an alternative form of an unsplit multidimensional Higher Order Godunov method has been developed by Bell, Dawson and Shubin [3]. In this formulation a limited piecewise bilinear approximation of the solution in each grid cell is used to ensure oscillation free results. The left and right states at the cell edges being traced using the geometry of the characteristic surfaces. However this method has only been applied to scalar conservation laws, the authors of [3] stating that extension to systems of conservation laws would be difficult; we do not consider this method any further.

4.3.2 Details of the Scheme

Firstly we state that we are considering the following 2-Dimensional systems of hyperbolic conservation laws

$$\frac{\partial \mathbf{U}}{\partial t} + \frac{\partial \mathbf{F}}{\partial x} + \frac{\partial \mathbf{G}}{\partial y} = 0,$$

where $\mathbf{U} = \mathbf{U}(x, y, t)$ and with initial data

$$\mathbf{U}(x, y, 0) = \mathbf{U}_0(x, y).$$

The numerical solution procedure largely proceeds as in the 1-Dimensional case. We calculate left and right traced states at each cell edge and hence solve the Riemann problems there. The jump between these two states is assumed to take place perpendicular to the cell edge, hence we solve 1-Dimensional Riemann problems at all the cell edges. The resulting fluxes, which are calculated in both coordinate directions at the same time, are then used in a conservative difference formula to update the cell averages.

We focus our attention on the calculation of the left and right traced states since that is the portion of the scheme that differs from the 1-D case. In particular these traced states will contain extra terms arising from the influence of the extra coordinate direction as we are about to see. We will only consider calculation of

the state

$$\mathbf{U}_{i+\frac{1}{2},j}^{n+\frac{1}{2},L},$$

since the other left states are calculated by interchanging the roles of i and j, x and y, and the right (R) states follows on naturally from our experience of the 1-D algorithm. We proceed as in the 1-D algorithm and use a Taylor's series extrapolation to the half time level and the cell edge in the x coordinate direction. We again use the quasi-linear form, with respect to the x direction, of the hyperbolic equations i.e. we use

$$\frac{\partial \mathbf{U}}{\partial t} + H^x \frac{\partial \mathbf{U}}{\partial x} + \frac{\partial \mathbf{G}}{\partial y} = 0,$$

to replace the temporal derivative of $\mathbf{U}$ in the formula for $\mathbf{U}_{i+\frac{1}{2},j}^{n+\frac{1}{2},L}$, where H^x is the x-directional Jacobian $\frac{\partial \mathbf{F}}{\partial \mathbf{U}}$. We therefore have

$$\mathbf{U}_{i+\frac{1}{2},j}^{n+\frac{1}{2},L} = \mathbf{U}_{i,j}^{n} + \frac{1}{2}(\Delta x I - \Delta t H_{i,j}^{x}) \frac{\partial \mathbf{U}}{\partial x} - \frac{\Delta t}{2} \frac{\partial \mathbf{G}}{\partial y},$$

which looks like the 1-D traced states with an extra term due to the extra coordinate direction, i.e. the fact that we are working in two dimensions. We again apply the characteristic projection operators to the second order tracing terms, they are neglected here to simplify the exposition.

The tracing of this left state can be viewed as a 2 step procedure by firstly calculating the traced states as in the 1-D case by replacing $\frac{\partial \mathbf{U}}{\partial x}$ with its monotonised central difference approximation, i.e.

$$\widehat{\mathbf{U}}_{i+\frac{1}{2},j}^{L} = \mathbf{U}_{i,j}^{n} + \frac{1}{2}(I - \frac{\Delta t}{\Delta x} H_{i,j}^{x}) \Delta \mathbf{U}_{i,j}^{x}.$$

Secondly we add on the effect of the transverse flux gradient $\frac{\partial \mathbf{G}}{\partial y}$, i.e.

$$\mathbf{U}_{i+\frac{1}{2},j}^{n+\frac{1}{2},L} = \widehat{\mathbf{U}}_{i+\frac{1}{2},j}^{L} - \frac{\Delta t}{2} \frac{\partial \mathbf{G}}{\partial y}. \tag{4.3.13}$$

To complete the calculation the term $\frac{\partial \mathbf{G}}{\partial y}$ is approximated by an upwind flux difference. The simplest choice would be to use Godunov's first order method to calculate $\frac{\partial \mathbf{G}}{\partial y}$. This is a sufficiently accurate approximation to give an algorithm that is second order accurate. Equation (4.3.13) is approximated by

$$\mathbf{U}_{i+\frac{1}{2},j}^{n+\frac{1}{2},L} = \widehat{\mathbf{U}}_{i+\frac{1}{2},j}^{L} - \frac{\Delta t}{2\Delta y} \left(\mathbf{G}^R(\mathbf{U}_{i,j+\frac{1}{2}}^{L}, \mathbf{U}_{i,j+\frac{1}{2}}^{R}) - \mathbf{G}^R(\mathbf{U}_{i,j-\frac{1}{2}}^{L}, \mathbf{U}_{i,j-\frac{1}{2}}^{R}) \right),$$

where

$$\mathbf{G}^R(\mathbf{U}^L, \mathbf{U}^R),$$

denotes the flux obtained from solving the Riemann problem with the indicated left and right states. So Godunov's first order method used to approximate $\frac{\partial \mathbf{G}}{\partial y}$ would take

$$\begin{aligned} \mathbf{U}^L_{i,j+\frac{1}{2}} &= \mathbf{U}^n_{i,j}, \\ \mathbf{U}^R_{i,j+\frac{1}{2}} &= \mathbf{U}^n_{i,j+1}, \end{aligned} \tag{4.3.14}$$

i.e. the cell centred quantities.

However for problems involving moderately strong discontinuities traveling obliquely to the grid directions, it is necessary to use a more accurate approximation to the transverse derivative. This is because if the approximation calculated is sufficiently different from the actual change calculated in the conservation (conservative update) step then the solution will overshoot or the discontinuity will spread. To address this possible problem more accurate left and right states (4.3.14) are needed in the flux calculations used to approximate the transverse flux derivative. This is accomplished by using the following left and right states

$$\begin{aligned} \mathbf{U}^L_{i,j+\frac{1}{2}} &= \widehat{\mathbf{U}}^L_{i,j+\frac{1}{2}}, \\ \mathbf{U}^R_{i,j+\frac{1}{2}} &= \widehat{\mathbf{U}}^R_{i,j+\frac{1}{2}}, \end{aligned} \tag{4.3.15}$$

i.e. the 1-Dimensional traced left and right states in the y direction. For completeness we also give the right traced state at cell edge $i+\frac{1}{2}, j$

$$\widehat{\mathbf{U}}^R_{i+\frac{1}{2},j} = \mathbf{U}^n_{i+1,j} - \frac{1}{2}(I + \frac{\Delta t}{\Delta x} H^x_{i+1,j}) \Delta \mathbf{U}^x_{i+1,j},$$

$$\mathbf{U}^{n+\frac{1}{2},R}_{i+\frac{1}{2},j} = \widehat{\mathbf{U}}^R_{i+\frac{1}{2},j} - \frac{\Delta t}{2\Delta y} \left(\mathbf{G}^R(\mathbf{U}^L_{i+1,j+\frac{1}{2}}, \mathbf{U}^R_{i+1,j+\frac{1}{2}}) - \mathbf{G}^R(\mathbf{U}^L_{i+1,j-\frac{1}{2}}, \mathbf{U}^R_{i+1,j-\frac{1}{2}}) \right).$$

The usual CFL stability condition is used to calculate a stable time step, i.e.

$$\Delta t \leq \min\left(\frac{\Delta x}{\max_{i,j}(\lambda^x_{i,j})}, \frac{\Delta y}{\max_{i,j}(\lambda^y_{i,j})}\right),$$

where λ^x denotes the eigenvalues of H^x (i.e. $\frac{\partial \mathbf{F}}{\partial \mathbf{U}}$) and the λ^y the eigenvalues of H^y ($\frac{\partial \mathbf{G}}{\partial \mathbf{U}}$).

The steps in the calculation of the 2-D left and right states can be summarised by the following:

1. Compute 1-D left and right traced states at each cell interface in each coordinate direction,
2. Add on the effect of the transverse flux derivatives to all the traced states,
3. Solve 1-D Riemann problems at every cell interface,
4. Use a conservative difference formula to update the cell averages,

$$\mathbf{U}_{i,j}^{n+1} = \mathbf{U}_{i,j}^{n} - \frac{\Delta t}{\Delta x}(\mathbf{F}_{i+\frac{1}{2},j}^{n+\frac{1}{2}} - \mathbf{F}_{i-\frac{1}{2},j}^{n+\frac{1}{2}}) - \frac{\Delta t}{\Delta y}(\mathbf{G}_{i,j+\frac{1}{2}}^{n+\frac{1}{2}} - \mathbf{G}_{i,j-\frac{1}{2}}^{n+\frac{1}{2}}).$$

In the next chapter we describe the implementation of the Higher Order Godunov scheme on the Black-Oil model, and show results of numerical reservoir simulations in 1 and 2 dimensions.

Chapter 5

Implementation of the Higher Order Godunov Method on the Black-Oil Flow Equations

5.1 Introduction

In this chapter we discuss the implementation of the Higher Order Godunov method on the Black-Oil fluid flow equations. We also describe the general computational details associated with the numerical modelling, such as time step control and the type of computational grid used, and also discuss the discretisation of the parabolic pressure equation. A 1-D and a dimensionally unsplit 2-D Fortran code were written to numerically solve the flow equations so we may perform reservoir simulations in 1 and 2 dimensions. The 1-D code was validated by comparison of results with those presented by Trangenstein and Bell in [46], who also applied the Higher Order Godunov method to the Black-Oil equations. We show results of three of these comparison problems.

Results of a 2-D cross-sectional problem, using the same numerical method and mathematical model, are shown by Bell et al. in [2] but the initial conditions are not supplied therein. No other 2-D Black-Oil results have appeared in the literature, so the 2-D code was validated by comparison of results with those from a commercial reservoir simulator. These comparisons relate more closely to the discussions in Chapter 7 and can be found there. However, in this chapter we

present results of a 2-D Areal problem which was used to investigate the effect on the numerical results of the accuracy of the transverse flux derivatives (4.3.15) and (4.3.14), described in Section 4.3.2.

It is not possible to construct analytic solutions to the Black-Oil fluid flow equations but analytic solutions to 3-phase incompressible flow equations are possible. Comparison of the analytic solutions of these problems with the corresponding numerical results has not appeared in the literature. Incompressible flow problems are a good test of a numerical method since analytic solutions exist for comparison with numerical results. Construction of analytic solutions in this case is straightforward since the mathematical model for incompressible flow reduces to a 2-system of conservation laws. The model also exhibits local linear degeneracies and eigenvector deficiencies, as does the Black-Oil model, and hence is a good test of the numerical method, although for the types of problem considered, namely those with no gravitational effects and therefore no counter-current flow, the Higher Order Godunov scheme used to simulate the problems is not fully tested. This is because the phase space construction of the Riemann problem described in Section 4.2.3, will not be needed because the flux computation reduces to upwind determination. Physical assumptions and experience of incompressible flow problems are used to aid the solution construction process. The Higher Order Godunov method was found to be successful at simulating these incompressible (Buckley-Leverett) flow problems and so confidence is provided that the numerical method is resolving the solutions to the analogous Black-Oil model problems well. Some numerical results of 3-phase incompressible flow problems were also presented by Bell et al. [6] but these were not compared against analytic solutions since they were used to investigate the prescence of elliptic degeneracies in the conservation laws.

Finally in this chapter we describe the incorporation of source terms to model injection of fluid into and production of fluid from the reservoir. Source terms are traditionally used in the computer codes used by the reservoir simulation community to model these processes. However as far as we know source terms have not previously been used in conjunction with the form of the Black-Oil model in [46] but have been used with the much simpler Polymer Flood Model

[49], neither of these models being used in commercial reservoir simulation codes. Locally implicit procedures are usually utilised when applying source terms to remove the numerical stability problem associated with their use. We follow this approach when applying source terms in conjunction with the Black-Oil model and Higher Order Godunov method.

5.2 Computational Approach

5.2.1 Computational Grids

The discretisations of the differential equations are based on a block (or cell) centred grid system. The block centred grid is particularly suitable for reservoir simulation problems because fluid and rock properties can be assigned, and assumed to hold throughout each computational cell. The 1-Dimensional grid is specified by giving the grid block interfaces which are denoted by

$$\cdots x_{j-\frac{1}{2}} < x_{j+\frac{1}{2}} < \cdots,$$

with an analogous definition of the grid in higher dimensions. The block centred grid can be distinguished from the more standard point (or node) centred grid in the following way. The block centred grid can be considered as the computational region having been distributed with cells, with the nodes residing in their centres, whereas the node centred grid having been distributed with nodes. Therefore the two ends of the block centred grid align with block edges, whereas in the case of the point centred grid the ends of the grid align with nodes and hence a half cell is present at the ends of the grid. Again in two dimensions all the boundaries of the grid, assuming it is regular, align with block edges. In 1-Dimension grid block B_j is bounded by $x_{j-\frac{1}{2}}$ and $x_{j+\frac{1}{2}}$ and is of length $\Delta x = x_{j+\frac{1}{2}} - x_{j-\frac{1}{2}}$.

For each grid block B_j we define a vector of component densities at time t which is denoted by $\mathbf{n}_j^n$, and provides a piecewise constant approximation to $\mathbf{n}$ at time t. A pressure p_j^n is associated with each $\mathbf{n}_j^n$ and at time $t = 0$, i.e. the initial conditions, p and $\mathbf{n}$ should be paired such that the volume balance equation (3.4.4) is satisfied. A staggered grid is used with pressure and component densities stored at grid block centres and with total velocities stored at grid block interfaces, see

Figure 5.1. This is due to the centred discretisation of Darcy's law (5.2.2) and is standard in reservoir simulation work, see Aziz and Settari [1].

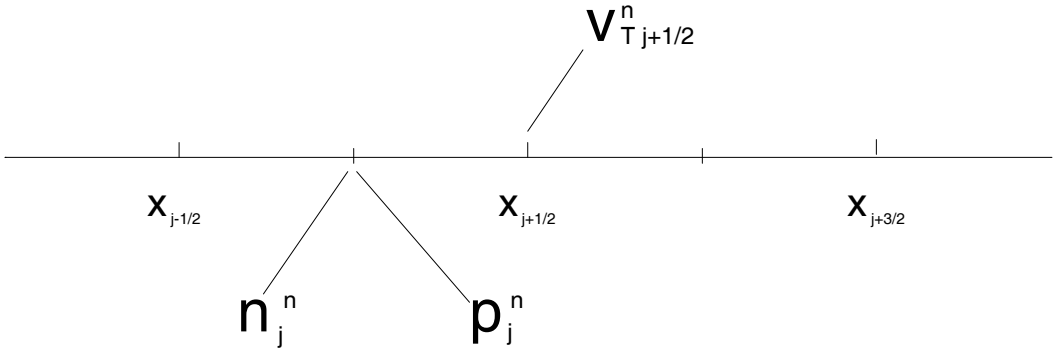

Figure 5.1: The staggered 1-D grid, indicating where the variables pressure (p), component density ($\mathbf{n}$) and total velocity (v_T) are stored.

The use of a block centred grid with the Higher Order Godunov method is also particularly suitable due to the cell based nature of the scheme. Also specification of numerical boundary conditions is straightforward. For example at $x = 0$ we have the first cell edge where we need to specify a flux, so if we have an inflow boundary we assign the physical inflow flux there. On the other hand if the boundary is of no-flow type then we simply set the flux to zero. At the other end of the 1-D grid, at $x = x_{max}$ say, we also need to specify a flux. The no-flow boundary is treated as before, but if we have an outflow boundary then we can perform a characteristic tracing of $\mathbf{n}$ to the boundary, as in the internal flowfield, and calculate the resulting outflow flux.

5.2.2 Conservation Law and Pressure Discretisations

The system of conservation laws (3.5.8) is discretised using the Higher Order Godunov method described in the previous chapter. There are a number of points regarding implementation with the Black-Oil model worth mentioning. Firstly, due to the high component density of gas, because of its high compressibility, the component densities are poorly scaled. This results in an unreliable calculation of the average wavespeed (4.2.8), used to determine the reference state for the flux computation. This can be overcome, see [49], by multiplication of $\mathbf{U}$ and $\mathbf{F}$

in (4.2.8) by the formation volume factors at the appropriate state, i.e. left or right. Secondly, since the characteristic tracing step is derived from a Taylor's series expansion, with removal of wavespeeds of the wrong sign, it is possible that the traced component densities could be unphysical. More specifically we could trace to a negative component density or to a state outside the current state of phase equilibrium. When an unphysical traced state is detected the slope $\Delta\mathbf{n}$ is set to zero, which leaves the cell centred value plus the source term from the quasi-linear form of the equation (3.5.9). We then test again and if we still find an unphysical state we use the cell centred value $\mathbf{n}_j^n$. Each grid block of fluid has an associated number of fluid phases present, i.e. a particular saturation state, if we trace to a block edge where a different number of phases are present we perform the same process as before, i.e. set the slopes to zero and test again.

Under certain reservoir conditions the Higher Order Godunov flux computation is simplified. Namely, if we have a linear reservoir with no depth variation then gravitational effects are removed. If we also have pressure boundary conditions that guarantee flow from left to right then the total velocity will be positive for all time. This guarantees positive wavespeeds which means that the reference state for the flux computation (4.2.9) will always be the left-hand state, and the flux computation itself reduces to upwind determination, i.e.

$$\mathbf{F}^{EO}(\mathbf{U}^L, \mathbf{U}^R) = \mathbf{F}(\mathbf{U}^L).$$

In fact even if gravity is present, as long as no counter-current flow occurs, i.e. all phase velocities are the same sign (and hence wavespeeds), then flux computation will still simplify to determination of the upwind direction.

The pressure equation (3.4.6) is discretised using a backward Euler (i.e. implicit) approach, namely

$$c_j^n(p_j^{n+1} - p_j^n) + \frac{\Delta t}{(\Delta x)^2}(\mathbf{w}^T)_j^n[\mathbf{f}_{j+\frac{1}{2}}^n(v_T)_{j+\frac{1}{2}}^{n+1} + \mathbf{g}_{j+\frac{1}{2}}^n\tau_{j+\frac{1}{2}}^n - \mathbf{f}_{j-\frac{1}{2}}^n(v_T)_{j-\frac{1}{2}}^{n+1} - \mathbf{g}_{j-\frac{1}{2}}^n\tau_{j-\frac{1}{2}}^n]$$
$$= \Delta t q_j^n, \tag{5.2.1}$$

with the following discretisation of total velocity

$$(v_T)_{j+\frac{1}{2}}^{n+1} = [-\frac{(p_{j+1}^{n+1} - p_j^{n+1})}{\Delta x} + \gamma_{j+\frac{1}{2}}^n]\ \tau_{j+\frac{1}{2}}^n. \tag{5.2.2}$$

As the numerical solution of the pressure equation is of implicit type there is no restriction on the time step due to stability considerations. The solution of (5.2.1) after substitution of (5.2.2) is accomplished by solving a tridiagonal linear system every time step. This system is straightforward to solve directly via a standard forward/backward substitution algorithm, and in any case is the most efficient, see Golub and van Loan [21].

We note however, that the fluid parameters in the discretisations (5.2.1) and (5.2.2) can only be evaluated at the current time level, because they are functions of the quantities we are trying to calculate. This results in the approximation of pressure being second order accurate in space but only first order in time. The fact that pressure is only first order accurate in time is not thought to be too serious by Trangenstein [49]. This is because although pressure effects are quickly felt throughout the reservoir, once the fluid flow has settled down the pressure field is slowly varying in time because of the small compressibilities in the reservoir fluids, i.e. the coefficient c of $\frac{\partial p}{\partial t}$ is of the order 10^{-5}. Therefore the time truncation errors associated with the pressure equation should not be too large compared to those in the hyperbolic conservation laws.

The transmissibilities $\tau^n_{j+\frac{1}{2}}$ in (5.2.1) and (5.2.2), at the cell interfaces are formed by a harmonic weighting

$$\tau^n_{j+\frac{1}{2}} = \frac{2\tau^n_j \tau^n_{j+1}}{\tau^n_j + \tau^n_{j+1}},$$

the other quantities at the cell interfaces being evaluated by arithmetic averaging, for example

$$\mathbf{f}^n_{j+\frac{1}{2}} = \frac{1}{2}(\mathbf{f}^n_j + \mathbf{f}^n_{j+1}).$$

The reason for the differing methods of calculation of the quantities needed at the cell interfaces is as follows. Quantities which are functions of saturation are termed strong non-linearities whereas quantities which are functions of pressure are termed weak non-linearities. The strong non-linearities are stated to need special treatment, i.e. the harmonic weighting as opposed to arithmetic averaging to obtain the cell edge values, see Aziz and Settari [1]. Actually all four of the coefficients $\mathbf{f}$, $\mathbf{g}$, γ and τ, needed at the cell edges, are functions of saturation and pressure but Trangenstein [49] only recommends harmonic weighting of the

transmissibilities τ. This is because he is very keen to stress the equivalence of the discretisation, along with the given method of obtaining the cell edge coefficients, with the mixed finite element formulation of the pressure equation. If all the coefficients were harmonically averaged, as the above reason dictates, this would not then be the case.

5.2.3 Time Step Control

Time step control for the component conservation equations is based on CFL [13] considerations,

$$\Delta t^n \leq \frac{\Delta x}{S^n_{max}},$$

where S^n_{max} is the largest wavespeed at the current time level. As we are approximating the solution of the differential equations with the numerical method, the possibility exists that the maximum wavespeed calculated S^n_{max} could be smaller than the maximum wavespeed in the analytic solution. This would result in the calculated time step being an unstable one. To allow for this possibility the calculated time step is reduced by a multiplicative factor termed a CFL number. A CFL number of 0.9 is usually sufficient for use with the Higher Order Godunov method, to achieve stable numerical solutions.

This time step is also suitable for correctly capturing the transient behaviour in the parabolic pressure equation. To justify this we can examine how the time step responds to fluctuations in the pressure field. The time step is inversely proportional to the wavespeed which is proportional to the total velocity v_T, i.e.

$$\Delta t \propto \frac{\Delta x}{S_{max}} \propto \frac{\Delta x}{v_T},$$

and since in the absence of gravitational effects $v_T \propto \frac{\Delta p}{\Delta x}$, we have

$$\Delta t \propto \frac{(\Delta x)^2}{\Delta p}. \tag{5.2.3}$$

Time steps of $O(\Delta x^2)$ are of the correct size for ensuring stability in explicit numerical solutions of parabolic equations, however, we are using an implicit discretisation which has a far less severe stability criteria, if indeed any. The relation (5.2.3) tries to ensure that the $O(\Delta t)$ and $O(\Delta x^2)$ leading terms in the truncation error balance.

When we solve the pressure equation we use a time step based on CFL considerations at the current time level. Once the pressure field at the advanced time level is obtained we may calculate the maximum wavespeed and hence an associated stable time step at this level. If this time step is greater than that at the current time level we complete the update procedure by solving the conservation laws, if this is not the case we repeat the pressure equation with the stable time step from the advanced time level. Thus this process represents an extra technique of ensuring stability and is important in problems with high injection rates. This strategy of ensuring a stable time step can be summarised by

$$\Delta t^n \leq \frac{\Delta x}{\max_k(S_{max}(\mathbf{n}_k^n, p_k^n), S_{max}(\mathbf{n}_k^n, p_k^{n+1}))}.$$

The time stepping used in the Higher Order Godunov code is based on CFL criteria with a CFL number of 0.9. However we need to supply the code with an initial time step since at $t = 0$ all wavespeeds are zero. We supply a very small time step of 0.001 days to break the computation in. Also we do not allow the increase of the time step to go beyond a specified limit, an increase of a factor of 1.5-2.0 is usually acceptable which has the effect of controlling the volume error discrepancy which can become large near the wells early on, due to the comparatively large changes in pressure and component density there. Once the computations have settled down the usual CFL criteria then takes over in controlling the time steps. Also, during the course of the computation, if large volume error discrepancies are generated, for instance $O(10^{-2})$, then the time step is reduced by a factor of 10 which has the effect of re-establishing the smooth running of the computation by reducing the discrepancy.

5.2.4 Multidimensional Considerations

In 2-Dimensions, application of the Higher Order Godunov method to the component conservation laws is straightforward, there is nothing that needs to be taken into account that was not mentioned for the 1-D case. However we will describe the solution of the pressure equation in 2-D because it is more complex than the 1-D case. The discretisation of the 2-D pressure equation is of the same type as in the 1-D case but we now have the standard 5-point stencil shown in

Figure 5.2 instead of the 3-point stencil.

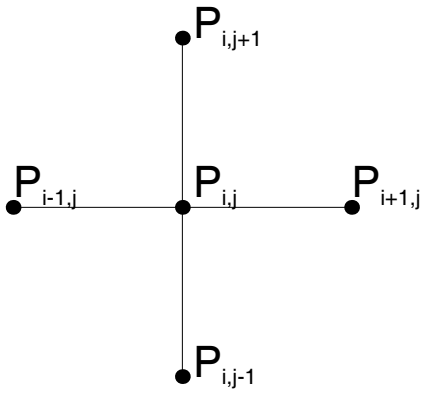

Figure 5.2: The 5 point pressure stencil resulting from the discretisation of the 2-D parabolic pressure equation.

This results in a pentadiagonal matrix equation

$$A\mathbf{p} = \mathbf{f}, \tag{5.2.4}$$

to solve for pressure, assuming that we used natural ordering to form the matrix equation, i.e. cycling along the x-direction first. A is a pentadiagonal $N \times N$ matrix where $N = N_x \times N_y$ and is the total number of grid blocks used in the simulation. N_x and N_y are the number of grid blocks in the x and y directions respectively. Vector $\mathbf{p}$ is the N vector of unknown pressures $p_{i,j}^{n+1}$ and $\mathbf{f}$ is the right hand side vector. A is of block tridiagonal form as below

$$A = \begin{bmatrix} M_{11} & M_{12} & 0 & \dots & \dots & \dots & \dots \\ M_{21} & M_{22} & M_{23} & 0 & \dots & \dots & \dots \\ 0 & M_{32} & M_{33} & M_{34} & 0 & \dots & \dots \\ \vdots & \vdots & \ddots & \ddots & \ddots & \vdots & \vdots \\ \dots & \dots & \dots & M_{i,i-1} & M_{ii} & M_{i,i+1} & \dots \\ \vdots & \vdots & \vdots & \vdots & \ddots & \ddots & \vdots \\ \dots & \dots & \dots & \dots & \dots & M_{N_{y-1},N_y} & M_{N_y,N_y} \end{bmatrix}.$$

Each of the sub-matrices $M_{i,j}$ is itself an $N_x \times N_x$ matrix, with the matrix entries M on the diagonal being tridiagonal and the off-diagonal matrices being diagonal.

The linear system (5.2.4) may be solved directly by, for instance, Gaussian Elimination, however in two dimensions the solution of the pressure equation takes

up a considerable amount of the total CPU time, i.e. around 20%. Therefore we require the method of solution to be as efficient as possible so we prefer an iterative method such as the Successive Line Over Relaxation (SLOR) method, see Varga [52] for details, or the pre-conditioned Conjugate Gradient method see Golub and van Loan [21] for general details and Van Der Vorst [53] for the algorithm used. We tried both methods of solution and found the pre-conditioned conjugate gradient method to be more efficient as the grid was refined.

We now describe the implementation of boundary conditions for a 2-D Areal reservoir simulation problem. An Areal problem takes place in the $x - y$ plane, gravity is assumed to act in the z-direction, therefore there are no gravitational effects in the problem, if there is no dip angle in either coordinate direction. See Aziz and Settari [1] for a more detailed description of the Areal problem and for other types of reservoir simulation performed in 2-D, for example cross-sectional problems which do include gravitational effects. The Areal region is usually square with injection of fluid taking place in the bottom left hand corner and production of fluid in the top right hand corner. All boundaries other than the injection and production points are of no normal flow type. The computational region is shown in Figure 5.3.

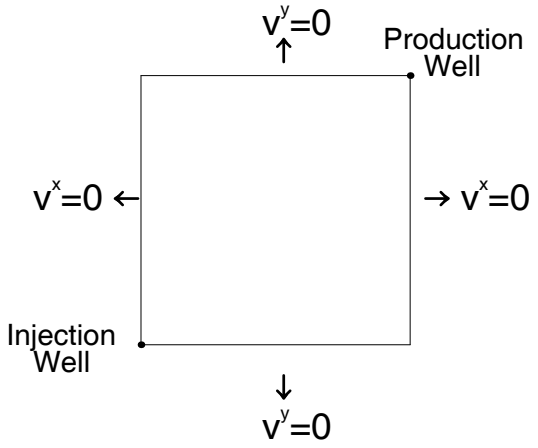

Figure 5.3: The geometry of the Areal problem, indicating the locations of the wells and the no-flow boundaries.

The grid block in the bottom left hand corner containing the injection well is shown in Figure 5.4.

We need to specify the four fluxes shown on Figure 5.4 to update the compo-

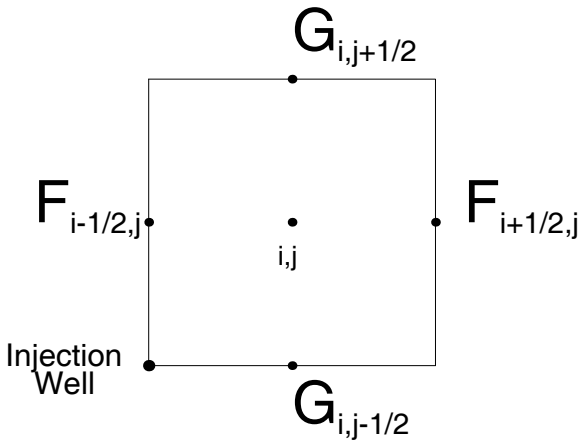

Figure 5.4: The injection grid block, indicating the 4 fluxes needed to update the component density vector.

nent density held at the block $B_{i,j}$. The two fluxes $\mathbf{F}_{i+\frac{1}{2},j}, \mathbf{G}_{i,j+\frac{1}{2}}$ are calculated using the methods explained in Chapter 4. We see that the fluxes $\mathbf{F}_{i-\frac{1}{2},j}, \mathbf{G}_{i,j-\frac{1}{2}}$ are located on no-flow boundaries and therefore would expect to set them to zero. However we also see that the point $(x = 0, y = 0)$ where the injection well is physically located does not enter into the stencils of our numerical schemes for either the conservation laws or the pressure equation. Therefore we must find a way of modelling it, the most obvious way is the inclusion of a local source term in the hyperbolic conservation laws. However dealing with source terms in hyperbolic conservation laws is problematical, for instance with explicit treatment of source terms time steps need to be significantly reduced to ensure stable solutions. We will discuss the use of source terms to model injection and production wells in the Black-Oil model equations and their treatment later in this chapter.

There is another way to model injection that is very straightforward, we simply set the injection conditions to hold on the boundaries of the grid block at points $i - \frac{1}{2}, j$ and $i, j - \frac{1}{2}$, the fluxes $\mathbf{F}_{i-\frac{1}{2},j}, \mathbf{G}_{i,j-\frac{1}{2}}$ then become the physical injection fluxes. We can justify this by pointing out that the total mass flux into the grid block is the same as if the injection took place at $(x = 0, y = 0)$. This technique is also used in the pressure equation discretisation. We also use this process to model the production well in its containing block. Basically we assume that production of fluid takes place at two points, $N_x, N_y + \frac{1}{2}$ and $N_x + \frac{1}{2}, N_y$, we trace the component densities to these points and compute an outflow flux to use in the

conservative finite difference update, the same process as in the 1-D case. Again this modelling of production is also used in the pressure equation.

5.3 Validation of the Higher Order Godunov Code

A Fortran code was written to solve the Black-Oil fluid flow equations given in Chapter 3 using the Higher Order Godunov method described in Chapter 4. Both a 1-D and a dimensionally unsplit 2-D code were written, the 2-D code being obtained from extension of the 1-D code. In order to use the the codes to perform the investigations in this thesis, they need to be validated. The 1-D code was validated by comparison of results with those given by Trangenstein and Bell in [46], who also used the Higher Order Godunov method [2] to solve the Black-Oil flow equations [46]. There is only one set of 2-D Black-Oil results in the literature, in [2], but the initial conditions are not included therein. Therefore an alternative method of validating the 2-D code was required and was performed by comparison of results with those from a commercial reservoir simulation code (VIP) used by B.P., written by Western Atlas, these results relate to the discussions in Chapter 7 and so are shown there. However we also show some 2-D results in this section to investigate the accuracy of the transverse flux derivatives (4.3.15), (4.3.14), used to construct the left and right traced states, see Section 4.2.2. In 1-D three of the reservoir flow problems from [46] were simulated, these being a saturated flow problem, an undersaturated flow problem, and a mixed saturated-undersaturated flow problem. In 2-D a saturated flow Areal problem was simulated which was based on the 1-D saturated flow problem.

The problems given in [46] were said to have not been typical of Black-Oil reservoir simulations, but were designed to test the resolution capabilities of the numerical method for problems involving sharp fronts. The Pressure-Volume-Temperature properties and the relative permeability data was the same for all of the problems and can be found in Section 3.9. The physical setting in 1-D was as follows, a reservoir 1000 feet in length with no dip angle (i.e. horizontal), with permeability of 100 millidarcy's was initially filled with a mixture of oil, gas and

water. The initial fluid distribution was taken to be uniform along the length of the reservoir, and had an associated pressure. Fluid of given composition and pressure was injected at $x = 0$ and the fluid resident in the reservoir was produced at a specified pressure at $x = 1000$. We remark that the initial data, of the problems given in [46], including that at injection and production did contain a volume error discrepancy, i.e. the volume balance equation (3.4.4) was not satisfied exactly.

The problems were simulated using the second order scheme with 200 grid blocks to accurately resolve the fronts, a CFL number of 0.9 was used throughout the computation. The reservoir data used guarantees that the fluid flow is from left to right for the entire computation, hence flux computation reduces to upwind determination as described in Section 5.2.2.

We now give a description of the test problems from [46] which we simulated. Problem 1 is a saturated flow problem throughout with injection and initial reservoir compositions given by

$$\mathbf{n}_{inj} = \begin{bmatrix} 0.0414 \\ 66.23 \\ 0.497 \end{bmatrix} \quad , \quad \mathbf{n}_{res} = \begin{bmatrix} 0.703 \\ 70.30 \\ 0.0502 \end{bmatrix} .$$

The injection, initial reservoir and production pressures are 2000, 1800 and 1600 psi respectively. We refer to this as problem A2 in this thesis. The problem was simulated for 150 days with the results from the Higher Order Godunov code shown in Figure 5.5. The corresponding results shown by Trangenstein and Bell in [46] are shown in Figure 5.6.

In the saturation plots shown in this section, the lower curve is the vapour saturation and the upper curve the sum of the vapour and liquid saturations. Hence the distance between these two curves represents the liquid saturation and the distance between the second curve and the top of the graph represents the aqueous saturation. For the saturated flow example, in Figure 5.5, both non-zero wave families are not genuinely non-linear and therefore rarefaction-shock compound waves are possible and can be observed with the shocks, in these waves, located at about 150 and 720 feet.

The second simulation problem was problem 3 from [46], which we refer to as

problem A3, and has injection and initial reservoir compositions given by,

$$\mathbf{n}_{inj} = \begin{bmatrix} 0.404 \\ 4.042 \\ 0.647 \end{bmatrix} \quad , \quad \mathbf{n}_{res} = \begin{bmatrix} 0.734 \\ 32.10 \\ 0.1835 \end{bmatrix} .$$

This problem is an undersaturated flow example with the vapour phase missing. The injection, initial reservoir and production pressures are 1400, 1200 and 1000 psi respectively. The simulation time being 300 days with the results from the Higher Order Godunov code shown in Figure 5.7. The corresponding results shown by Trangenstein and Bell in [46] are shown in Figure 5.8.

Both wavespeeds in the saturated flow problem 1 are termed Buckley-Leverett modes, due to their similarity to the 3-phase incompressible wavespeeds. In undersaturated flow only one of the wavespeeds is of this form, the other being the linearly degenerate particle velocity. Hence only one of the two wave modes was expected to yield a compound wave similar to those observed in problem 1. The compound wave in Figure 5.7 can be identified, with the shock located around 750 feet.

The last 1-D example is problem 5 from [46], which we refer to as problem A4, and has injection and initial reservoir compositions given by,

$$\mathbf{n}_{inj} = \begin{bmatrix} 0.0179 \\ 178.68 \\ 0.357 \end{bmatrix} \quad , \quad \mathbf{n}_{res} = \begin{bmatrix} 0.668 \\ 100.19 \\ 0.0668 \end{bmatrix} .$$

In this problem a 2-phase mixture with the liquid phase missing is injected into a 2-phase reservoir with the vapour phase missing. During the course of the simulation a saturated region also develops in the middle of the reservoir, thus we have a mixed flow problem. The injection, initial reservoir and production pressures are 4300, 4200 and 4100 psi respectively. The fluid flow was simulated for 400 days with the results from the Higher Order Godunov code shown in Figure 5.9. The corresponding results shown by Trangenstein and Bell in [46] are shown in Figure 5.10. The results of problem 5 in Figure 5.9 shows two phase changes located at about 150 and 650 feet.

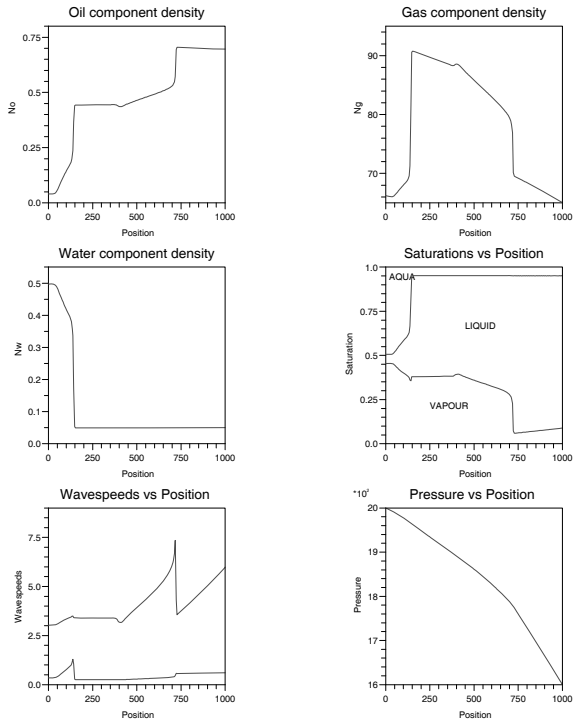

Figure 5.5: The numerical results obtained from simulating problem A2 with the Higher Order Godunov code using 200 grid blocks and a CFL number of 0.9.

Figure 5.6: The corresponding numerical results of simulating problem A2 presented by Trangenstein and Bell.

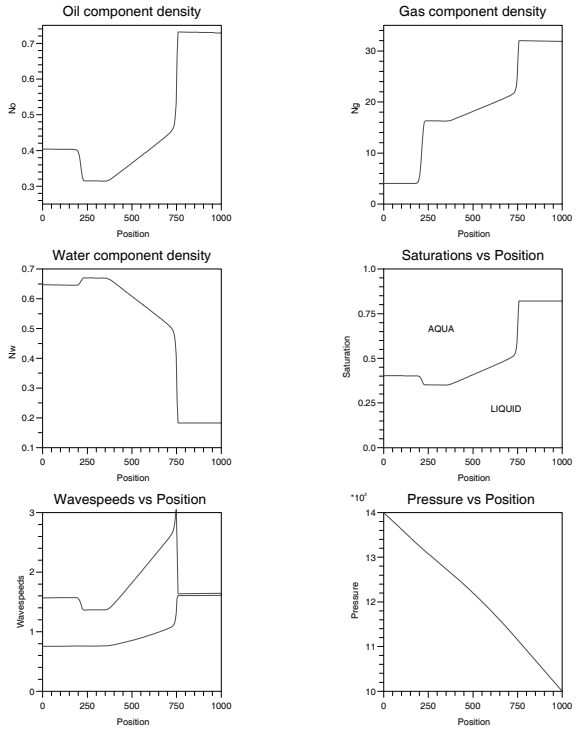

Figure 5.7: The numerical results obtained from simulating problem A3 with the Higher Order Godunov code using 200 grid blocks and a CFL number of 0.9.

Figure 5.8: The corresponding numerical results of simulating problem A3 presented by Trangenstein and Bell.

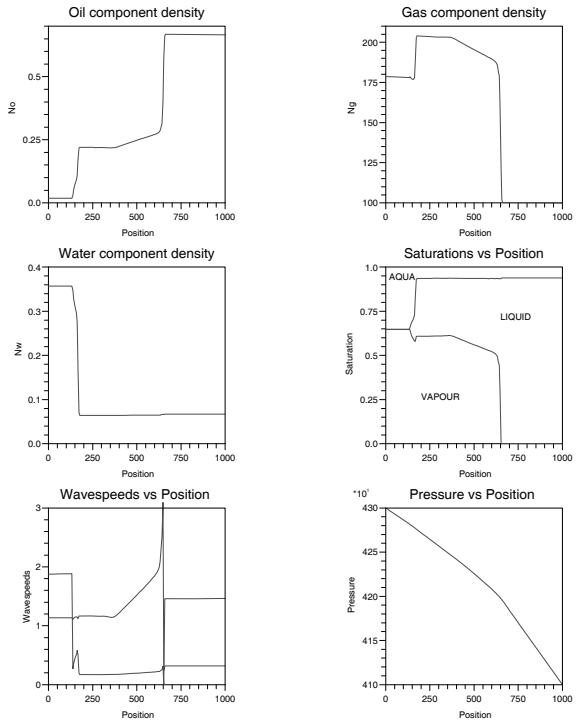

Figure 5.9: The numerical results obtained from simulating problem A4 with the Higher Order Godunov code using 200 grid blocks and a CFL number of 0.9.

Figure 5.10: The corresponding numerical results of simulating problem A4 presented by Trangenstein and Bell.

The simulations shown in Figures 5.5, 5.7 and 5.9 show good agreement with the corresponding numerical results in [46], which are shown in Figures 5.6, 5.8 and 5.10, hence validating the 1-D Higher Order Godunov code. Of note in these results, and those in [46], are the spikes in the wavespeeds at the points of local linear degeneracy which are commonly observed in simulating such problems.

The 2-D Areal problem was simulated in order to examine the effect on the numerical results of the accuracy of the transverse flux derivatives in the calculation of the left and right traced states, described in Section 4.3.2. The Black-Oil model parameters were the same as in the 1-D problems, with the rock permeability of 100 milliDarcy's in both coordinate directions. The problem takes place in the $x - y$ (horizontal) plane and is simulated on a region of 100 square feet. The reservoir has no dip angle in either direction and hence flux computation again simplifies as in the 1-D problems, i.e. upwind determination in both coordinate directions. Fluid is injected at the bottom left hand corner, i.e. at (0,0) and fluid is produced at the top right hand corner, i.e. at (100,100). All boundaries other than at the injection and production points are of no-flow type. The injection, initial reservoir and production conditions are the same as in the 1-D saturated flow problem.

The problem was simulated with 40 grid blocks in both directions using a CFL number of 0.9 and to a time of 5.0 days. The results shown in Figure 5.11 were simulated with the second order scheme using the most accurate transverse flux derivatives, calculated using (4.3.15), (see Section 4.3.2).

In the Areal problem the contours start out at an early time as circular in nature. However the greatest pressure gradient is along the diagonal connecting the injection and production wells, which forces the contours to square off, as can clearly be seen. A section of the results along this diagonal was plotted and found to exhibit the same qualitative structure as the corresponding 1-D problem, which was to be expected.

The corresponding results with the less accurate transverse flux derivatives calculated using (4.3.14), are shown in Figure 5.12.

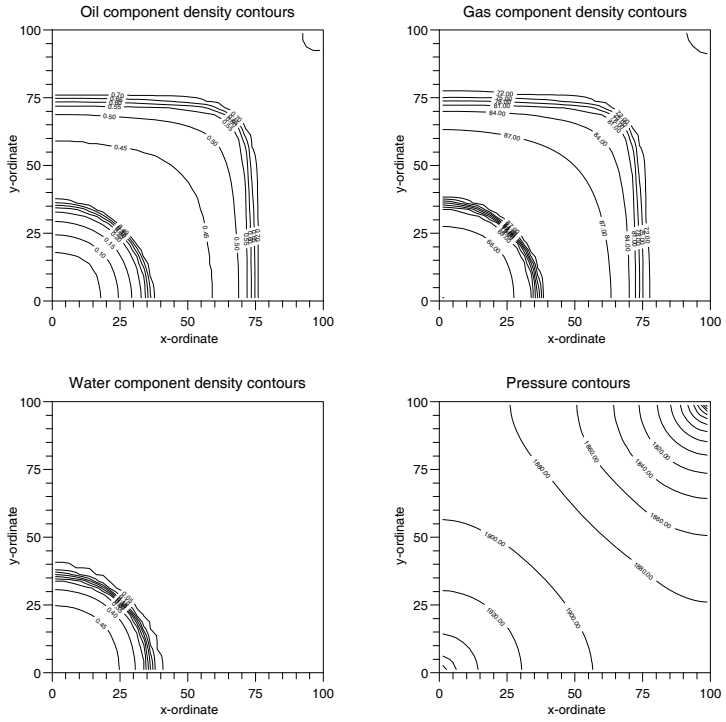

Figure 5.11: Results of simulating the 2-D Areal problem with the most accurate transverse terms, using a 40×40 grid and a CFL number of 0.9.

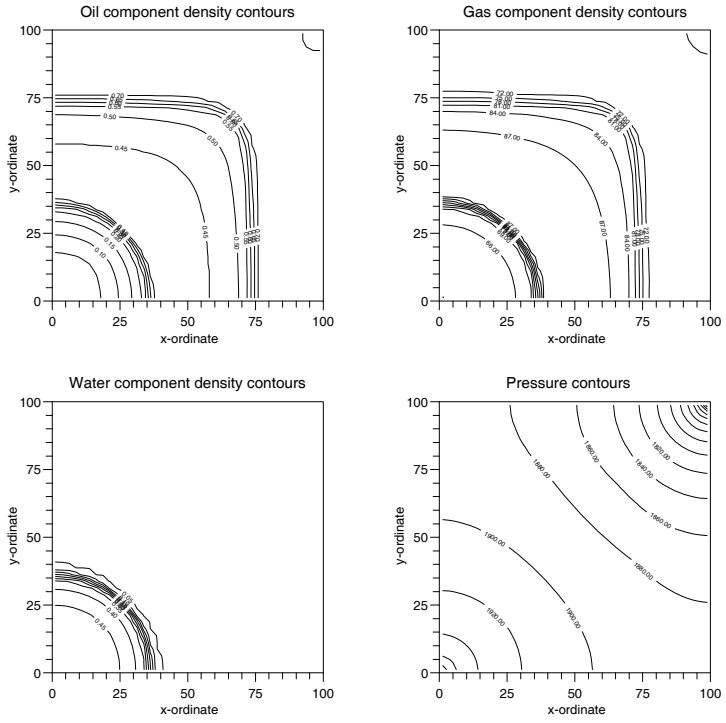

Figure 5.12: Results of simulating the 2-D Areal problem with less accurate transverse terms, using a 40×40 grid and a CFL number of 0.9.

Figure 5.13 shows the effect of neglecting the transverse flux derivatives completely.

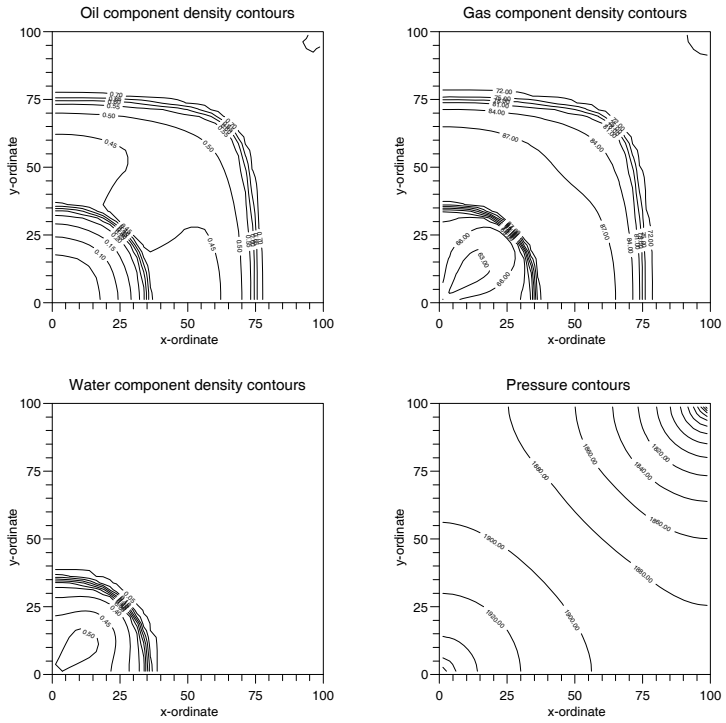

Figure 5.13: Results of simulating the 2-D Areal problem with no transverse terms, using a 40×40 grid and a CFL number of 0.9.

In these contour plots, when the contours are closely spaced the prescence of a shock is indicated, whilst comparatively widely spaced contours indicate rarefaction regions. Two shocks are clearly visible in the results of this Areal problem. A close comparison of Figure 5.11, obtained with the most accurate transverse terms, and Figure 5.12, with the less accurate transverse terms, although still maintaining second order accuracy, was performed. This indicated that the contours in Figure 5.11 near the injection well are slightly more square whilst those further into the region are slightly less square, compared to Figure 5.12, but there not being much difference between the two. The result of using no transverse terms, in Figure 5.13 is that the contours in the middle of the region are not properly formed. Also unphysical cavities are introduced in the gas and water component densities near the injection well. Therefore one form of transverse flux calculation is needed in the 2-D Higher Order Godunov algorithm to simulate the Areal problems. In the 2-D cross-sectional problems the effect of the

accuracy of the these terms is expected to be more noticeable since transverse flow is more prevalent.

Experience of Black-Oil computations have provided a feel for the level of volume error discrepancy that is acceptable in terms of the accuracy of the numerical results. For instance in 1-D computations without gravity the maximum volume error discrepancies generated are typically in the range $O(10^{-3}) - O(10^{-5})$ which are deemed acceptable. If discrepancies of $O(10^{-2})$ are generated these are thought to be unacceptable and may usually be reduced by reducing the time step. For example when fluid is injected having an associated volume error discrepancy of $O(10^{-2})$ boundary layers develop in the results at the injection point. This is due to the mismatch in discrepancy between the injected fluid and the fluid in the reservoir, and represents unphysical behaviour. In 2-Dimensional simulations the volume error discrepancies generated are typically an order of magnitude higher than those in 1-D.

5.4 Construction of Analytic 3-Phase Flow Riemann Problem Solutions

We now move on to the construction of analytic solutions to the Riemann problem associated with 3-phase incompressible flow equations in order to test the accuracy of the Higher Order Godunov method when applied to degenerate systems of conservation laws. Analytic Riemann problem solutions for 3-phase compressible flow problems do not exist due to the complexity of the mathematical model. However analytic Riemann problem solutions for 3-phase incompressible problems without gravitational effects are relatively straightforward to construct. We construct some 3-phase incompressible analytic solutions and compare these with the corresponding results from the Higher Order Godunov code. Some analytic constructions were also performed by Smith in [40], we extend this work to consider more general solution behaviour. We now outline the derivation of the mathematical model and then describe the solution construction process.

The mathematical model describing 3-phase incompressible (Buckley-Leverett) flow of oil, gas, and water in a porous medium is quite straightforward, reduc-

ing to a 2-system of equations due to the volume balance condition. The mass conservation equations for the 3 fluid components (or phases) are as follows

$$\frac{\partial}{\partial t}(n_i\phi) + \frac{\partial}{\partial x}(\rho_i v_i) = 0,$$

where $i = o, g, w$ and refers to the fluid component with component density n_i. ϕ is the porosity, ρ_i is the density of the phase and v_i is the gravity free Darcy phase velocity given by

$$v_i = \frac{\lambda_i v_T}{\lambda_o + \lambda_g + \lambda_w},$$

where λ_i are the phase mobilities and v_T is the total fluid velocity. No mass transfer effects are modelled and so the phases and components are equivalent. For example oil exists in the liquid phase only and so the liquid phase could equally well be referred to as the oil phase, similarly for gas and water. The following equations describe phase equilibrium

$$n_i = \rho_i s_i, \quad i = o, g, w,$$

where s_i is the phase saturation which is the volume fraction of the phase. Hence the saturations sum to one, which gives the volume balance equation

$$s_o + s_g + s_w = 1. \tag{5.4.5}$$

The conservation of mass equations may be manipulated to give

$$\phi\frac{\partial \mathbf{s}}{\partial t} + \frac{\partial \mathbf{v}}{\partial x} = 0,$$

where $\mathbf{s}$ and $\mathbf{v}$ are vectors of the component quantities. These 3 equations may be summed to give the relation

$$\frac{\partial v_T}{\partial x} = 0,$$

which states that the total fluid velocity is independent of position in the reservoir. This means that the boundary conditions specify the velocity field throughout the reservoir. Only 2 of the saturation equations need to be considered, namely

$$\frac{\partial s_w}{\partial t} + \frac{\partial v_w}{\partial x} = 0,$$

and

$$\frac{\partial s_g}{\partial t} + \frac{\partial v_g}{\partial x} = 0,$$

since (5.4.5) then implies conservation of the oil saturation s_o. Hence we have a conserved variable $\mathbf{U} = [s_w, s_g]^T$ of saturations and a flux function vector $\mathbf{F} = [v_w, v_g]^T$ of phase velocities.

The characteristic structure of the model is as follows, the wavespeeds are given by

$$\lambda_{1,2} = \frac{1}{2}\left[\frac{\partial v_w}{\partial s_w} + \frac{\partial v_g}{\partial s_g} \mp \sqrt{\left((\frac{\partial v_w}{\partial s_w} - \frac{\partial v_g}{\partial s_g}) + 4\frac{\partial v_g}{\partial s_w}\frac{\partial v_w}{\partial s_g}\right)}\right],$$

and the right eigenvectors by

$$\mathbf{r}_1 = \begin{bmatrix} 1 \\ \frac{\lambda_1 - \frac{\partial v_w}{\partial s_w}}{\frac{\partial v_w}{\partial s_g}} \end{bmatrix}, \mathbf{r}_2 = \begin{bmatrix} 1 \\ \frac{\lambda_2 - \frac{\partial v_w}{\partial s_w}}{\frac{\partial v_w}{\partial s_g}} \end{bmatrix}.$$

It is known that the wavemodes of this model are not genuinely non-linear. Therefore shock/rarefaction compound waves which also occur in the 2-phase Buckley-Leverett model will be expected.

Weak solutions of the flow equations are sought as discontinuous solutions are expected. The Riemann problem considered is of the form

$$\mathbf{s}(x,0) = \begin{cases} \mathbf{s}^L & \text{if } x = 0 \\ \mathbf{s}^R & \text{if } x > 0 \end{cases},$$

so that s^L corresponds to the injected fluid composition and s^R the initial reservoir composition. The theory of the Riemann problem solution to a 2-system of strictly hyperbolic conservation laws can be found in Smoller [41]. Liu [30] describes the solution of the Riemann problem for systems not satisfying the genuine non-linearity condition.

The calculated analytic solutions are plotted against the wavespeed x/t which leads to a clearer interpretation of the results. Some analytic results will be shown after a description of the construction process and compared to numerical results from the Higher Order Godunov code. We use the same relative permeability functions as were used with the Black-Oil computations, given in Section 3.9, and the following phase viscosities in Centipoise

$$\mu_o = 1.0, \quad \mu_g = 0.05, \quad \mu_w = 0.8.$$

For the Riemann problems under consideration we take unit porosity ($\phi = 1$) and total velocity ($v_T = 1$). The positive total fluid velocity ensures that fluid flow takes place from left to right and hence that both wavespeeds are non-negative.

The aim in solving the Riemann problem is to connect the left and right states in the problem with either shocks or rarefactions which are separated by constant states. The system considered exhibits a lack of genuine non-linearity and so rarefaction-shock compound waves are also possible. The solution to the Riemann problem can also be exhibited in phase space, that is in conserved variable (s_w, s_g) space. In this representation the Riemann problem can be considered as tracking the various shock, rarefaction, or rarefaction-shock composite wave curves and finding the points of intersection, and thus determining the path between the left and right states taken by the solution.

The approach of determining the waves present in the solution is influenced by physical assumptions, and in particular the behaviour of 2-phase Buckley-Leverett systems. In the 2-phase Buckley-Leverett system water injection will typically give a rarefaction-shock compound wave. The rarefaction fan stretches from the injection composition to an intermediate saturation state which is connected by a shock to the initial water saturation in the reservoir. Similar behaviour is expected with the 3-phase system, where the compound wave would be expected to be a 1-rarefaction-shock, a faster 2-wave will also appear in the solution. This is because the shock in the first wave will clearly be the slower of the two waves which constitute the Riemann problem solution, and hence be associated with λ_1, defining a 1-wave, due to the condition $\lambda_1 \leq \lambda_2$. If the first wavespeed λ_1 is non-zero at the injection point ($x = 0$) then the injection conditions can propagate into the region and a constant state connecting the injection conditions with the left state of the rarefaction is expected. If on the other hand $\lambda_1 = 0$ then the rarefaction connects directly to the injection saturations at $x = 0$.

Firstly the 1-rarefaction in the 1-compound wave is tracked by choosing a water saturation increment ds_w and calculating the corresponding increment in the gas saturation from

$$ds_g = \frac{(\lambda_1 - \frac{\partial v_w}{\partial s_w})}{\frac{\partial v_w}{\partial s_g}} ds_w,$$

which is derived from the first right eigenvector $\mathbf{r}_1$, see Smith [40]. The increment

ds_w is successively applied to the injected water saturation, which defines the left state of the rarefaction. The wavespeed λ_1 is calculated and plotted against x/t since for a 1-rarefaction we have $\lambda_1 = x/t$. The incrementation procedure on the water saturation s_w which constructs the 1-rarefaction is continued until the location of the shock which connects the current water saturation on the rarefaction wave to the initial reservoir water saturation is found. The 1-shock is located as follows; since the shock is part of a compound wave connected to a 1-rarefaction then at the connection point the fastest wavespeed in the rarefaction will be equal to the first characteristic speed to the left of the shock. At the connection point, $\mathbf{s}^{con}$ say, the 1-rarefaction is given by

$$\frac{x}{t} = \lambda_1(\mathbf{s}^{con}),$$

the 1-shock is located at $x/t = \sigma$, where σ is the shock speed and hence the shock will have speed

$$\sigma = \lambda_1(\mathbf{s}^{con}),$$

which satisfies the extended entropy condition for shocks which are not genuinely non-linear, see Liu [30]. As the 1-rarefaction is tracked a shock speed based on the water component is calculated

$$\sigma = \frac{[\mathbf{F}_w]}{[\mathbf{U}_w]} = \frac{v_w^k - v_w^{res}}{s_w^k - s_w^{res}},$$

where $\mathbf{s}^k$ is each incremented state on the rarefaction wave. The square brackets refer to the jump between the values to the left and right of the shock. This shock speed can only be calculated for the water component as only the water saturation to the right of the shock is known in advance, i.e. the initial reservoir water saturation. Since λ_1 increases from left to right along the rarefaction, at the left end $\lambda_1 < \sigma$ so the shock can be detected when the condition $\lambda_1(\mathbf{s}^k) \geq \sigma$ arises. When this condition is met the current value of $\mathbf{s}^k$ connects the rarefaction to the shock. Figure 5.14 shows an example of a 1-rarefaction wave curve from the left state in the Riemann problem connecting to a 1-shock wave curve in phase space. The point where the two composite wave curves coincide is given by $\mathbf{s}^{con}$.

Once the shock is detected the gas saturation to the right of the shock may be calculated. This is done by using the jump condition for the gas phase

$$v_g^L(s_w^L, s_g^L) - v_g^R(s_w^R, s_g^R) = \sigma(s_g^L - s_g^R),$$

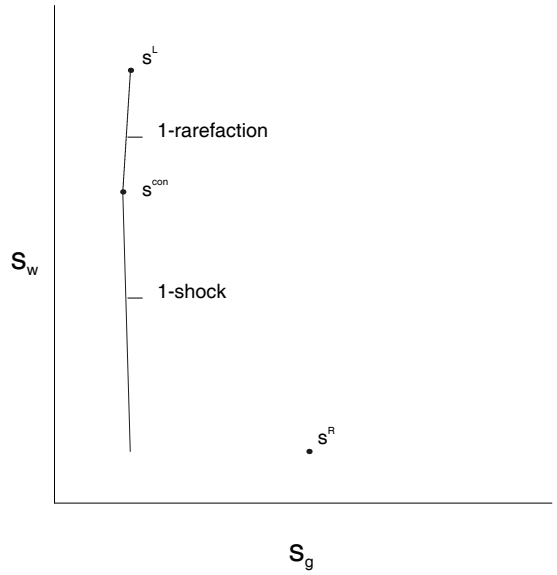

Figure 5.14: Example wave curves in phase space emanating from the left state in the Riemann problem.

where σ is the shock speed and the superscripts indicate the left and right states associated with the shock. The only unknown in this non-linear equation is s_g^R since the oil saturation to the right of the shock may be expressed in terms of s_g^R and s_w^R, and may be calculated by using an iterative method such as Newton. Now the characterisation of the shock can be checked to see if it satisfies the appropriate entropy condition, namely that it is a 1-shock. Assuming this to be the case, we can now attempt to connect the local right state associated with the 1-shock to the right state in the Riemann problem, i.e. the initial reservoir conditions, by a 2-wave. A triple (transitional) wave is not considered a possibility, as these are not typically seen in gravity free 3-phase flow problems, and would only occur at an umbilic point, so a constant state connects the local right state to the 2-wave.

The wavespeeds associated with the local right state and the reservoir initial conditions can then be used to determine whether the 2-wave is a shock only or a rarefaction/shock compound wave. This is done by calculating a shock speed based on a shock having a left state of the constant state mentioned in the previous paragraph, $\mathbf{s}^c$ say, and a right state of the reservoir initial conditions, i.e.

$$\sigma = \frac{v_g^c - v_g^{res}}{s_g^c - s_g^{res}}.$$

The Lax entropy condition for a 2-shock can then be used to check that a shock

with this speed is an admissible one, namely

$$\lambda_2^c > \sigma > \lambda_2^{res}.$$

If this is the case then it is assumed this shock from the constant state to the initial reservoir state completes the solution of the Riemann problem. Figure 5.15 shows how the composite wave curve in Figure 5.14 intersects with a shock wave curve emanating from the right state in the Riemann problem when the solution is completed by a 2-shock. The state $\mathbf{s}^c$ refers to the constant state separating

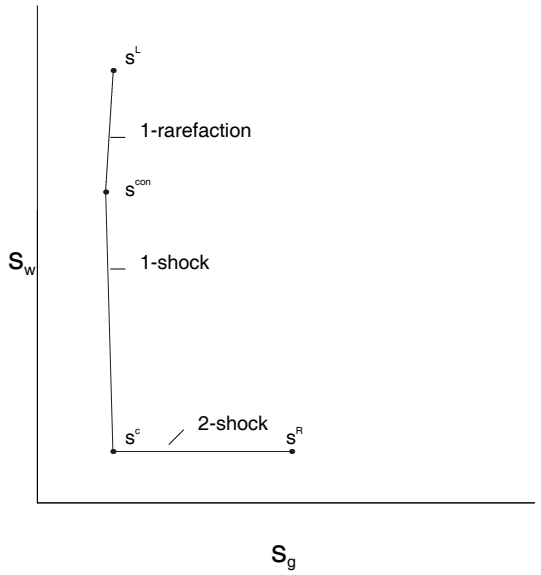

Figure 5.15: Example wave curves in phase space connecting the left and right states in the Riemann problem.

the 1-rarefaction-shock compound wave from the 2-shock.

If this 2-shock cannot be found then it is assumed the 2 states are connected with a 2-rarefaction-shock. The 2-rarefaction is defined by $\lambda_2 = x/t$, therefore we calculate $\lambda_2(\mathbf{s}^c)$ to determine the starting point (left state) of the rarefaction on the x/t axis. The gas saturation is then incremented, starting from s_g^c, using a similar procedure to that previously described, to track the rarefaction wave. The water saturation is constant across this wave since the initial reservoir water saturation was reached by the 1-shock in the first wave. Hence the corresponding increment in the oil saturation is trivial to calculate because the saturations sum to 1. Once each new saturation state, s_g^k say, on the rarefaction wave has been calculated, the corresponding wavespeed λ_2 is calculated to see if a 2-shock can

be connected from s_g^k to the initial reservoir state. This is done by calculating the shock speed

$$\sigma = \frac{v_g^k - v_g^{res}}{s_g^k - s_g^{res}},$$

and then using this in the entropy condition

$$\lambda_2^k \geq \sigma \geq \lambda_2^{res},$$

which is of the required form for determining the admissibility of a shock in a rarefaction-shock compound wave. If this condition is satisfied then we have found the 2-shock in the compound wave located at $x/t = \sigma$. This then completes the solution of the Riemann problem.

Two Riemann problems were considered, the first of which corresponds to essentially a waterflood into a reservoir containing half oil and half gas. The injected and initial reservoir saturations are given by

$$\mathbf{s}_{inj} = \begin{bmatrix} 0.0 \\ 0.06 \\ 0.94 \end{bmatrix} \quad , \quad \mathbf{s}_{res} = \begin{bmatrix} 0.5 \\ 0.5 \\ 0.0 \end{bmatrix},$$

where the vectors are ordered oil, gas, and lastly water. In Figure 5.16 we show the analytic solution in phase space. In this diagram the triangle defined by the dotted line indicates all possible fluid saturations. The left and right states defining the Riemann problem are shown together with the wave curves that connect them. On these diagrams shocks are indicated by straight lines which connect the left and right states associated with the shock although the actual shock curve (Hugoniot) will not necessarily be a straight line. Rarefaction curves are indicated by smooth curves. For a 2-system of hyperbolic conservation laws the wave curve out of the left state in the Riemann problem intersects the wave curve out of the right state at exactly one point in phase space. This point is referred to as the intermediate state in the Riemann problem. For systems that are not genuinely non-linear either or both of the wave curves can be composed of both shock and rarefaction wave curves as in the Riemann problems considered here. In Figure 5.16 a composite rarefaction-shock wave curve can be seen intersecting the shock curve from the right state at the intermediate state denoted by $\mathbf{s}^{int}$.

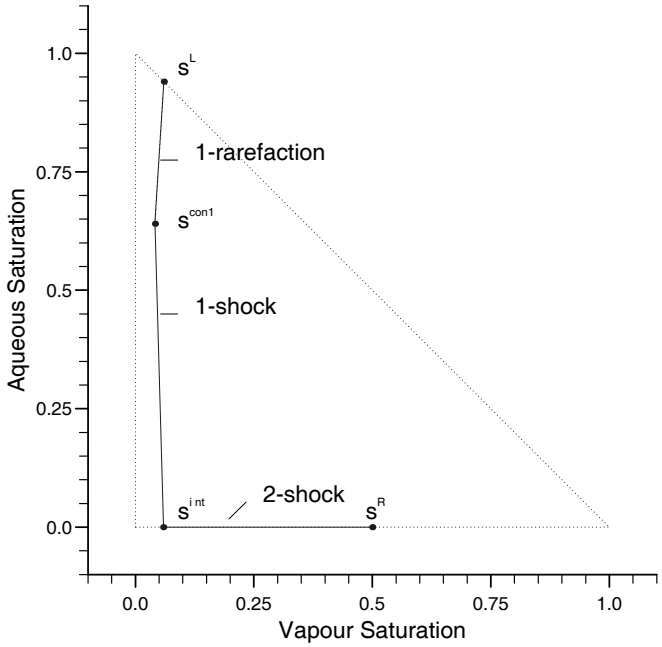

Figure 5.16: The phase space solution for problem 1 indicating the types of waves that connect the left and right states in the Riemann problem.

The state $\mathbf{s}^{con1}$ denotes the connection point of the rarefaction and shock wave curves associated with the 1-rarefaction-shock compound wave.

The results of the analytic constructions are shown in Figure 5.17. Here a constant state connecting the injection conditions to the left state on the 1-rarefaction can be observed, and occurs because $\lambda_1(\mathbf{s}_{inj}) \neq 0$. A 1-rarefaction-shock compound wave connecting the injected water saturation to the initial reservoir water saturation is clearly visible, the shock in this wave has a speed of $\sigma = 1.220$. The calculations then indicate that the constant state to the right of the 1-shock can be connected to the initial reservoir state with a 2-shock with speed $\sigma = 1.994$. In comparison the results of simulating this problem with the Higher Order Godunov code are shown in Figure 5.18. The simulation was run with 100 grid blocks and a CFL number of 0.9. The numerical results agree well with the analytic constructions, the shocks are captured in the correct positions as expected and the rarefaction waves are resolved accurately. Of particular note is the spike in the wavespeeds of the numerical solution at the location of the shock in the compound wave which is the characteristic signature of a local linear degeneracy, i.e. a point where the genuine non-linearity condition fails.

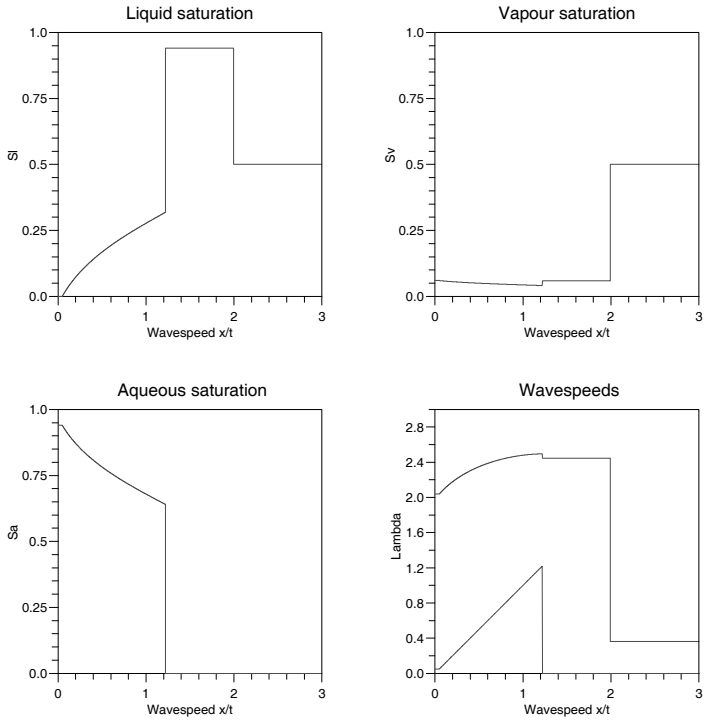

Figure 5.17: The analytic solution for problem 1 showing a 1-rarefaction-shock compound wave and a faster 2-shock.

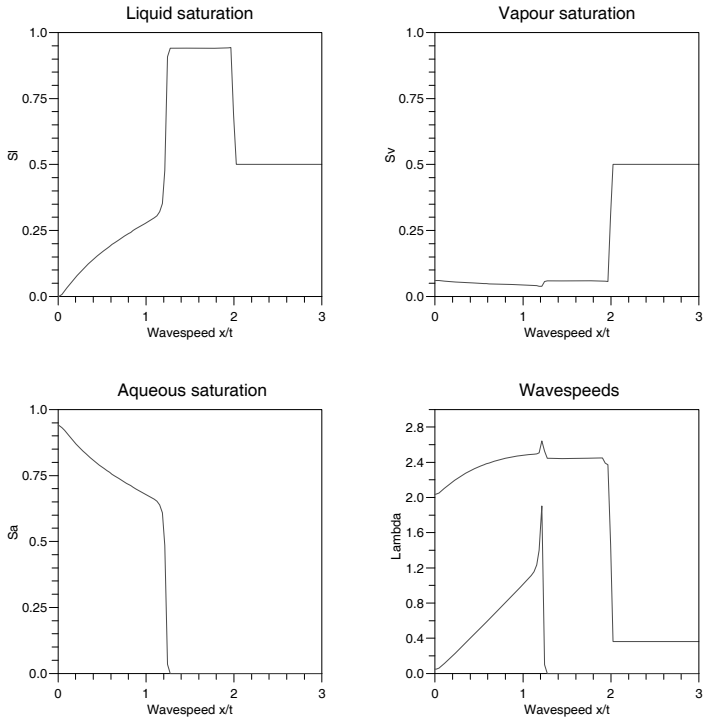

Figure 5.18: The numerical solution for problem 1 simulated using 100 grid blocks and a CFL number of 0.9.

If the analytic and numerical solution results are overlaid the agreement is such that only the spikes in the wavespeeds show up as a clear difference.

The second Riemann problem considered corresponds to a gas and waterflood into an oil saturated reservoir. The initial conditions are as follows

$$\mathbf{s}_{inj} = \begin{bmatrix} 0.0 \\ 0.5 \\ 0.5 \end{bmatrix} \quad , \quad \mathbf{s}_{res} = \begin{bmatrix} 1.0 \\ 0.0 \\ 0.0 \end{bmatrix} .$$

In Figure 5.19 we show the analytic solution in phase space. This time the solution consists of two rarefaction-shock compound waves, separated by the intermediate state in the Riemann problem $\mathbf{s}^{int}$. The states $\mathbf{s}^{con1}$ and $\mathbf{s}^{con2}$ indicate where the rarefaction and shock portions of the compound waves are connected.

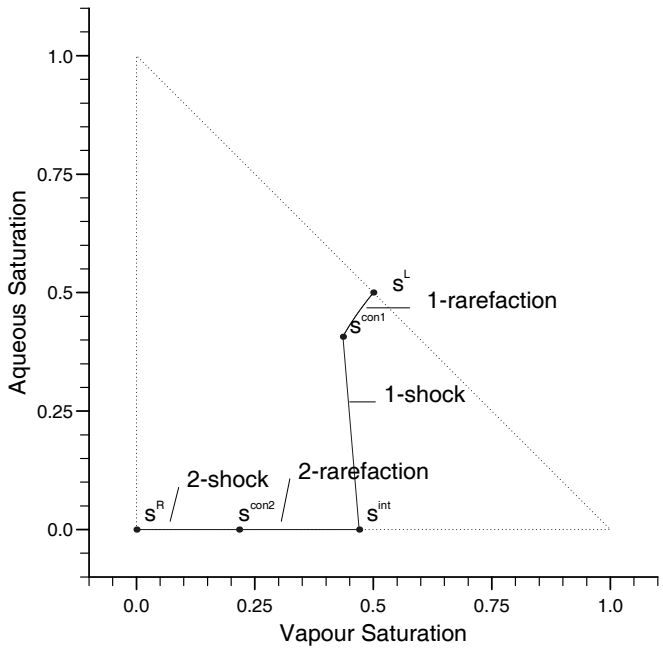

Figure 5.19: The phase space solution for problem 2 indicating the types of waves that connect the left and right states in the Riemann problem.

The analytic constructions are shown in Figure 5.20. Here the left state of the 1-rarefaction again connects to the injected saturations via a constant state. The shock in the 1-rarefaction-shock compound wave has a speed of $\sigma = 0.125$. In this case a valid shock which connects the constant state to the right of the 1-shock, with the initial reservoir saturations cannot be found. Therefore the solution to the Riemann problem is completed with a 2-rarefaction-shock compound wave.

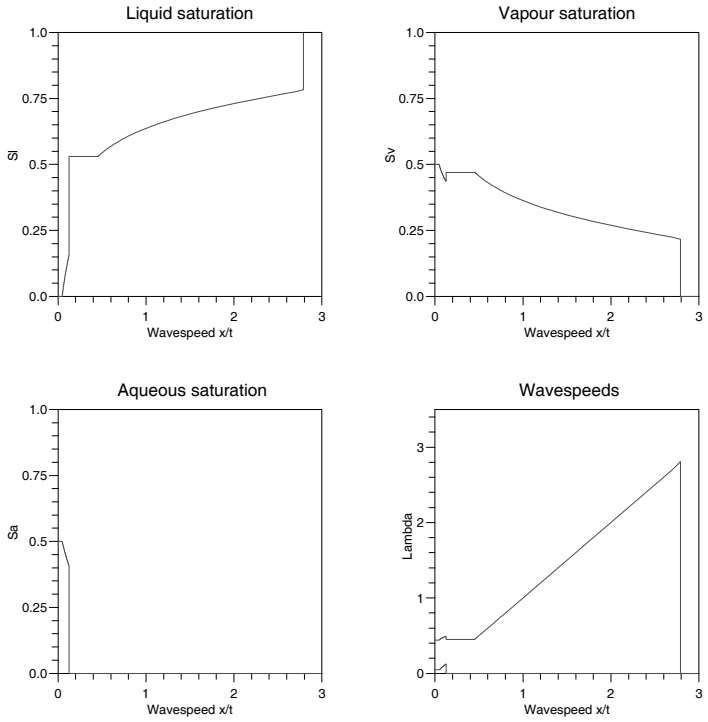

Figure 5.20: The analytic solution for problem 2 showing a 1-rarefaction-shock compound wave and a faster 2-rarefaction-shock compound wave.

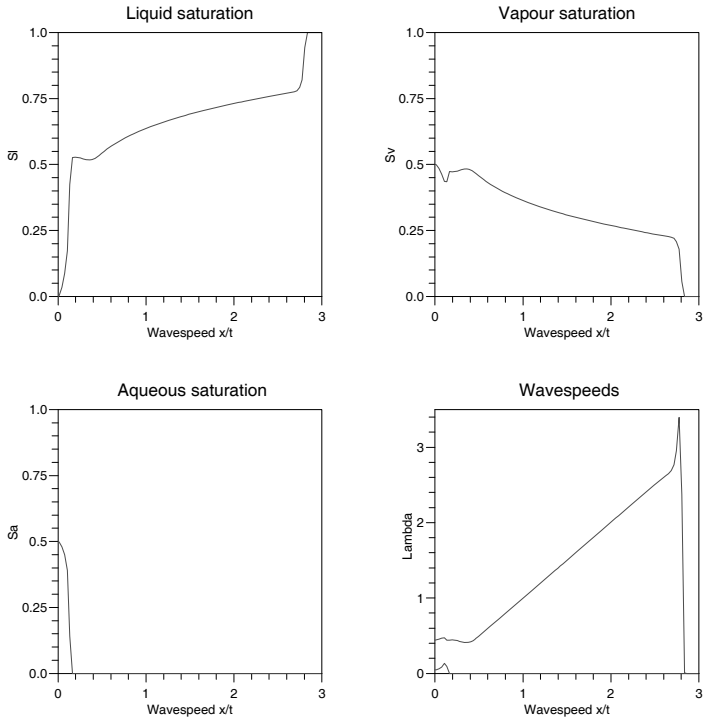

Figure 5.21: The numerical solution for problem 2 simulated using 100 grid blocks and a CFL number of 0.9.

The 2-rarefaction is tracked until a valid 2-shock can be found which connects the rarefaction to the initial reservoir state. A 2-shock with speed $\sigma = 2.791$ was found to accomplish this. The corresponding numerical results, again run with 100 grid blocks, are shown in Figure 5.21. The analytic solution contains some fine detail in the vapour saturation profile, the 1-rarefaction-shock poses a difficult test for the numerical method. The plots in Figure 5.21 show that the numerical method resolves this wave pattern fairly well. The spikes in the wavespeeds at the points of local linear degeneracy are again apparent.

Although the mathematical model describing 3-phase incompressible flow is a 2-system of equations with a conserved variable of two of the saturations, the Black-Oil model is a 3-system with a conserved variable of component density. When the Higher Order Godunov code is used to simulate the incompressible flow problems, we actually solve the 3-system for component density and compute the saturations from these results. The numerical results obtained agree well with the analytic solutions to the Riemann problem. The shocks in the problems are captured with the correct speed and the rarefaction waves are resolved accurately. The only deficiency associated with the numerical results are the spikes in the wavespeeds at the points of local linear degeneracy, however these are commonly observed in the numerical results of simulating such problems, for example [6] and [46].

5.5 Incorporation of Source Terms

The investigation of applying source terms in the Black-Oil model was prompted by the Areal (2-D) simulations, which were described in Chapter 4. In these problems the positions of the injection and production wells do not coincide with the nodes of the stencils of either the pressure equation or conservation law discretisations. Therefore the way of specifying injection and production fluxes was not clear and hence it was thought that injection and production of fluid would have to be modelled via point source terms in the relevant grid block centres. Use of a source term enables the pressure of the injected fluid and its injection rate to be specified whereas when boundary fluxes are used either one or the

other may only be specified, similarly with production of fluid. In the petroleum reservoir simulation community inflow and outflow of fluid are typically modelled by assigning all boundaries to be of no flow type and using source terms where appropriate. There is a lack of implementation details in the literature regarding source terms, especially in relation to the fluid model and numerical method we use.

The main problem associated with using source terms is one of stability. This arises through the fact that non-homogeneous conservation laws will have curved characteristics whereas in the homogeneous case these are straight. Therefore the CFL condition on stability, which is derived using straight characteristics, no longer applies and so explicit finite difference schemes must be operated at a lower CFL number. The required reduction of the CFL number depends on the stiffness of the source term and can represent a considerable increase in computational effort. For this reason implicit procedures are usually incorporated to remove the stability problem. A locally implicit approach is usually adopted and used only in those cells where variables associated with the well cells are used in the calculations.

Bell et al. [3] use a locally implicit procedure in their reservoir simulations modelled by a scalar hyperbolic conservation law, with an alternative Higher Order Godunov method, but no details are given. Whereas Holing et al. [26] provide some, but only minor, details of application of sources in their reservoir simulations using the Higher Order Godunov method applied to 2-D polymer flooding, which is modelled by a system of 2 conservation laws.

Inclusion of a source term in the mass conservation laws associated with the Black-Oil model results in the following non-homogeneous system in the 1-D case

$$\frac{\partial}{\partial t}(\mathbf{n}\phi) + \frac{\partial}{\partial x}(RB^{-1}\mathbf{v}) = RB^{-1}\mathbf{r},$$

where $\mathbf{r}$ is the vector of phase injection rates of fluid measured in day^{-1}. Production of fluid at a production well would be accomplished with a negative value of $\mathbf{r}$. A source term in the conservation laws means that an extra source term will also appear in the parabolic pressure equation since the conservation laws are substituted into the pressure equation in the course of its derivation. The

pressure equation now becomes

$$c\frac{\partial p}{\partial t} + \mathbf{w}^T \frac{\partial}{\partial x}(\mathbf{f}v_T + \mathbf{g}\tau) = q + \mathbf{w}^T RB^{-1}\mathbf{r}.$$

The additional source term here represents no problem in its numerical solution. However this is not the case when we come to solve the conservation laws as previously described. If we wish to model injection of fluid into the reservoir, then the source term will only appear in the equations associated with that grid block. Hence the implicit procedure to be described need only be used when variables associated with that grid block are used in the calculations.

The locally implicit procedure for a source in block j as outlined by Holing et al. [26] is as follows. The cell edge fluxes $\mathbf{h}_{j+\frac{1}{2}}$ and $\mathbf{h}_{j-\frac{1}{2}}$ are calculated as the first order upstream implicit fluxes. Therefore for flux $\mathbf{h}_{j+\frac{1}{2}}$ this means that if the fluid flow is into this cell edge from right to left then the flux calculation is explicit. If the flow is from left to right then the well cell variables will be needed to calculate the flux and hence the implicit procedure is needed. For example the implicit procedure for a constant source in cell j with flow from left to right would be

$$(\mathbf{n}\phi)_j^{n+\frac{1}{2}} = (\mathbf{n}\phi)_j^n - \frac{\Delta t}{2\Delta x}\left[\mathbf{h}(\mathbf{n}_j^{n+\frac{1}{2}}, p_{j+\frac{1}{2}}^{n+\frac{1}{2}}, (v_T)_{j+\frac{1}{2}}^{n+\frac{1}{2}}) - \mathbf{h}_{j-\frac{1}{2}}^{n+\frac{1}{2}}\right] + \frac{\Delta t}{2}\mathbf{s}_j^n, \qquad (5.5.6)$$

where $\mathbf{s}_j^n$ is the source term. The flux $\mathbf{h}_{j-\frac{1}{2}}^{n+\frac{1}{2}}$ is calculated to second order, explicitly in the usual manner as the well cell is not upstream for this flux calculation. Equation (5.5.6) is implicit in $\mathbf{n}_j^{n+\frac{1}{2}}$ and so we need to solve it by an iterative method. Hence the main idea behind the procedure is calculation of an implicit well cell flux rather than an implicit update of the component density in the well cell. Once the unknown $\mathbf{n}_j^{n+\frac{1}{2}}$ has been calculated the flux $\mathbf{h}_{j+\frac{1}{2}}^{n+\frac{1}{2}}$ may be recalculated explicitly using $\mathbf{n}_j^{n+\frac{1}{2}}$ and used in the usual finite difference update procedure, which will also include the source term, i.e.

$$(\mathbf{n}\phi)_j^{n+1} = (\mathbf{n}\phi)_j^n - \frac{\Delta t}{\Delta x}\left[\mathbf{h}_{j+\frac{1}{2}}^{n+\frac{1}{2}} - \mathbf{h}_{j-\frac{1}{2}}^{n+\frac{1}{2}}\right] + \Delta t\ \mathbf{s}_j^n.$$

The modelling of injection and production of fluid in a 1-D reservoir simulation was tried using point source terms. Firstly injection of fluid will take place via a source term in the centre of grid block 1 and hence the flux $\mathbf{h}_{j-\frac{1}{2}}$ (with $j = 1$) in

(5.5.6) will be zero as that cell boundary corresponds to $x = 0$ and is assigned to be of no-flow type. The source term in this case is

$$\mathbf{s} = RB^{-1}\mathbf{r}_{inj},$$

where $\mathbf{r}_{inj}$ is the vector of fluid phase injection rates. The matrix RB^{-1} indicates the injected fluid composition at reservoir conditions. Equation (5.5.6) was solved iteratively for $\mathbf{n}_1^{n+\frac{1}{2}}$ using simple iteration, i.e. we iterated on each component equation of (5.5.6) at a time. The first iterate was provided by the component density in cell 1 at the current time level, i.e. $\mathbf{n}_1^n$. The simulation problem used to test the implicit technique was as follows. The initial reservoir component densities were

$$\mathbf{n}_{res} = \begin{bmatrix} 0.703 \\ 70.3 \\ 0.0502 \end{bmatrix},$$

at a pressure of 1800 psi. The injected fluid had a composition of

$$\mathbf{n}_{inj} = \begin{bmatrix} 0.0414 \\ 66.23 \\ 0.497 \end{bmatrix},$$

at a pressure of 2000 psi and was injected at a total rate of 0.1 day^{-1}. The individual phase rates being distributed by their mobility weighting. The production pressure was held at 1600 psi. This problem corresponds to problem 1 from [46] except that an injection rate is also specified here. The iteration in grid block 1 to solve for $\mathbf{n}_1^{n+\frac{1}{2}}$ was performed to a tolerance of 1.0×10^{-6} with about 11 iterations needed at each time step to reach convergence once the simulation had settled down. The results of the simulation, with the locally implicit method, using 100 grid blocks and a CFL number of 0.9 are shown at 50 days in Figure 5.22. The corresponding results using a totally explicit algorithm with a CFL number of 0.9 are shown in Figure 5.23.

The two sets of results compare well, however a small boundary effect occurs with the explicit treatment of the source. There is an unsmooth transition in the gas and water component densities over the first few grid blocks when the explicit formulation is used. The corresponding region when the implicit formulation is

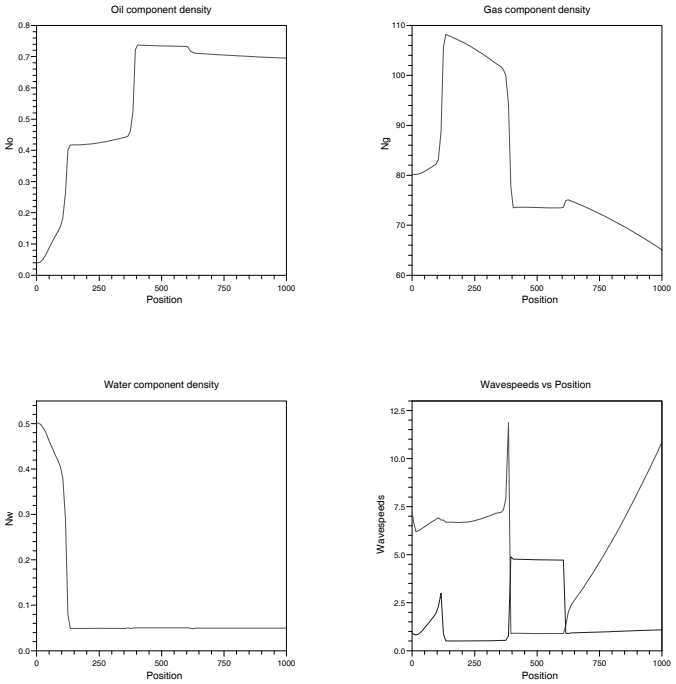

Figure 5.22: Numerical results of the 1-D source problem at 50 days using the implicit treatment of the injection source simulated with 100 grid blocks and a CFL number of 0.9.

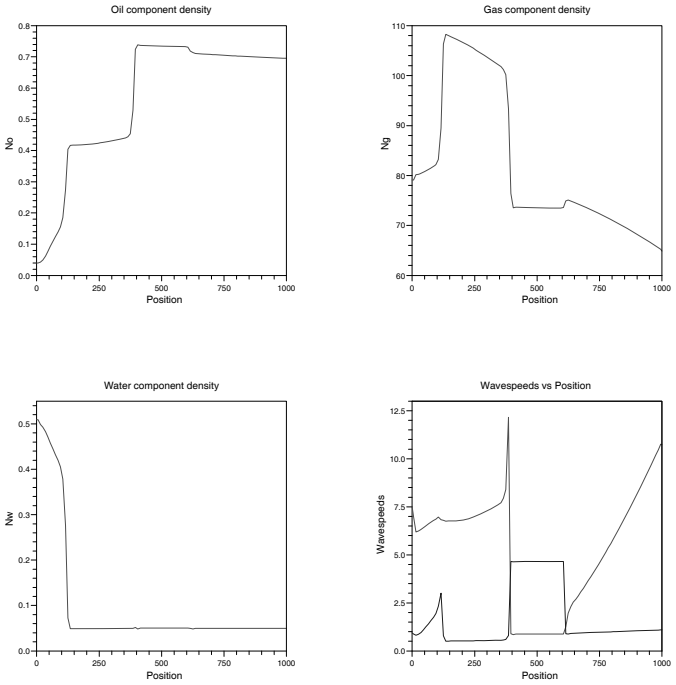

Figure 5.23: Numerical results of the 1-D source problem at 50 days using the explicit treatment of the injection source simulated with 100 grid blocks and a CFL number of 0.9.

used is smooth, an improvement on the results from the explicit case. The results consist of two rarefaction-shock compound waves connecting to a constant state at about 400 feet. The region from 400 to 600 feet is an undersaturated region, hence the discontinuity in the slower wavespeed at these distances. This problem cannot be simulated using boundary fluxes rather than source terms, for comparison of results purposes, since both the pressure of the injected fluid and its injection rate may not simultaneously be specified.

In using the explicit second order flux calculation it should be noted that the source term in the conservation laws will appear in the characteristic tracing step of the Higher Order Godunov procedure. This is because the quasi-linear form of the conservation laws are used in that step of the computation. When we perform the characteristic tracing step we neglect the source term from that step since its inclusion causes unphysical solution behaviour. This can be justified since the presence of the source term causes the characteristics to be modified so instead of deriving these modified characteristics we simply neglect the source term.

We now discuss the modelling of a production source to model production of fluid from a production well. The source term will be located in cell Nx where Nx is the total number of grid blocks used in the simulation. The composition of the fluid being produced is the composition of the fluid that resides in cell Nx. The implicit flux calculation is of the form

$$(\mathbf{n}\phi)_{Nx}^{n+\frac{1}{2}} = (\mathbf{n}\phi)_{Nx}^{n} - \frac{\Delta t}{2\Delta x}\left[\mathbf{h}_{Nx+\frac{1}{2}}^{n+\frac{1}{2}} - \mathbf{h}_{Nx-\frac{1}{2}}^{n+\frac{1}{2}}\right] + \frac{\Delta t}{2}\mathbf{s}_{prod}^{n},$$

where $\mathbf{s}_{prod}^{n}$ is the source term representing the production fluid. The flux $\mathbf{h}_{Nx+\frac{1}{2}}^{n+\frac{1}{2}}$ is zero since the boundary at $x = x_{max}$ is of no-flow type. The flux $\mathbf{h}_{Nx-\frac{1}{2}}^{n+\frac{1}{2}}$ may be calculated explicitly to second order accuracy since the production source is not upstream with respect to the cell interface $Nx-\frac{1}{2}$. Hence the resulting equation is not implicit in $\mathbf{n}_{Nx}^{n+\frac{1}{2}}$ and hence need not be solved since the normal explicit update may be used instead, i.e.

$$(\mathbf{n}\phi)_{Nx}^{n+1} = (\mathbf{n}\phi)_{Nx}^{n} - \frac{\Delta t}{\Delta x}\left[-\mathbf{h}_{Nx-\frac{1}{2}}^{n+\frac{1}{2}}\right] + \Delta t\ \mathbf{s}_{prod}^{n}.$$

A totally implicit update of $\mathbf{n}_{j}^{n+1}$, using a first order implicit upstream flux $\mathbf{h}_{j+\frac{1}{2}}^{n+1}$, was also tried instead of the implicit flux calculation of $\mathbf{h}_{j+\frac{1}{2}}^{n+\frac{1}{2}}$. The implicit

update for a source in cell j is then of the form

$$(\mathbf{n}\phi)_j^{n+1} = (\mathbf{n}\phi)_j^n - \frac{\Delta t}{\Delta x}\left[\mathbf{h}(\mathbf{n}_j^{n+1}, p_{j+\frac{1}{2}}^{n+1}, (v_T)_{j+\frac{1}{2}}^{n+1}) - \mathbf{h}_{j-\frac{1}{2}}^{n+\frac{1}{2}}\right] + \Delta t\ \mathbf{s}_j^n, \qquad (5.5.7)$$

where the source term is upstream with respect to cell edge $j+\frac{1}{2}$ so that (5.5.7) is implicit in $\mathbf{n}_j^{n+1}$. However this procedure was not effective at modelling source terms since the iteration, of simple type, used to solve (5.5.7) would not converge.

The implicit flux calculation was also used to model a source term in the Areal 2-D problem. In this problem injection of fluid takes place in the lower left hand grid block and production of fluid in the upper right hand grid block. Also there are no gravitational effects in the problem. The production source may be incorporated explicitly as the well cell is not upstream for the relevant flux computations, similarly to the 1-D case. The injection source is located in grid block 1,1. The implicit flux calculation to model the source is as follows

$$\begin{aligned}(\mathbf{n}\phi)_{1,1}^{n+\frac{1}{2}} = (\mathbf{n}\phi)_{1,1}^n &- \frac{\Delta t}{2\Delta x}\left[\mathbf{h}(\mathbf{n}_{1,1}^{n+\frac{1}{2}}, p_{\frac{3}{2},1}^{n+\frac{1}{2}}, (v_T)_{\frac{3}{2},1}^{n+\frac{1}{2}})\right] \\ &- \frac{\Delta t}{2\Delta y}\left[\mathbf{g}(\mathbf{n}_{1,1}^{n+\frac{1}{2}}, p_{1,\frac{3}{2}}^{n+\frac{1}{2}}, (v_T)_{1,\frac{3}{2}}^{n+\frac{1}{2}})\right] + \frac{\Delta t}{2}\mathbf{s}_{inj}^n. \qquad (5.5.8)\end{aligned}$$

The fluxes $\mathbf{h}_{\frac{1}{2},1}$ and $\mathbf{g}_{1,\frac{1}{2}}$ are both zero as they lie on no-flow boundaries. The Areal problem usually takes place on a square computational domain and hence the problem is usually simulated with the same number of grid blocks in both coordinate directions hence $\Delta x = \Delta y$. This also means that the fluxes out of block 1,1 namely $\mathbf{h}_{\frac{3}{2},1}$ and $\mathbf{g}_{1,\frac{3}{2}}$ are equal, assuming we have a homogeneous medium, which simplifies the iterative procedure. In fact the problem is symmetric about the diagonal connecting the injection and production wells.

The 2-D Areal simulation problem had the same injection, initial reservoir and production parameters as the 1-D source problem except that the total injection rate was 4.0 day^{-1}. The problem was simulated with a 40×40 grid and a CFL number of 0.9, the tolerance to which we calculate $\mathbf{n}_{1,1}^{n+\frac{1}{2}}$ being 1.0×10^{-4}. The simulation with the explicit treatment of the source generated unacceptably high discrepancies of $O(10^{-1})$ and therefore these results were considered too unphysical and so the simulation problem was repeated using a lower CFL number. Even at a CFL number of 0.5 the unacceptably high discrepancies were still produced, with these results being shown in Figure 5.24, the problem having been simulated

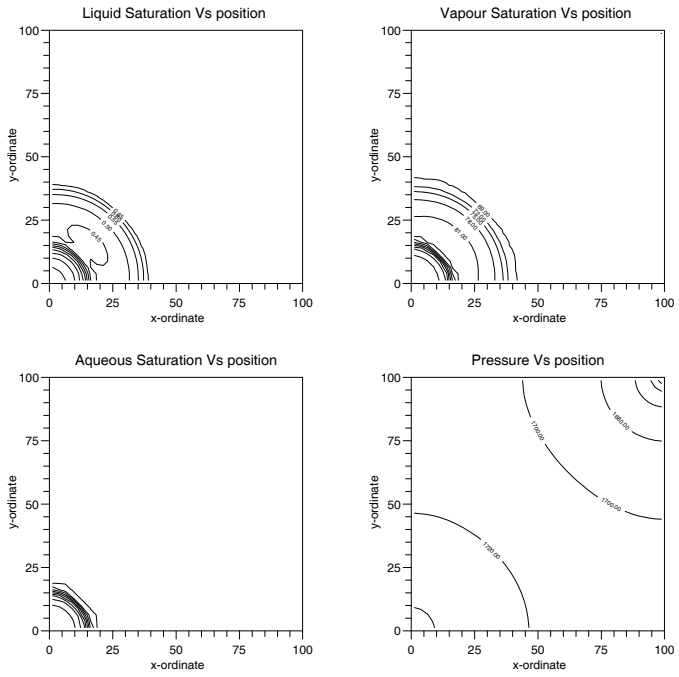

Figure 5.24: Numerical results of the 2-D Areal source problem at 3 days using the explicit treatment of the injection source simulated with a 40×40 grid and using a CFL number of 0.5.

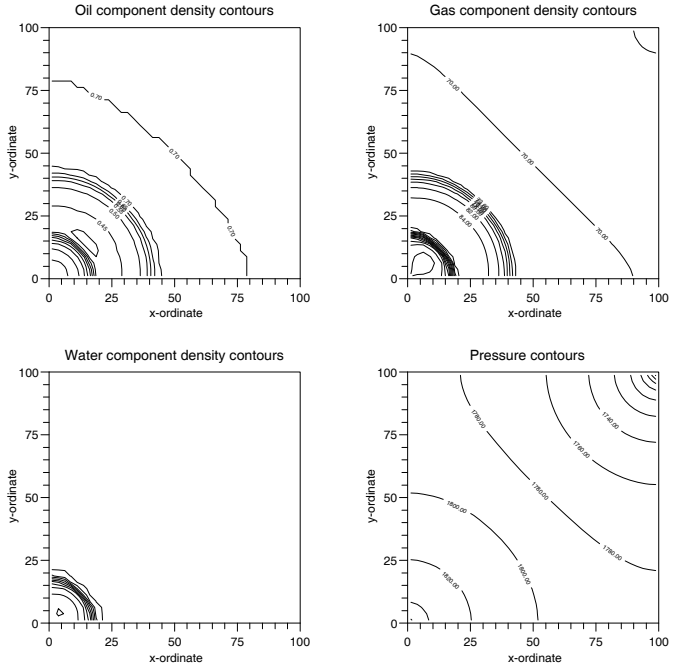

Figure 5.25: Numerical results of the 2-D Areal source problem at 3 days using the implicit treatment of the injection source simulated with a 40×40 grid and using a CFL number of 0.9.

for 3 days. Simulating the problem with the explicit treatment of the source at a lower CFL number would be prohibitively expensive even if the discrepancies were decreased. The results with the implicit treatment of the source are shown in Figure 5.25, with about 11-15 iterations needed to achieve convergence of the iteration (5.5.8) once the computation had settled down.

The two sets of results show a marked difference, which is due to the unacceptably large volume error discrepancies being generated in the results of the explicit treatment of the injection source term.

In 1-D the implicit treatment of the source term used to model injection of fluid into the reservoir has been shown to give improved results compared to an explicit treatment. No reduction of the CFL number is necessary with the implicit treatment. In 2-D the improvement when the implicit treatment is used is more apparent. The explicit treatment of an injection source produces unphysical results even at reduced CFL numbers. The implicit treatment of the source enables the simulation to generate reasonable results in terms of the magnitude of the volume error discrepancies and again can be run with a CFL number of 0.9.

In the next chapter we investigate the impact of the volume error discrepancy on the numerical results, which results from the splitting of the flow equations, and describe potential methods of reducing it.

Chapter 6

The Impact and Reduction of the Volume Error Discrepancy

6.1 Introduction

The work in this chapter concerns the volume error discrepancy associated with the splitting of the flow equations into hyperbolic and parabolic parts, namely equations (3.5.8) and (3.4.6). The resulting volume error discrepancy essentially indicates how well the equation of state, or volume balance equation, is satisfied in terms of pressure but more importantly indicates the error associated with the splitting methodology. These errors must therefore be kept as low as possible and controlled where necessary. In this chapter the impact of the volume error discrepancy is investigated as are two potential methods of reducing it.

The impact of the volume error discrepancy on the numerical results of reservoir simulations has not, as far as we know, been investigated. We perform this investigation for 2-component 2-phase flow since a Black-Oil model without an inherent volume error discrepancy [5] exists for this situation. This model is the forerunner to the more general Black-Oil model with which we are working with elsewhere in this thesis, which does have an inherent volume error discrepancy. Comparisons of the numerical results from both formulations, with and without the inherent volume error discrepancy, are made by simulating 2-component 2-phase problems within the 3-component 3-phase Black-Oil model by setting the relevant fluid component, water in this case, to zero. These comparisons are made

and assessed in the next section of this chapter.

The system of conservation laws in the Black-Oil model are discretised to second order accuracy in both space and time whereas the pressure equation is only discretised to first order in time but having the same spatial accuracy. A formally second order accurate overall algorithm would therefore require a more accurate prediction of pressure. Achievement of second order time accuracy for pressure is possible in such a non-linear parabolic equation by using a predictor corrector approach, otherwise this accuracy could only be obtained using non-linear iteration. Although the predictor corrector procedure can itself be regarded as a non-linear iteration only one extra iteration would be needed for an additional corrector step compared to iterating to a given tolerance on pressure. This predictor corrector procedure is applied and investigated in terms of the effect on the volume error discrepancy and the extra computation required.

In the 2-component 2-phase Black-Oil model [5] the pressure field is obtained by direct solution of the volume balance equation, which is straightforward for this model. This is in contrast to the 3-component 3-phase Black-Oil model [46] in which the pressure field is obtained from the parabolic pressure equation which was derived from the linearisation of the volume balance equation. Experience of the model in [5] provided the idea of solving the volume balance equation for pressure in the 3-phase Black-Oil model to reduce the volume error discrepancy. In this case the volume balance equation is non-linear in pressure and has to be solved iteratively, which is done at the end of the time step. This procedure results in a corrected pressure field which has the effect of substantially reducing the volume error discrepancy.

Another issue regarding the volume error discrepancy arises in reservoir simulations, using a thermal model developed by Trangenstein [48], which include highly compressible fluids. These problems have run into difficulties when the split methodology, i.e. a splitting of the flow equations as mentioned above, has been used, see [48]. Large volume error discrepancies were blamed for causing these difficulties and were stated by Trangenstein to be due to the large variations in compressibilities between the different fluid components. The effect of increased fluid compressibility in the Black-Oil model was investigated to ascer-

tain whether the same type of problem occurred and to offer possible remedies if needed.

6.2 Impact of the Volume Error Discrepancy

The impact of the volume error discrepancy on numerical results of reservoir simulations is assessed for 2-component 2-phase flow. The effect on the positioning and resolution of the fronts, if any, is of particular interest as is a general comparison of the results. The sequential (or split) solution methodology was first applied to 2-component 2-phase flow problems by Bell et al. [5], see Section 3.7. This model considers oil and gas fluid components and has a 'solution gas ratio' R_l only, i.e. the only mass transfer effect modelled is gas dissolving in oil. This formulation has no volume error discrepancy due to the simple nature of the volume balance equation which is a quadratic in pressure and hence can be solved exactly. The 2-component 2-phase problems with the volume error discrepancy can be simulated within the full 3-phase Black-Oil model [46] which does have an inherent volume error discrepancy, by setting the appropriate parameters, connected with the water component in this case, to zero. The corresponding problems without the volume error discrepancy can also be run within the full 3-phase Black-Oil model by making appropriate modifications to the algorithm so as to agree with that in [5].

In [5] Bell et al. calculated time steps for their computations by basing them on a maximum possible wavespeed. They calculated this maximum possible wavespeed based on the given relative permeability data and for all pressures between 500 and 4500 psi and for all possible fluid compositions. Hence it is unlikely that this wavespeed will appear in the computations and so Bell et al. state that they were operating at local CFL numbers which were considerably less than 1. We also calculate this maximum possible wavespeed and use it to determine the time steps to be used for the method. We also use this procedure to calculate time steps for the simulations with the volume error discrepancy. This was done so that the time steps used for both methods would be about the same and hence approximately the same amount of numerical diffusion would be introduced by

both formulations. If this was not done then different amounts of diffusion would be introduced by the two methods and comparison of the results would not be so informative. It was found that the formulation of the model without the volume error discrepancy can be run with time steps calculated using the CFL criteria (2.5.3) with a CFL number of 0.9, however we still follow Bell et al. and use their method.

The first simulation problem from [5] was chosen to compare the formulations as the results of this problem contain some fine detail as well as two phase changes and so will be a good test of the numerical methods. We refer to this as problem number A1 in this chapter of the thesis. The Black-Oil model parameters used were those contained in Section 3.9 except for the following. The porosity ϕ was set to 1, the rock permeability κ was 1 milliDarcy and square saturation relative permeabilities were used for both phases. The numerical results shown below were simulated for 200 days with 100 grid blocks and a CFL number of 0.9 was used to further reduce the time step, as calculated in the description above. This ensures that we were using the same time stepping as in [5], where they quoted the number of time steps used by their method, so we could compare results. The initial component densities for this problem were

$$\mathbf{n}_{inj} = \begin{bmatrix} 0.0001 \\ 120.0 \end{bmatrix} \quad , \quad \mathbf{n}_{res} = \begin{bmatrix} 0.8 \\ 60.0 \end{bmatrix}.$$

The equation of state was used to determine the injection and initial reservoir pressures which to 2 decimal places, were

$$P_{inj} = 1900.09, \qquad P_{res} = 1436.29,$$

whilst the production pressure used was set at $P_{prod} = 1000$ psi. The results of simulating this problem with the formulations of the Black-Oil model with and without the volume error discrepancy are very similar so we overlay the two sets of results. This is shown in Figure 6.1, where the solid line indicates results without the volume error discrepancy and the crosses, results with the volume error discrepancy.

The results show a rarefaction-shock compound wave connecting to a constant state at around 35 feet which is the start of an undersaturated region which

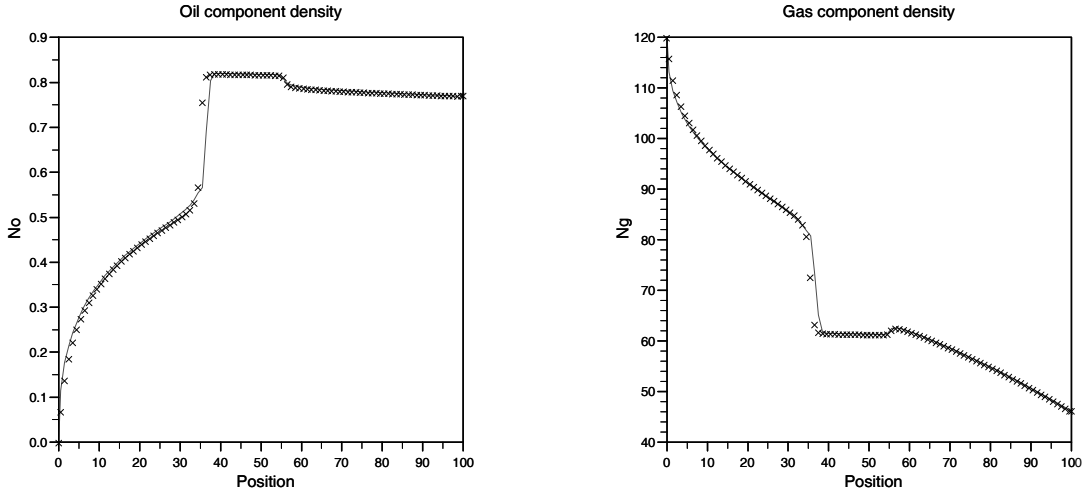

Figure 6.1: The oil and gas component densities from problem A1 simulated with 100 grid blocks and a CFL number of 0.9, solid line - with no volume error discrepancy, crosses - with the volume error discrepancy.

continues to about 55 feet. The results from the formulation with the volume error discrepancy were in good agreement with the very fine grid results from [5]. However small spikes were generated in the pressure fields when the volume balance equation was solved for pressure, during the course of some time steps, and were located at the positions of the phase changes in the problem. The pressure fields are not shown in [5] so we do not know whether Bell et al. encountered the same effect, which does not cause any difficulties in simulating the problems. The results from the formulation with the volume error discrepancy, were also in good agreement but the fronts were not located in the same positions, the same for the rarefactions, when compared to the results without the volume error discrepancy, the resolution of the fronts being comparable between the two sets.

As the two sets of results shown look almost identical we also plot the percentage differences between them, which are shown in Figure 6.2. It can be seen the differences between the two sets of results is significant at the front which is located at about 35 feet. This means that the front is slightly displaced as previously mentioned. A large difference in the oil component density occurs near the injection well at $x = 0$, this is due to the fact that larger discrepancies exist

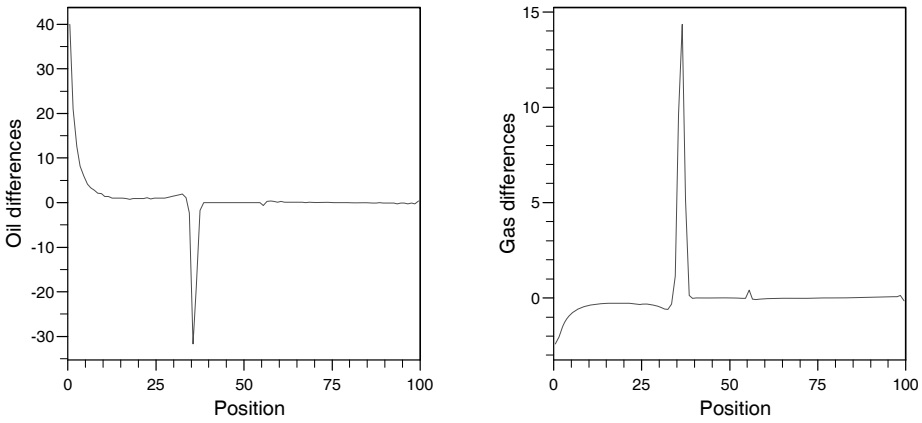

Figure 6.2: The percentage differences between the oil and gas component densities obtained from simulating problem A1 with and without the volume error discrepancy (100 grid blocks).

there, compared to other smooth regions of the flowfield, so the differences in the pressure fields is greater there, which ultimately effects the mass fluxes in this region.

It is therefore concluded that the formulation of the Black-Oil model with the inherent volume error discrepancy provides a good approximation to the more physically accurate flow behaviour, at least for the 2-component 2-phase problems, even though discrepancies as large as $O(10^{-2})$ were occasionally generated at the phase changes in these problems. Therefore use of the formulation without the inherent volume error discrepancy is not essential for a 2-component 2-phase simulation of acceptable physical accuracy, simulation of the other 2 problems from [5] support this.

6.3 Second Order Pressure Correction

The discretisation of the parabolic pressure equation is second order accurate in space but only first order accurate in time. A truly second order algorithm would therefore require a more accurate time discretisation of the pressure equation. The reason for first order time accuracy is that the spatial derivatives of pressure, and the fluid composition dependent coefficients in the discretisation (5.2.1) are not centred in time. Such a discretisation would result in a pressure equation

which would need to be solved by a non-linear iteration and thus would add considerable computational complexity since the coefficients in the equation would have to be updated every iteration. Trangenstein [49] justifies the reduced time accuracy by the fact that in secondary and tertiary recovery processes, which we are considering, the pressure field is slowly varying in time and hence the time truncation errors would not be expected to be too large. However a method does exist of obtaining second order time accuracy without the need of a non-linear iteration, namely a Predictor-Corrector approach. This method is described for general parabolic equations by Douglas and Dupont [15], who use a Galerkin formulation of the problem. We use a finite difference analogue of the Galerkin method given in [15] to investigate the second order pressure correction technique. The effect of this procedure on the volume error discrepancy is of particular interest since Trangenstein claims in [48] that the method should reduce the volume error discrepancy without claiming to have implemented it.

To aid the description we recall that the parabolic pressure equation is of the form

$$c\frac{\partial p}{\partial t} + \mathbf{w}^T \frac{\partial}{\partial x}(\mathbf{f}v_T + \mathbf{g}\tau) = q,$$

with the total velocity v_T being given by

$$v_T = [-\frac{\partial p}{\partial x} + \gamma]\tau,$$

where the coefficients in these equations are given explicitly in Section 3.4. The standard first order Backward-Euler time discretisation of the pressure equation is as follows

$$c_j^n(p_j^{n+1} - p_j^n) + \frac{\Delta t}{\Delta x}(\mathbf{w}^T)_j^n[\mathbf{f}_{j+\frac{1}{2}}^n(v_T)_{j+\frac{1}{2}}^{n+1} + \mathbf{g}_{j+\frac{1}{2}}^n\tau_{j+\frac{1}{2}}^n - \mathbf{f}_{j-\frac{1}{2}}^n(v_T)_{j-\frac{1}{2}}^{n+1} - \mathbf{g}_{j-\frac{1}{2}}^n\tau_{j-\frac{1}{2}}^n]$$
$$= \Delta t q_j^n, \qquad (6.3.1)$$

with the following discretisation of total velocity

$$(v_T)_{j+\frac{1}{2}}^{n+1} = \left[-\frac{(p_{j+1}^{n+1} - p_j^{n+1})}{\Delta x} + \gamma_{j+\frac{1}{2}}^n\right] \tau_{j+\frac{1}{2}}^n. \qquad (6.3.2)$$

In these equations the coefficients dependent on pressure and component density, i.e. c, $\mathbf{w}$, $\mathbf{f}$, $\mathbf{g}$, γ, q and τ, must be evaluated at the current time level, since at this stage of the computation nothing at the next time level is known. If these

coefficients and the total velocities at the cell edges $(v_T)_{j+\frac{1}{2}}$ were evaluated at the half time level in both (6.3.1) and (6.3.2), a Crank-Nicholson type of finite difference approximation would arise, which gives second order accuracy in space and time. Douglas and Dupont [15] introduced a Predictor-Corrector approach to obtaining second order accuracy in such parabolic equations. For the parabolic equation we use, the predictor step is given by

$$c_j^n(\overline{p}_j^{n+1} - p_j^n) + \frac{\Delta t}{\Delta x}(\mathbf{w}^T)_j^n[\mathbf{f}_{j+\frac{1}{2}}^n(v_T)_{j+\frac{1}{2}}^{n+\frac{1}{2}} + \mathbf{g}_{j+\frac{1}{2}}^n\tau_{j+\frac{1}{2}}^n - \mathbf{f}_{j-\frac{1}{2}}^n(v_T)_{j-\frac{1}{2}}^{n+\frac{1}{2}} - \mathbf{g}_{j-\frac{1}{2}}^n\tau_{j-\frac{1}{2}}^n]$$
$$= \Delta t q_j^n, \tag{6.3.3}$$

with the total velocity at the half time level given by

$$(v_T)_{j+\frac{1}{2}}^{n+\frac{1}{2}} = \left[-\frac{\frac{1}{2}(\overline{p}_{j+1}^{n+1} + p_{j+1}^n) - \frac{1}{2}(\overline{p}_j^{n+1} + p_j^n)}{\Delta x} + \gamma_{j+\frac{1}{2}}^n\right]\tau_{j+\frac{1}{2}}^n, \tag{6.3.4}$$

where $\overline{p}^{n+1}$ is the predicted pressure and we define

$$p_j^{n+\frac{1}{2}} = \frac{1}{2}(p_j^n + \overline{p}_j^{n+1}).$$

The corrector equation takes the following form

$$c_j^{n+\frac{1}{2}}(p_j^{n+1} - p_j^n) + \frac{\Delta t}{\Delta x}(\mathbf{w}^T)_j^{n+\frac{1}{2}}[\mathbf{f}_{j+\frac{1}{2}}^{n+\frac{1}{2}}(v_T)_{j+\frac{1}{2}}^{n+\frac{1}{2}} + \mathbf{g}_{j+\frac{1}{2}}^{n+\frac{1}{2}}\tau_{j+\frac{1}{2}}^{n+\frac{1}{2}} -$$
$$\mathbf{f}_{j-\frac{1}{2}}^{n+\frac{1}{2}}(v_T)_{j-\frac{1}{2}}^{n+\frac{1}{2}} - \mathbf{g}_{j-\frac{1}{2}}^{n+\frac{1}{2}}\tau_{j-\frac{1}{2}}^{n+\frac{1}{2}}] = \Delta t q_j^{n+\frac{1}{2}}, \tag{6.3.5}$$

with the total velocity at the half time level given by

$$(v_T)_{j+\frac{1}{2}}^{n+\frac{1}{2}} = \left[-\frac{\frac{1}{2}(p_{j+1}^{n+1} + p_{j+1}^n) - \frac{1}{2}(p_j^{n+1} + p_j^n)}{\Delta x} + \gamma_{j+\frac{1}{2}}^{n+\frac{1}{2}}\right]\tau_{j+\frac{1}{2}}^{n+\frac{1}{2}}. \tag{6.3.6}$$

The coefficients in the corrector are now evaluated at the half time level, i.e. with $p_j^{n+\frac{1}{2}}$. The corrector step should be performed after the update of the conservation laws which uses the predicted pressure $\overline{p}_j^{n+1}$, so that the component densities at the half time level may be calculated and used to evaluate the coefficients needed in the corrector step. In the remainder of this section we abbreviate the second order pressure correction technique by SOPC.

The term on the right hand side of the pressure equation is

$$q = \frac{(\mathbf{e}^T\mathbf{u} - 1)}{\Delta t}\,\phi,$$

and needs special consideration. This is because the Taylor series linearisation of the volume balance equation, used to derive the pressure equation, dictates that the volume discrepancy term in q should be evaluated at the current time level n rather than the half time level $n + \frac{1}{2}$ as in the corrector (6.3.5). Therefore the discrepancy term $\mathbf{e}^T\mathbf{u} - 1$ must be treated as a constant and only the porosity term ϕ evaluated at the time level $n + \frac{1}{2}$ in the q term in (6.3.5).

Douglas and Dupont point out that the dependent variable p and the coefficients c, $\mathbf{w}$, $\mathbf{f}$ etc. in the parabolic equation must satisfy certain continuity and boundedness properties for the Galerkin formulation of the predictor corrector approach to achieve second order time accuracy. If the continuity property is not maintained for the coefficients in the pressure equation then a time accuracy of one and a half is obtained, i.e. $O(\Delta t^{\frac{3}{2}})$, after the predictor corrector technique has been applied. Douglas and Dupont then state that a further pass through the corrector will achieve the desired second order time accuracy. In the finite difference case the continuity of the coefficients has a greater consequence on the accuracy of the scheme. For instance if one or more of the coefficients is discontinuous at a given point then the Taylor series expansion of that coefficient is not valid. Hence the truncation error analysis does not follow through as in the continuous case and the numerical scheme looses its formal order of accuracy at discontinuous points. In the finite difference case a further pass through the corrector will not increase the formal order of accuracy at the discontinuous points as the formal order of accuracy is lost in both the predictor and corrector equations.

Use of the SOPC technique to achieve second order accuracy in time is consistent with the derivation of the pressure equation since the error in the Taylor series linearisation of the volume balance equation is $O(\Delta t)^2$. The error in the derivation of the pressure equation can be reduced by adding the extra term in the Taylor series expansion of the volume balance equation. However that introduces a $\frac{\partial^2 p}{\partial t^2}$ term into the pressure equation which means then that the equation has lost its parabolic character. Hence adding the higher order term in the derivation of the pressure equation is not a possibility since the pressure field in reservoir fluid flow is known to have parabolic character.

The SOPC procedure was applied to both a saturated and undersaturated fluid flow problem to assess its effect. The problems were simulated with 100 grid blocks and using a CFL number of 0.9. Small oscillations were introduced by the method into the pressure fields from both problems near the injection and production wells, i.e. unphysical behaviour was introduced. Figure 6.3 shows the pressure and gas component density from problem 1 from [46] using the SOPC technique, we refer to this as problem number A2 which we defined in Chapter 5. The oscillations in the pressure field near the injector (at $x = 0$) and the producer (at $x = 1000$) are clearly visible, which also causes oscillation in the gas component density field. A similar kind of effect occurred with the undersaturated problem, which was problem 3 from [46], our reference, problem A3.

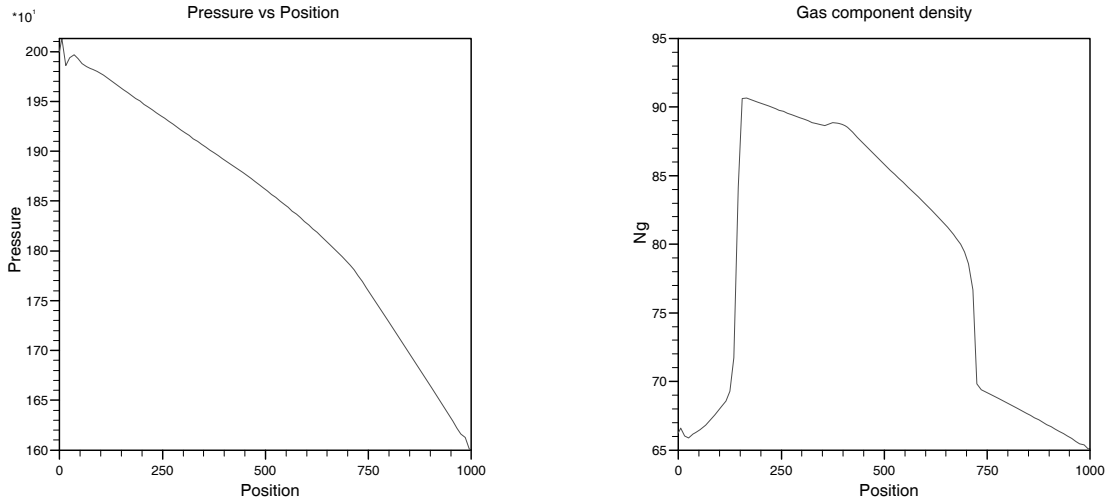

Figure 6.3: The pressure and gas component density fields obtained from simulating problem A2 with 100 grid blocks using the SOPC technique with a CFL number of 0.9.

The oscillation in the pressure field, which can also cause oscillation in the component density field when the SOPC technique is applied, can be removed by controlling the growth of time steps early on in the computations. The simulations were supplied with an initial time step of 0.001 days, which was not allowed to increase by more than a factor of 1.5. This method of controlling the growth of time steps early on in the computations was described in Section 5.2.3. Using this

time step growth factor of 1.5 in conjunction with the SOPC technique enables the method to be used without generating any oscillation in the results, and was the largest factor possible such that the oscillations were removed from both simulations. Actually problem A2 only needed a maximum time step growth factor of 2.0. Use of these factors does not seriously increase the total number of time steps used during the simulations, for example problem A2 needed less than 10 extra time steps to complete the simulation, compared to simulating the problem without any restriction on the growth of the time step. If these time step growth factors are not used then it was found that the CFL number had to be reduced to as low as 0.1 in some cases for the SOPC technique to generate oscillation free results. The effect of the technique on the inherent volume error discrepancy may now be investigated.

The volume error discrepancies generated when the SOPC was used were compared to those generated without the SOPC technique, both simulations using the same maximum time step growth factor. The maximum volume error discrepancies generated at each time step were found to have been increased as much as an order of magnitude over the course of some time steps. Also the corrector equation was applied a number of times until a desired tolerance on pressure was met. A tolerance of 10^{-10} was chosen which usually required less than 10 applications of the corrector equation. Again the results obtained were similar to before, the discrepancies were not improved. A possible explanation for the lack of success of the technique could have been due to the averaging of the pressure and component density fields to give $p_j^{n+\frac{1}{2}}$ and $\mathbf{n}_j^{n+\frac{1}{2}}$, which are then used to calculate the coefficients at the half time level. Large volume error discrepancies could then possibly be introduced at the half time level resulting in unphysical coefficients, but this was not found to be the case. A pairing of both $\mathbf{n}_j^n$ and $\mathbf{n}_j^{n+1}$ with $p_j^{n+\frac{1}{2}}$ was used to calculate the coefficients needed in the corrector equation but neither of these modifications improved the results.

In 1-D simulations the solution of the pressure equation uses in the region of 5-15% of the total computation time. However in 2-D the solution of the pressure equation can take up to 20% of the total computation time. The larger computational time associated with higher dimensions is due to the fact that

in 1-D the pressure equation can be solved by a direct method but in higher dimensions an iterative method must be used to solve the resulting linear system. The above percentage time for the 2-D pressure equation is based on using a typical engineering tolerance of 0.1 psi, and would obviously increase if lower tolerances were used. Therefore the SOPC technique is less viable in dimensions higher than 1, even if it had been found to have been successful at reducing the volume error discrepancy.

Since the SOPC technique was not found to reduce the volume error discrepancy an alternative method was devised, which is similar to the SOPC procedure, to try to reduce the volume error discrepancy. This simply involved repeating the pressure equation at the end of the time step, i.e. after the first pass through the pressure equation and conservation laws, with the coefficients c, $\mathbf{w}$, $\mathbf{f}$, $\mathbf{g}$, γ, q and τ evaluated at the advanced time level. A reduction of the volume error discrepancy was expected since pressure at the advanced time level is now recalculated from the first order accurate in time prediction of pressure and component densities, both being at the advanced time level, whereas previously the pressure there was calculated with p and $\mathbf{n}$ both from the current time level. On implementation of this procedure however, the maximum volume error discrepancies generated at each time step were found to be of the same order of magnitude, namely usually $O(10^{-4})$ for the problems considered but more often than not were numerically larger. There is no obvious explanation for this behaviour.

In the next section we discuss a successful method of reducing the volume error discrepancy that is also less computationally demanding. This method is based on a local calculation to correct the pressure field rather than the global calculation associated with the SOPC technique.

6.4 Iterative Solution of the Volume Balance Equation

The volume balance equation $\mathbf{e}^T\mathbf{u} = 1$ is a non-linear equation involving pressure and component density, however the possibility exists of solving it for pressure by an iterative method, such as Newton's method. This procedure would be

hoped to have the effect of substantially reducing the volume discrepancy errors. Controlling these errors is thought to be important in problems involving highly compressible fluids, such as steam in thermal simulations [48]. The volume error discrepancy also indicates the deviation in some sense of the numerical solution from the true physical solution behaviour, and so a high volume error discrepancy means that unacceptable errors have been introduced into the results. The results of test problems from [46] and those from [5] when run with the volume error discrepancy formulation, indicate that the highest volume discrepancies occur around phase changes. The errors are worse for problems involving 1-phase/2-phase fluid boundaries such as in the simulation problems from [5]. The reservoir model in [5] is a 2-phase (liquid, vapour), 2-component (oil, gas) model with a solution gas ratio (R_l) only. In this formulation the volume balance equation amounts to a quadratic in pressure and hence can be solved exactly so that volume error discrepancies do not arise.

The pressure computed from the parabolic pressure equation is only approximate since the equation was obtained from the linearisation of the volume balance equation. A technique to improve on this was introduced in the following way. After solving the pressure equation and conservation laws these results were used to determine the current state of phase equilibrium in each grid block at time level $n+1$. The volume balance equation (3.4.4) is then solved iteratively for pressure with the component densities as determined from the advancement of the conservation laws, using the pressure computed from the pressure equation as the first iterate. The resulting pressure from the local iterative solution of the volume balance equation is then assigned to be the pressure at time level $n+1$ and is consistent with the component densities there, the discrepancy having been made negligible.

The Newton iteration for pressure takes the following form

$$p^{\nu+1} = p^{\nu} - f(\mathbf{n}, p)/\frac{\partial f(\mathbf{n}, p)}{\partial p},$$

where $f(\mathbf{n}, p) = \mathbf{e}^T\mathbf{u} - 1 = 0$, and the component density vector $\mathbf{n}$ is held fixed and the superscript ν indicates the ν^{th} iterate. For saturated flow we have

$$f(\mathbf{n}, p) = B_l(n_o - R_v(n_g - R_a n_w)) - B_v(R_l n_o + R_a n_w - n_g) + (1 - R_l R_v)(B_a n_w - 1),$$

whilst for undersaturated flow with the vapour phase missing, $f(\mathbf{n}, p)$ becomes

$$f(\mathbf{n}, p) = \overline{B}_l(p, p_b)n_o + \overline{B}_a(p, p_b)n_w - 1,$$

and for undersaturated flow with the liquid phase missing

$$f(\mathbf{n}, p) = \overline{B}_v(p, \overline{R}_v)(n_g - R_a n_w) + B_a n_w - 1,$$

where, in this case, $\overline{R}_v$ is a function of pressure if water is present and gas is allowed to dissolve in the water.

The local iterative solution of the volume balance equation technique was first tried on problems 1 and 3 from [46] which are problems with no phase changes. Firstly problem 1 (which we have referred to as problem A2 and defined in Chapter 5) was simulated, using 100 grid blocks, with and without the volume error discrepancy reduction technique, with the maximum discrepancy errors being reduced from $\sim 10^{-4}$ to $\sim 10^{-10}$ with two iterations in each grid block. The two sets of results obtained look almost identical, so in Figure 6.4 we show the percentage differences between the two sets. Figure 6.4 indicates that the resulting

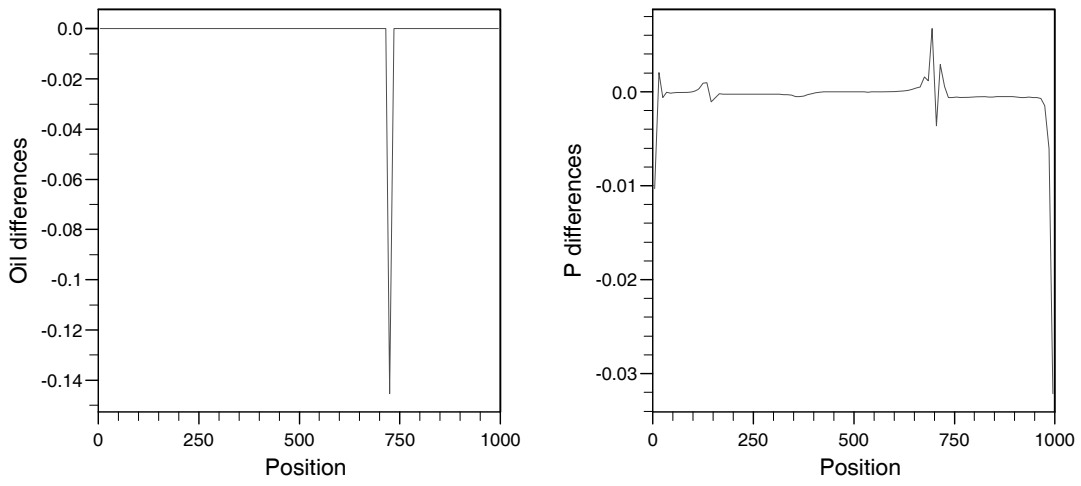

Figure 6.4: The percentage differences in the oil component density and pressure fields of problem A2, between the results of applying and not applying the discrepancy reduction technique.

corrected pressure field has very slightly shifted the second front in the problem.

The technique was then applied to an undersaturated flow problem, namely problem 3 from [46], (our reference A3 defined in Chapter 5), again with two

iterations in each grid block, the maximum errors being reduced still further compared to problem A2. The two sets of results look almost identical so we again only show the differences. Figure 6.5 shows the percentage differences between the two sets of results and shows that both fronts in the problem have been displaced very slightly. The technique was also tried on a saturated flow 2-D

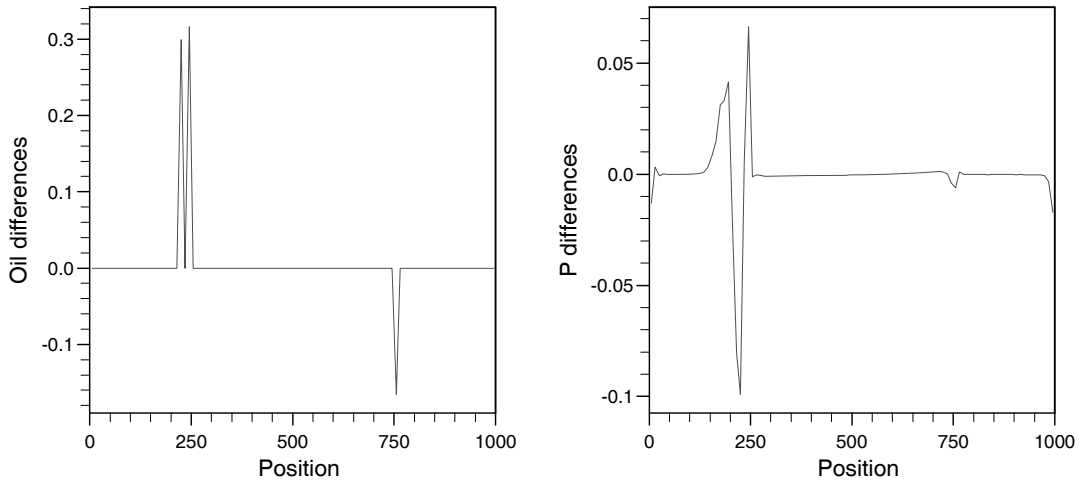

Figure 6.5: The percentage differences in the oil component density and pressure fields of problem A3, between the results of applying and not applying the discrepancy reduction technique.

Areal problem with the maximum discrepancy errors being reduced from $\sim 10^{-3}$ to $\sim 10^{-7}$ with 3 iterations in each grid block. These results will be discussed in the next chapter since they relate to the discussions therein.

The iteration was then tried on a mixed saturated/undersaturated flow problem 5 from [46], (our reference A4 defined in Chapter 5), again using 2 iterations. In Figure 6.6 we again shown the oil component density and pressure plots without the iteration, whilst Figures 6.7 show these plots with the iteration.

The resulting corrected pressure profile exhibits 'blips' which occur at the phase changes, these produce local large negative and positive total velocities, which are responsible for distortions in the wavespeeds at the phase changes. As well as resulting in unphysical solution behaviour, the technique was not so effective at reducing the discrepancy errors. This was because the highest discrepancies occur at the phase changes and hence the pressure needs a greater

modification there in order to satisfy the volume balance equation, hence the reason for the large changes needed in pressure at the phase changes. Therefore the problem of the unsmooth pressure profile with the 'blips', which in turn produces spurious wavespeeds, needs to be remedied.

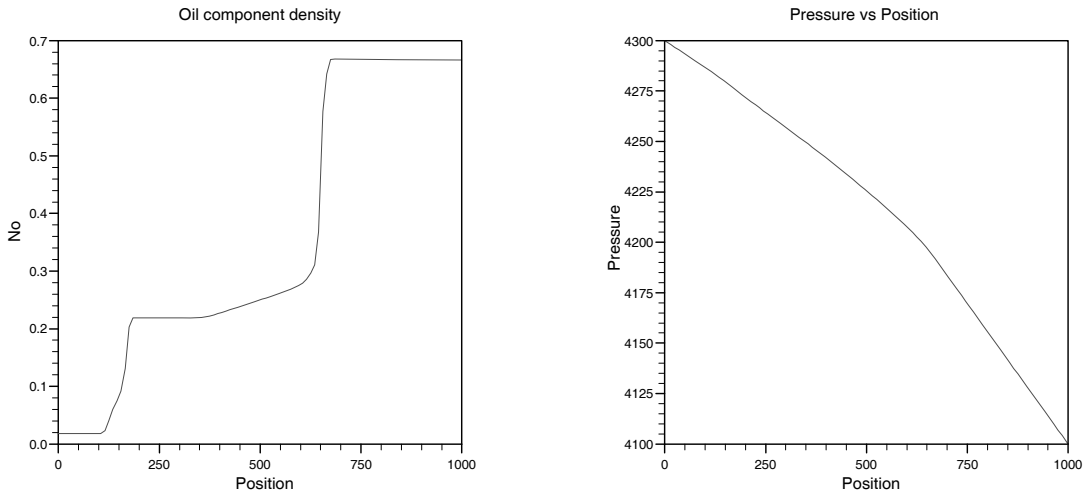

Figure 6.6: The oil component density and pressure fields obtained from a standard simulation of problem A4, using 100 grid blocks and a CFL number of 0.9.

Suppressing the iteration one grid point either side of the phase changes removes the 'blips' on the pressure profile. The resulting pressure profile was smooth, but we are left with the original volume discrepancy either side of the phase changes, the error in the regions of smooth flow having been reduced. As an alternative, iteratively solving the volume balance equation with respect to the component density at the phase changes should improve upon this by reducing the volume error discrepancy at the phase changes. This was implemented in the same fashion as with the pressure iteration, we iterate with respect to one of the component densities at a time, holding the others and pressure constant. For example in the case of iterating with respect to the oil component density n_o:

$$n_o^{\nu+1} = n_o^{\nu} - f(\mathbf{n}, p) / \frac{\partial f(\mathbf{n}, p)}{\partial n_o}.$$

When the flow is undersaturated the function f is also a function of the undersaturation parameter ω ($= p_b$ or $\overline{R}_v$), which itself is a function of component

density. Introducing iteration on the component densities at phase changes and iterating on pressure in regions of smooth flow had the desired effect in that the discrepancies at the phase changes were also reduced.

In this mixed flow problem we had to suppress the iteration for pressure two grid blocks either side of the phase changes, and iterate on the component densities instead, to ensure the resulting pressure field was smooth. Figure 6.8 shows plots of oil component density and pressure, when we suppressed the pressure iteration at the phase changes and instead iterated with respect to component density. The resulting discrepancy errors at the phase changes were reduced and the maximum errors over the course of the simulation were reduced to $\sim 10^{-8}$. The resulting corrected pressure profile is smooth, a large improvement on that in Figure 6.7. In this mixed flow example, it can be seen from Figure 6.9, that the fronts have been displaced to a greater extent than in the previous two simulation problems. This is due to the fact that higher discrepancies are associated with phase changes and hence the p and $\mathbf{n}$ variables need a greater correction to ensure satisfaction of the volume balance equation.

The results of applying the iterative solution of the volume balance equation technique has shown it to be successful for problems without any phase changes.

The technique is also successful for problems with phase changes when the modification just described is applied, i.e. solving the volume balance equation with respect to component density rather than pressure at the phase changes. However the modification of the component density vector $\mathbf{n}$ by iterating on the volume balance equation has a consequence in that conservation of mass is not maintained at these points. But the modification of the vector $\mathbf{n}$ to reduce the volume error discrepancy is usually small, namely less than 1.0%. Therefore loss of conservation of mass at the phase changes does not seem to pose a problem due to this small correction and since the results obtained in the process are qualitatively as before, the volume error discrepancy having been reduced substantially.

When the iteration on the volume balance equation is performed it is possible to reduce the discrepancy errors to below 10^{-6}, usually much lower. In such a case it is not unreasonable to assume that the volume balance equation is satisfied in terms of machine accuracy and hence exactly which means that p and $\mathbf{n}$ would not be independent, as mentioned in Section 3.6. Hence the effect of $\frac{\partial p}{\partial \mathbf{n}}$ should be included in the characteristic analysis, whereas at present it is assumed $\frac{\partial p}{\partial \mathbf{n}} = 0$. This would mean the characteristic analysis would have to be reformulated which is not within the scope of this thesis.

The method of reducing the volume error discrepancy described in this section was tried on the 2-component 2-phase problem from Section 6.2, (problem A1), which was used to compare the formulations of the method with and without the volume error discrepancy. This was done to assess the success of the technique to reduce the volume error discrepancy and hence whether its application leads to more physically accurate results, like those from the formulation with no volume error discrepancy. The reservoir problem in question exhibits two phase changes over the length of the reservoir, an undersaturated region lies between two saturated fluid regions. Hence the component density vector will be corrected instead of pressure at the phase changes. The results of this simulation are shown in Figure 6.10, all parameters being the same as in Section 6.2. These results are in closer agreement to those results from the no volume error discrepancy formulation shown in Figure 6.1 compared to those from the volume error discrepancy formulation without the discrepancy reduction also shown in Figure

6.1, we justify this statement below.

Although the three sets of results look very similar, tests on the norms of the differences between the solution values indicate that the results of applying the discrepancy reduction techniques gives results closer to those from the no volume error discrepancy formulation and hence more physically accurate results. We calculated both the 1 and 2-norms and found these both to have been reduced for course (50 blocks) and fine (100 blocks) grid simulations when the technique was used. The improvement being greater as the grid was coarsened. In Figure 6.11 we again show the percentage differences between the results without the volume error discrepancy (Figure 6.1) and with the discrepancy reduction (Figure 6.10). This Figure can be compared to Figure 6.2 in Section 6.2, and confirms that applying the discrepancy reduction techniques to the formulation of the Black-Oil model with the volume error discrepancy produces more physically accurate results for this problem. The third test problem from [5] was also simulated which confirmed the above findings. We also simulated the second problem from [5] but were unable to obtain as good an agreement with the results therein as with the first and third problems.

Results of applying the volume error discrepancy reduction techniques indicate that in terms of the effect on the numerical results, if the techniques are to be applied, then they are only necessary when problems with phase changes or maximum discrepancies of $O(10^{-3})$ or more are being simulated. Only when these types of problem are being considered is the pressure field, and the component density vector at phase changes, corrected a significant amount such that the results show a discernible difference to those from not applying the techniques. For example the fronts may be slightly displaced due to the modified pressure field as occurs with problem A4 in Figure 6.8.

The simulation problems used to investigate the reduction of the volume error discrepancy technique have all been performed using 100 grid blocks. The problems were repeated using a coarser grid of 20 blocks to assess the impact of the technique on coarser grids. The maximum volume error discrepancies generated using these coarse grids were usually of the same order of magnitude, although increased, compared to the 100 grid block simulations. Therefore the pressure,

and component density fields in the case of mixed flow problems, will need a greater correction. However the volume error discrepancy reduction technique does not have a significant impact on coarser grids due to the resulting level of volume error discrepancy not having been increased to $O(10^{-3})$ or more.

6.5 Effect of Increased Fluid Compressibility

We now look at the effect that a variation of fluid compressibilities has on the volume error discrepancy. Reservoir simulation with highly compressible fluid has been reported in the literature to cause some problems, particularly in a 2-component, 3-phase reservoir simulation model which includes thermal effects. This model, which was developed by Trangenstein [48], is similar to the Black-Oil model in that a splitting of the flow equations into a system of hyperbolic conservation laws and a parabolic pressure equation is performed.

Injection of steam, which is highly compressible, is an important tertiary oil recovery process, especially in the United States, therefore the simulation of such oil recovery processes is also important. However the numerical simulation of such processes has encountered difficulties with the particular formulation introduced by Trangenstein. The problems are stated in [48] to be due to the volume error discrepancy since larger volume error discrepancies were said to have been observed in steam flooding than those typically seen in Black-Oil simulations. The larger volume error discrepancies were stated to have caused unphysical backflow in the pressure equation which caused the simulation to abort. Trangenstein stated in [48] that the linearisation of the volume balance probably cannot handle the large variations in compressibility between the vapour (steam) and other phases. However these problems were not reported to have occurred with hot water flooding simulations. An investigation of the effects of increased compressibility in the context of the Black-Oil model was therefore needed to see if the same kinds of problem occurred. If the same problems are observed then the techniques of reducing the volume error discrepancy, described in the previous section, could be used to alleviate the problem.

The compressibility of each fluid component is given by

$$c_f = -\frac{1}{\rho}\frac{\partial \rho}{\partial p} = -B\frac{\partial}{\partial p}\left(\frac{1}{B}\right),$$

where p is the pressure, ρ is the density and B is the formation volume factor. Throughout this section we drop the negative sign associated with compressibility to simplify the discussion. We now derive expressions for the compressibilities of gas from the Black-Oil model and steam from the thermal model in order to compare the two. In the Black-Oil model the vapour formation volume factor is given by

$$B_v(p) = \frac{1}{(6 + 0.06p)}, \tag{6.5.7}$$

therefore the vapour compressibility is

$$c_v(p) = \frac{0.06}{(6 + 0.06p)}.$$

The steam density function is given by different functional forms over the pressure range, i.e.

$$\left(\frac{p}{p_b}\right)\frac{1}{\rho_v(p)} = \begin{cases} \frac{490.386}{p} - 0.04703 & \text{if } p \leq 1500 \text{ psi} \\ \frac{551.74}{p} - 0.0887 & \text{if } p > 1500 \text{ psi} \end{cases},$$

where ρ_v is the steam (vapour) density in lb ft^{-3}, p is the pressure and p_b is the bubble point pressure which is a function of the temperature. This is of the general form

$$\rho_v(p) = \frac{p^2}{p_b(a - bp)}, \tag{6.5.8}$$

where a and b are the constants above depending on which pressure interval p is in. The compressibility of steam in the thermal simulations is therefore given by

$$c_s(p) = \frac{2a - bp}{p(a - bp)}.$$

The compressibilities of steam from the thermal model and gas from the Black-Oil model are shown graphically in Figure 6.12, the steam compressibility can be seen to be an order of magnitude higher than that of the gas over most of the pressure range. The discontinuity in the steam compressibility is because the first derivative of $\rho_v(p)$ is discontinuous although $\rho_v(p)$ is continuous to only 3 decimal places.

In order to examine the effect of increased fluid compressibility within the Black-Oil model one of the fluid compressibilities must be increased. Gas is the most compressible fluid component in the Black-Oil model therefore it would be natural to try to increase the compressibility of the gas to match that of steam. A gas compressibility to match that of steam cannot be found by altering the parameters in (6.5.7). Instead a density function similar in form to (6.5.8) was converted into a formation volume factor for use in the Black-Oil model, the parameters used to accomplish this were $a = 450.0$ and $b = 0.09$. The resulting

gas compressibility compared to that of steam is shown in Figure 6.13 and can be seen to be just greater than that of steam throughout the pressure range.

A problem was devised which has a large variation in compressibility, namely gas injection into an oil saturated reservoir, therefore we have a 2-component, 2-phase problem. This type of problem gives a compressibility difference of 2 orders of magnitude between the injected and initial reservoir fluid. The mass transfer ratio $R_a \equiv 0$ since there is no water in the problem, the ratios R_l and R_v were also set to zero because no mass transfer effects were modelled in the thermal model. The absence of mass transfer effects in the Black-Oil model also ensures that the variation in compressibility occurs over a very narrow region, i.e. about 3 or 4 grid blocks, as would be expected in the thermal model.

A CFL number of 0.9 was used for this computation, after a few days into the simulation large volume error discrepancies were generated which caused oscillation in the pressure and component density fields. The same time as the large volume error discrepancies were generated the time steps being used were increasing to about 7 days which was much larger than those previously seen in Black-Oil computations performed thus far. Therefore this suggests that the wavespeeds in the problem were not being sampled well by the numerical method and the time steps calculated using the CFL criteria were unstable. Experience with Black-Oil computations has shown that unstable time steps can be responsible for generating large volume error discrepancies which cause unphysical oscillations in the results. The simulation was repeated using a CFL number of 0.5 and run to a late time, i.e. time for the front in the problem to have nearly reached the producer. The results obtained were free of any oscillation, the simulation proceeding smoothly, no large volume error discrepancies being generated. In particular no problems such as backflow in the pressure equation were observed. The maximum volume error discrepancies generated were of the order 10^{-3} to 10^{-4} with an occasional discrepancy of order 10^{-2}.

Further investigation showed that the large discrepancies occurred at the location of a shock in a rarefaction-shock compound wave. An entropy violation also occurred at this point, therefore extra numerical dissipation was needed at this point which was provided by the CFL number reduction of 0.9 to 0.5. A

local addition of dissipation to improve entropy satisfaction at this point may also be provided by decreasing the slope limiting parameter gamma in (4.2.4) to 1.0 when a local linear degeneracy is detected rather than using $\gamma = 1.5$. The problem was repeated with the above modification to the algorithm with a CFL number of 0.9 and also limiting the increase of time steps to a maximum of 20% as described in Section 5.2.3. The simulation proceeded with no entropy violations or unacceptably high volume error discrepancies.

It is therefore concluded that subject to the not unreasonable reduction of the CFL number, or addition of extra dissipation at local linear degeneracies, simulations of problems with the Black-Oil model involving highly compressible fluids does not pose a problem to the sequential methodology. This is similar to the findings of Trangenstein in [48], wherein the hot water flooding problems simulated needed a large amount of extra dissipation to ensure no entropy violations occurred in the numerical results near local linear degeneracies. It is assumed that Trangenstein tried reduced CFL numbers for the simulations involving steam injection in [48]. Therefore we can only conclude that the extra complications of thermal effects in comparing the Black-Oil model to the thermal model are in some way responsible for the problems reported by Trangenstein.

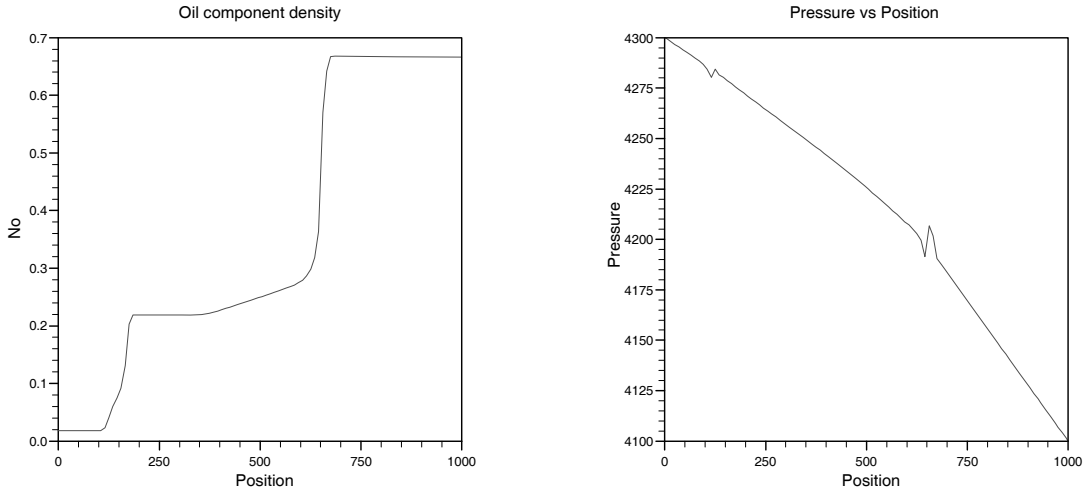

Figure 6.7: The oil component density and corrected pressure field, resulting from applying the discrepancy reduction technique to problem A4.

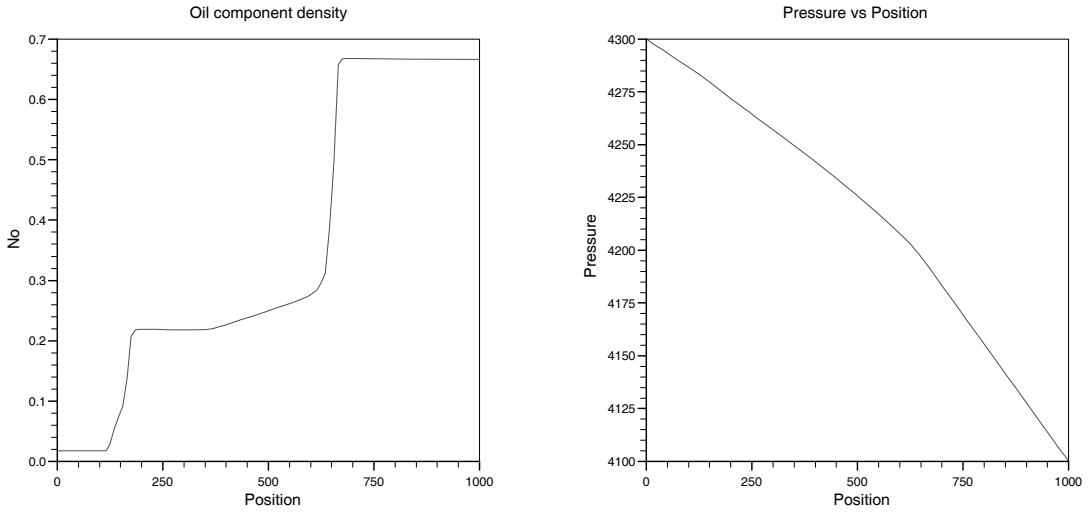

Figure 6.8: The oil component density and corrected pressure field with correction of component density instead of pressure at phase changes, applied to problem A4.

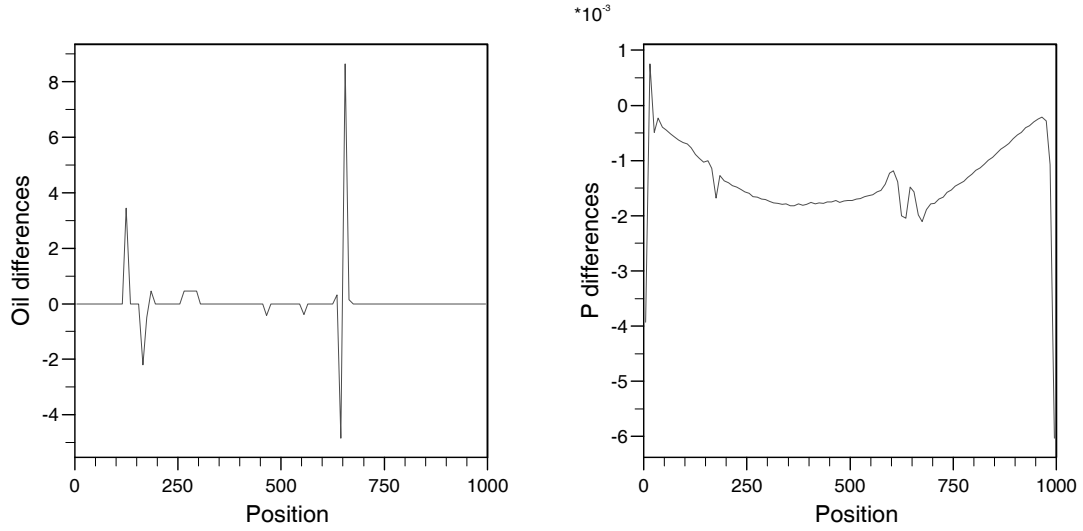

Figure 6.9: The percentage differences in the oil component density and pressure fields of problem A4, between the results of applying and not applying the discrepancy reduction technique.

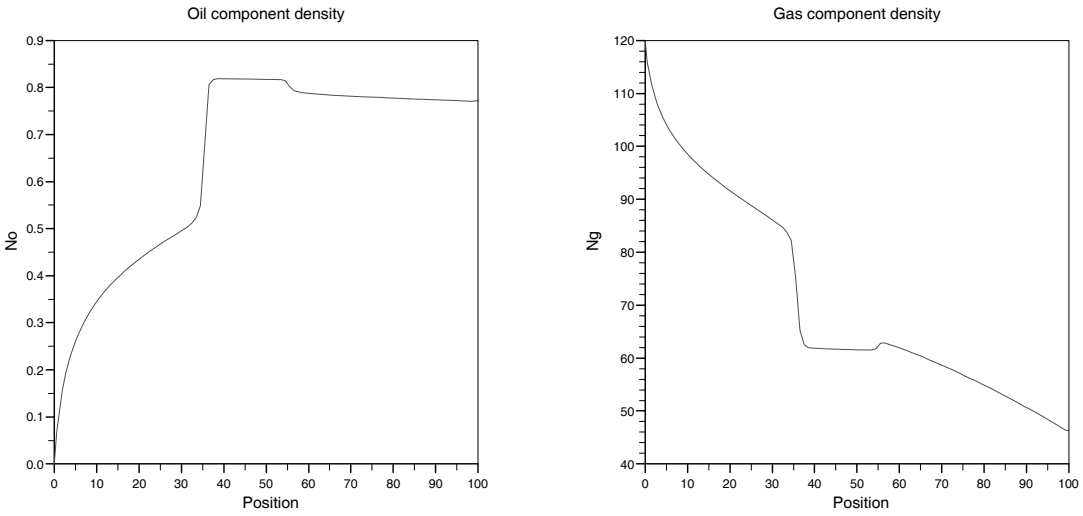

Figure 6.10: The oil and gas component densities from problem A1 using the volume error discrepancy formulation with reduction of the volume error discrepancy.

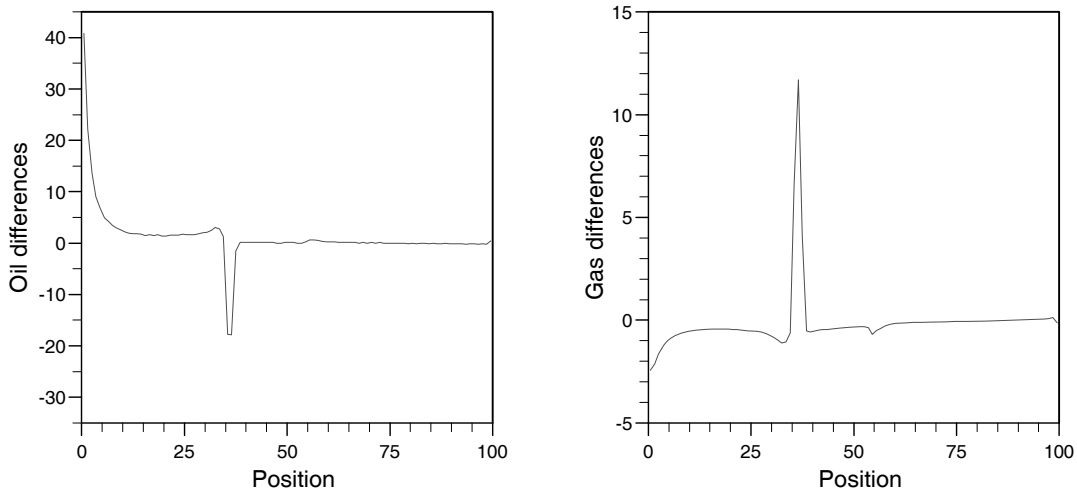

Figure 6.11: The percentage differences between the oil and gas component densities from problem A1 without the volume error discrepancy and with the discrepancy but the discrepancy reduction techniques having been applied.

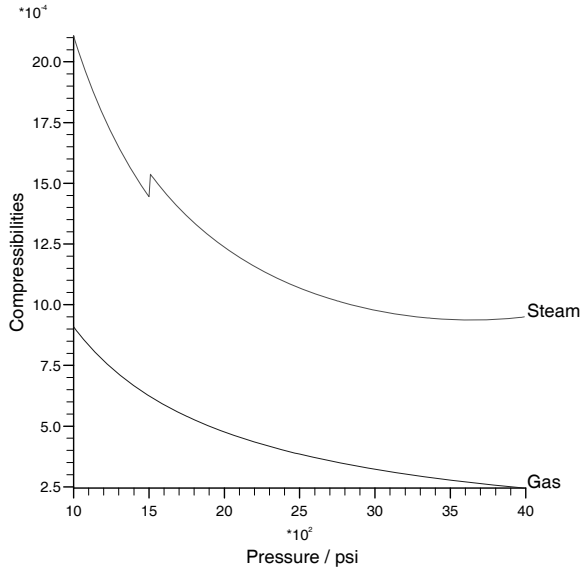

Figure 6.12: The steam and gas compressibilities, having units of psi^{-1}, used in the thermal and Black-Oil model respectively.

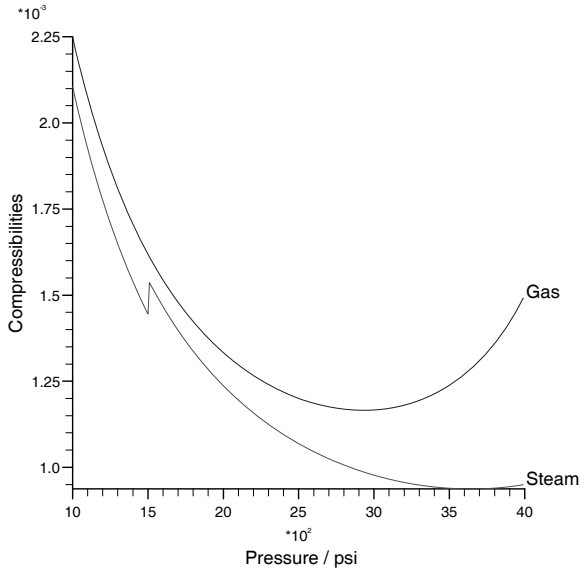

Figure 6.13: The increased gas compressibility, used in the Black-Oil model to simulate the injection of highly compressible fluid.

Chapter 7

A Comparison of TVD Flux-Limiter and Higher Order Godunov Schemes for Reservoir Simulation

7.1 Introduction

In this chapter we compare the numerical performance of the Higher Order Godunov scheme [2] and a TVD flux-limiter scheme, developed at B.P. Sunbury by Rubin and Edwards [36], when applied to the system of degenerate conservation laws arising from the Black-Oil flow equations. The Higher Order Godunov scheme was applied to the sequential (or split) form of the Black-Oil flow equations given in [46], a Fortran code having been written to perform the simulations, whereas the TVD flux-limiter scheme [36] was applied to the mass conservation laws present in the IMPES formulation of the Black-Oil flow equations. The IMPES acronym refers to the IMplicit Pressure Explicit Saturation formulation of the flow equations, see Aziz and Settari [1] for details, and is similar to the sequential formulation [46] except that it does not have an associated volume error discrepancy. Results of reservoir simulations with the flux-limiter scheme applied to the IMPES equations were gained through use of the commercial reservoir simulation code VIP (Vectorised Implicit Program), used by B.P.

Flux-limiter schemes were constructed with non-degenerate systems of conservation laws in mind, see [7, 36, 45] for details, i.e. systems that possess genuinely non-linear (or linearly degenerate) wave modes and that are strictly hyperbolic in nature. The Higher Order Godunov methodology was also originally developed for non-degenerate systems by Collela [10], with Bell et al. [2] presenting extensions of Collela's work enabling the scheme to be applied to degenerate systems, specifically those with local linear degeneracies and eigenvector deficiencies. The flux-limiter scheme in VIP does not rely on any knowledge of the characteristic structure of the conservation laws, i.e. it does not decompose the system into its characteristic components, and hence no clear mechanism exists of detection of the degeneracies and modification of the scheme. This is in contrast to the Higher Order Godunov methodology since the same characteristic information used to construct the scheme can also be used to test for the degeneracies. However since the characteristic information is used to construct the scheme, then suitable modifications to the scheme at degeneracies are now made a necessity.

Timings of individual subroutine calls in the Higher Order Godunov code indicate that the calculation of the eigenvectors can represent a significant amount of the total computational time, i.e. over 5%, in both 1 and 2 dimensions. The eigenvectors being used in the construction of second order accurate traced left and right states at cell interfaces, see Section 4.2.2. The eigenvectors are also used in the phase space construction needed to solve the Riemann problem at cell edges, see Section 4.2.3, and arises in problems in which counter-current flow occurs, due to the introduction of gravitational effects. However the relative computational time, associated with the calculation of the eigenvectors, decreases when gravity is introduced. This is because, although more eigenvector calculations will be needed compared to problems without gravity, extra computations are associated with introducing gravity, especially in solving the Riemann problems to compute the numerical fluxes. The timings indicate that in terms of calculating the eigenvectors, the most efficient problems are the 2-D cross-sectional problems, with the gravity-free 1-D problems the least efficient.

The Higher Order Godunov scheme has an advantage over the flux-limiter type schemes since it can usually be used with a CFL number of 0.9, whereas

flux-limiter schemes have to be used with lower CFL numbers, the greatest being 0.66 but usually 0.5, depending on the limiter used. But we have found that when problems involving counter-current flow are being simulated with the Higher Order Godunov code a reduced CFL number in the range 0.5-0.9 is needed for best performance of the method.

In the next section we describe the IMPES formulation of the Black-Oil model used in the VIP simulator. We also provide some details of the Riemann solver used in the Higher Order Godunov code since this step of the computation is crucial and required some fine tuning. Further details of the timings for the eigenvector calculations are also provided for various types of simulation problem. The numerical results of 1-D, 2-D Areal, and of most interest 2-D cross-sectional, reservoir simulations are presented to compare the two different types of numerical scheme. These comparisons are of interest since they have not previously appeared in the literature. The relative merits of the flux-limiter and Higher Order Godunov approaches to reservoir simulation being a current issue in the reservoir simulation community.

7.2 Description of the VIP Simulator

In this section we outline the IMPES formulation of the Black-Oil model and the numerical methods used in the commercial reservoir simulator VIP. The simulator is able to work in one of two modes, these being simultaneous solution (SS) or IMplicit Pressure Explicit Saturation (IMPES). All the unknown flow variables are solved for implicitly with the SS formulation and hence the IMPES mode most closely resembles the sequential formulation of the Black-Oil model [46] that we use in this thesis. For this reason we simulate problems using the VIP simulator in IMPES mode. The VIP simulator uses the standard Black-Oil model which deals with less general mass transfer effects between the phases than the Black-Oil model [46] that we use, namely a 'solution gas ratio' R_l only is considered.

The starting point for the derivation of the IMPES method for solution of the Black-Oil flow equations are the mass conservation laws for each fluid component. These equations are written in terms of primary variables, which are

the fluid pressure p and the vapour and aqueous saturations, s_v and s_a respectively. The three mass conservation laws are then discretised with a backward in time discretisation, and then combined in such a way that the time derivatives of the saturations are eliminated from the resulting equation. This equation then becomes the parabolic pressure equation and because of the backward time discretisation, is implicit in pressure. Once this pressure equation has been solved the saturations may be updated explicitly by using the original three mass conservation laws. For a more detailed description of the IMPES method see Aziz and Setarri [1].

The discretisations of both the pressure equation and the hyperbolic saturation equations, used in the the IMPES formulation ensure conservation of mass. The discretisation of the pressure equation being similar to that which we use for our pressure equation, in that second order accuracy in space and first order accuracy in time is achieved. The IMPES method does not have an inherent volume error discrepancy since there is no splitting of the flow equations as in the Black-Oil model [46]. The update of the saturation equations is explicit and hence the IMPES method has an associated stability criteria, see Aziz and Settari [1]. In practice commercial reservoir simulation codes ensure numerical stability by keeping changes in primary variables, over a time step, to within certain prescribed limits. If over the course of a time step these limits are violated the advancement of the equations would be repeated with a reduced time step.

The Higher Order Godunov algorithm [2] that we use to solve the Black-Oil flow equations [46], achieves second order accuracy in both space and time, at least in regions of smooth flow. The VIP simulator was originally written with a first order one-point upstream weighted algorithm, however a second order accurate TVD flux-limiter extension was programmed at B.P. Sunbury. This second order algorithm was a systems of equations extension of the Two Time Level Flux (TTLF) TVD scheme of Rubin and Edwards [36] described in Section 2.6.2, and used the van Leer limiter [50]. The extension of the scalar scheme to systems was performed by simply applying the scheme to the system component by component, which is a common method of solving systems of equations in oil reservoir simulation codes. This is in contrast to the rigorous approach of

decomposing the system into its characteristic components and then applying the scalar scheme to each characteristic family. Hence, although the scheme in VIP is simple to implement, a reduced resolution is expected from ignoring the coupling of the equations, but the formal order of accuracy of the scalar scheme is maintained. We also note that in the reservoir simulation community the upstream state is determined independently for each phase, and hence component of the system, by the sign of the Darcy phase velocity.

Hence comparisons of numerical results may be made between the Godunov and flux-limiter approaches of obtaining second order accuracy whilst maintaining the TVD property. It should be noted that in higher dimensions, although the schemes will be free of oscillation, in both cases the schemes will not be strictly TVD, as mentioned in Section 2.5.5. Also in higher dimensions both numerical schemes are dimensionally unsplit, the VIP code incorporates all coordinate directions simultaneously, see Section 4.3.2 for a description of how the Higher Order Godunov code remains unsplit.

7.3 The Higher Order Godunov Code

In this section we describe the introduction of gravitational effects into the Higher Order Godunov code that were needed in order to simulate the 2-D cross-sectional problems. We concentrate on the Riemann problem solver needed for counter-current flow, which requires the full phase space solution of the Riemann problem and caused some difficulties. Also, at the end of the section, details on the relative expense of the calculation of the eigenvectors are provided. This information is used in assessing the efficiencies of the two numerical approaches, under comparison, of solving the system of conservation laws arising from the Black-Oil model.

We first briefly review the phase space construction of the Riemann problem in order to aid the discussion, but see Section 4.2.3 for more details. The jump between the left and right traced states, which defines the Riemann problem at the cell edges, is decomposed into characteristic components corresponding to

each wave mode, i.e.

$$\mathbf{n}^R - \mathbf{n}^L = \overline{R}\,\overline{\boldsymbol{\alpha}},$$

where the matrix $\overline{R}$ is the matrix of eigenvectors evaluated at an expansion state $\overline{\mathbf{n}}$, i.e. $\overline{R} = R(\overline{\mathbf{n}})$. We have a system of 3 conservation laws and therefore the jump will be decomposed into 3 components or separate paths. If the eigenvectors (columns of $\overline{R}$) are normalised, the entries of $\overline{\boldsymbol{\alpha}}$ represent the lengths of the paths in phase space. The expansion state $\overline{\mathbf{n}}$ is calculate as an average of the traced left and right component densities, which define the Riemann problem at cell interfaces, i.e.

$$\overline{\mathbf{n}} = \frac{1}{2}(\mathbf{n}^L + \mathbf{n}^R).$$

Alternative expansion states are possible but the above form is recommended in [2] for problems involving flow in porous media.

The inherent volume error discrepancy associated with the flow equations can be a cause of concern when the expansion state $\overline{\mathbf{n}}$ is calculated. If we denote the pressure at the cell interface by $\overline{p}$ then the volume error discrepancy associated with the variables $\overline{\mathbf{n}}$ and $\overline{p}$ can exceed 10^{-2}, which is considered as bordering on the unphysical. It is also possible for the traced states $\mathbf{n}^L$ and $\mathbf{n}^R$ to be associated with high volume error discrepancies, in fact higher than those seen in problems without gravity where the volume error discrepancies of the traced states do not usually exceed 5.0×10^{-3}. Also the intermediate states in the Riemann problem defined by

$$\mathbf{n}^{is1} = \mathbf{n}^L + \overline{\alpha}_1 \overline{R}_1,$$

and

$$\mathbf{n}^{is2} = \mathbf{n}^{is1} + \overline{\alpha}_2 \overline{R}_2,$$

can also be associated with high volume error discrepancies. Despite all these perceived difficulties we find that the numerical results of such problems are improved if all of these phenomena are ignored, rather than making modifications to the Riemann problem solver such as lumping the paths in phase space when high volume error discrepancies are detected.

We now move on to two cases in which it is found necessary for the paths in phase space to be lumped (that is combined into 1 path) so that the numerical

results generated are free of oscillation. Firstly, if one of the intermediate states $\mathbf{n}^{is1}$ or $\mathbf{n}^{is2}$ given above, are unphysical by being negative (hence giving a negative component density) then the two paths connected with the relevant state should be lumped, or if both are unphysical then the whole path from $\mathbf{n}^L$ to $\mathbf{n}^R$ should be lumped into 1 path. When the paths are lumped the modifications to the flux computation are those given by Bell et al. in [2], described in Chapter 4. Secondly when eigenvector deficiencies are detected amongst the eigenvectors $\overline{R}_k$, used to expand the jump between the left and right states, modifications similar to those needed in the problems above, should be incorporated. In this case the problem manifests itself by a poor representation of the path in phase space. For instance if the eigenvectors $\overline{R}_1$ and $\overline{R}_2$ are nearly parallel, indicating an eigenvector deficiency in wave modes 1 and 2, then the calculated path lengths can become very large since the matrix $\overline{R}$ is nearly singular.

A further two circumstances exist for which the whole path in phase space, connecting $\mathbf{n}^L$ with $\mathbf{n}^R$, must be lumped. If we are unable to calculate a set of eigenvectors then clearly we cannot expand the jump into its characteristic components and the jump will have to be lumped. The failure of the eigenvector calculation occurs if the non-trivial wavespeeds are very small (effectively zero) or if one of the matrices used in the eigenvector calculation becomes singular. Also, in the case when we have the eigenvectors to expand the jump, it may not always be possible to solve for the path lengths (vector $\overline{\boldsymbol{\alpha}}$) and hence decompose the jump. This occurs if the matrix $\overline{R}$ is poorly conditioned, which suggests an eigenvector deficiency, and we again lump the whole path.

In Section 4.2.3 we follow Bell et al. [2] and describe a procedure for defining a reference state ($\mathbf{n}^L$ or $\mathbf{n}^R$), used in the numerical flux calculation to calculate a reference flux, which depends on the sign of an average wavespeed. We find that use of an alternative reference state, when a sonic state is detected on traversing the paths from $\mathbf{n}^L$ to $\mathbf{n}^R$, improves the numerical results. When one of the wavespeeds changes sign on one of the paths, near to one of the intermediate states in the Riemann problem solution, then we use that intermediate state for calculation of the reference flux, instead of $\mathbf{n}^L$ or $\mathbf{n}^R$, see equation (4.2.9). The contributions of the integral correction terms in the Engquist-Osher flux formula

(4.2.9) will then be modified, and are straightforward to deduce.

We now provide more details regarding the timings of the subroutine used to calculate the eigenvectors in the Higher Order Godunov code, in order to assess the impact on the total computational time associated with these calculations. We calculated the percentage of the total run time taken to calculate the eigenvectors for problems with and without gravity, in 1 and 2 dimensions. Firstly an example saturated 3-phase 1-D problem without gravity, simulated with 100 grid blocks, took about 8.9%, and an example undersaturated problem took about 9.3%, of the total computational time. These percentages change to 9.0% and 9.7% for the saturated and undersaturated flow problems respectively, when the grid was refined to 200 grid blocks. We also considered a 1-D problem with gravity, which now includes the calculation of the eigenvectors needed in the solution of the Riemann problems. We considered a vertical reservoir as this probably represents the most demand on the eigenvectors. The reservoir was divided into two halves, with a different fluid mixture in both halves. The fluids mix due to gravity and mass transfer effects, usually resulting in a mixed flow problem. The percentage time needed in the calculation of the eigenvectors was 4.6% for a 100 grid block simulation, which decreased to 4.4% when 200 blocks were used.

We then simulated the 2-D saturated flow Areal problem (with no gravity), from Chapter 5, using a 20×20 grid and found that 6.4% of the computational time was spent calculating the eigenvectors. This decreased to 6.0% when a 40×40 grid was used. The 2-D cross-sectional problems include gravity in the z direction with 3.6% of the total time needed to calculate the eigenvectors for a 20×10 grid block simulation. This decreased to 3.1% when the grid was refined to 40×20 grid blocks. These percentages are based on solving the pressure equation to a tolerance of 10^{-4} psi in each grid block, which represents accuracy to 8 figures. This tolerance is smaller than that which would be used in a commercial reservoir simulation, which would be about 0.1 psi, hence in this case, the percentage timings of the eigenvectors would be expected to increase. The 2-D simulations were repeated with the increased tolerance on pressure of 0.1 psi, with the timings of the eigenvectors increasing by at most 2%. Most noticeably, use of this increased tolerance resulted in the solution of the pressure equation

taking less than half the percentage time compared to before.

Given the percentage times above, it should be noted that the Higher Order Godunov code was not written with efficiency in mind, but was coded as efficiently as possible. In particular, we used a BI-CGSTAB pre-conditioned conjugate gradient solver, described by Van Der Vorst [53], to solve the linear system resulting from the 2-D parabolic pressure equation, so that this step of the computation is of high efficiency. We tried using optimisation of the Higher Order Godunov code, with the effect on the percentage timings mostly being within $\pm 2\%$ of those quoted.

Percentage timings of the calculations of the eigenvectors have been given, but these do not take into account the extra computation associated with performing the eigenvector decomposition. For instance we need to solve 3 $n \times n$ linear systems in each grid block to calculate the expansion coefficients (4.2.2), used in the calculation of the monotonised slopes, see Section 4.2.1, and a $n \times n$ linear system associated with the Riemann problem solution, where n is the number of conservation laws in the system. Taking into account all the computation associated with a full eigenvector decomposition, used in the Higher Order Godunov scheme, it is concluded that the time spent in performing these computations is significant and perhaps should be justified in terms of quality of numerical results compared to the flux-limiter schemes, which do not require the same computational effort.

7.4 Comparison of Numerical Results

In this section we show the numerical results from the Higher Order Godunov code and the VIP simulator to compare how well the numerical schemes handle the Black-Oil fluid flow equations. We show results of a 1-D and 2-D Areal problem which do not include gravitational effects, and a 2-D cross-sectional problem which does include gravity. The 2-D cross-sectional problem introduces counter-current fluid flow and hence will be a good test of the numerical methods, particularly the Higher Order Godunov method since all aspects of the scheme will be utilised. Also in this problem it is likely that points of a loss of strict hyperbolicity will occur and hence the modifications present in the Godunov

methodology, which were introduced by Bell et al. [2], will be used at such points. The flux-limiter scheme makes no such modifications at such points and hence how the schemes perform at these points is of particular interest.

The VIP simulator models injection of water and gas only since clearly oil would not be injected in a commercial recovery strategy. We have considered oil injection components previously in this thesis since a 3-phase injection usually yields more interesting numerical results. A water and gas injection is referred to as a 'WAG flood' in the oil industry, the ratio of the injected water flux to gas flux being known as the WAG ratio. The VIP code uses an extremely complicated well model to simulate the injection of fluid, so much so that it is very difficult to determine the injected fluid saturations. An exact replication of the simulation problems being solved by the VIP code is not essential for this work, since the main objective is to compare how well the scheme performs on degenerate systems of conservation laws compared to the Higher Order Godunov scheme. We determine the injected saturations by using the numerical results from the VIP code by assigning them to be the saturations present in the first grid block. The initial reservoir saturations in the VIP code are specified explicitly, so these will be identical in the simulations from both codes.

Simulation of the reservoir flow problems used to compare the numerical results of the two codes are performed at the same CFL number. However the VIP code does not use the wavespeeds associated with the hyperbolic saturation equations to calculate a stable time step as with the Higher Order Godunov code. A stability criteria for the IMPES formulation, based on the transmissibilities is used, see Aziz and Settari [1] for details. Therefore the time steps used by the IMPES method are calculated as above, but also having been reduced by a factor which we also term a CFL number. Hence the number of time steps used by the VIP and Higher Order Godunov codes will be different because of the differing stability criteria used. The simulations are also performed without any artificial viscosity since the VIP code does not use any, and we solve the pressure equation to the same tolerance in pressure, as in the VIP code, although the 1-D Higher Order Godunov code solves the system of unknown pressures directly, not iteratively.

We now describe the 1-D simulation problem used to compare the two approaches to solving the Black-Oil flow equations. The reservoir modelled was 500 feet in length and had a rock permeability of 100 milliDarcy's. The injection fluid consists of water and gas at a pressure of 2000 psi and had saturations of

$$\mathbf{s}_{inj} = \begin{bmatrix} 0.0 \\ 0.2235 \\ 0.7765 \end{bmatrix}.$$

The fluid initially resident in the reservoir was at a pressure of 1800 psi and had a composition of

$$\mathbf{s}_{res} = \begin{bmatrix} 0.7658 \\ 0.1406 \\ 0.0936 \end{bmatrix},$$

with the production pressure being 1600 psi. All the other reservoir, fluid and rock parameters are the same as those given in Section 3.9. We reiterate that the mass transfer ratios R_v and R_a are both identically equal to zero for all the reservoir simulations in this chapter. The results of this simulation problem from the VIP code at 30 days using 100 grid blocks, and with a CFL number of 0.5, are shown by the solid line in Figure 7.1. The tolerance used to solve the pressure equation for these results was an absolute value of 0.1 psi, representing 5 figure accuracy, i.e. pressure in every grid block was calculated to a tolerance of at worst 0.1 psi. The corresponding results from the Higher Order Godunov code, with the direct solution of the linear system resulting from the discretisation of the pressure equation, are shown by the crosses in Figure 7.1. We note that the IMPES formulation of the flow equations does not have an inherent volume error discrepancy therefore we could have applied the techniques, described in the previous chapter, to reduce the volume error discrepancy, to see the effect on the comparison. However at a CFL number of 0.5 the maximum volume error discrepancies generated are $O(10^{-5})$ therefore applying the techniques, although reducing the volume error discrepancy, do not noticeably effect the results, therefore we do not show the results of this computation.

In comparison of the results we see that the rarefaction stretching from about 10 to 110 feet is resolved almost identically by the two codes. However the

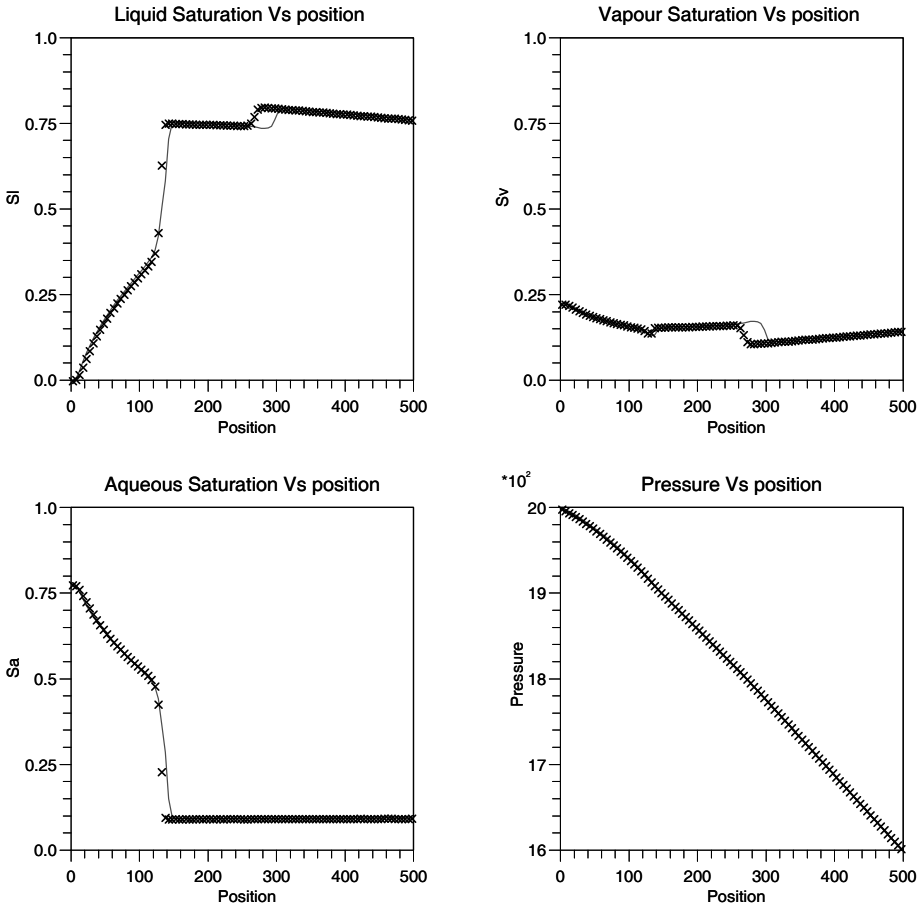

Figure 7.1: Numerical results of the 1-D problem from the VIP and Higher Order Godunov codes at 30 days using 100 grid blocks and a CFL number of 0.5, solid line - VIP, crosses - Higher Order Godunov code.

connecting shock, hence indicating the prescence of a local linear degeneracy, is resolved much more sharply (by about 2 or 3 grid blocks) with the Higher Order Godunov code, both codes predicting roughly the same shock height. Both codes then exhibit two linearly varying states, connected by a shock, separating the first shock (at about 110 feet) with the producer at 500 feet. These linearly varying states are not rarefaction waves but are due to pressure effects. The pressure fields can be seen to be almost identical. However, there is a significant difference in the location predicted of the second shock of about 30 feet ($\sim$ 6 grid blocks), the resolution of this shock between the two sets of results being comparable. Due to the complexity of the well model in VIP we might not be injecting the same fluid compositions, and numerical results from VIP at earlier times indicate that the injection saturations vary slightly before settling down.

Therefore the discrepancy in the location of the second shock is probably due to the different mass fluxes injected early on in the computation, with conservation of mass ultimately causing the differences. A similar kind of effect on 'the faster shock' was also observed in computations performed by Blunt and Rubin in [7]. The Higher Order Godunov code takes 146 time steps whereas the VIP code takes 2479 time steps to perform the simulation. Hence the Higher Order Godunov code is far more efficient at performing the simulation.

The 2-D Areal problem was simulated on a 100 feet square region with a rock permeability of 100 milliDarcy's in both coordinate directions. The injection, initial reservoir and production pressures were 2000, 1800 and 1600 psi respectively. The injection saturation vector was

$$\mathbf{s}_{inj} = \begin{bmatrix} 0.0 \\ 0.6957 \\ 0.3043 \end{bmatrix},$$

and the initial reservoir saturations were

$$\mathbf{s}_{res} = \begin{bmatrix} 0.7658 \\ 0.1406 \\ 0.0936 \end{bmatrix}.$$

The problem was simulated with a 60×60 grid of blocks, a CFL number of 0.3 and with a tolerance on the solution of the pressure equation of 0.1 psi. The results of this problem from the VIP code are shown in Figure 7.2. The corresponding results from the Higher Order Godunov code, using the most accurate transverse flux calculation, are shown in Figure 7.3.

Comparison of Figures 7.2 and 7.3 indicate that the results from the VIP code are at a more advanced state than those from the Higher Order Godunov code, and the computation has nearly 'broken through' to the producer in Figure 7.2. Since these Figures are not easily compared we plot the solution values along the diagonal connecting the injection and production wells against normalised distance and overlay the two Figures. This is shown in Figure 7.4, where the solid line indicates results from VIP and the crosses, results from the Higher Order Godunov code.

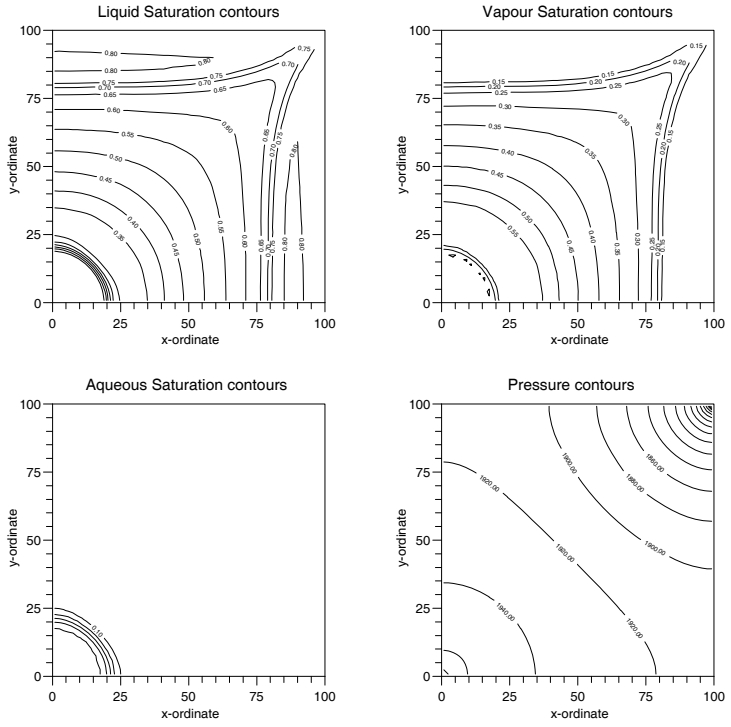

Figure 7.2: Numerical results of the 2-D Areal problem at 5 days from the VIP simulator using a 60×60 grid and a CFL number of 0.3.

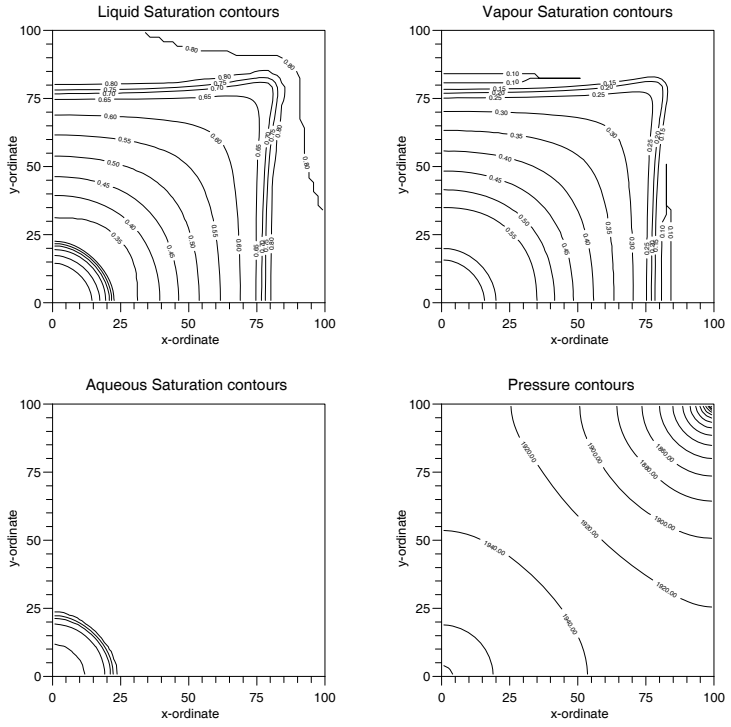

Figure 7.3: Numerical results of the 2-D Areal problem at 5 days from the Higher Order Godunov code using a 60×60 grid and a CFL number of 0.3.

The results in Figure 7.4 appear to show the same qualitative behaviour in the first half of the Figure, with the first shock, located at about 0.15 on the x-axis resolved far better by VIP. However the results from the Higher Order Go-

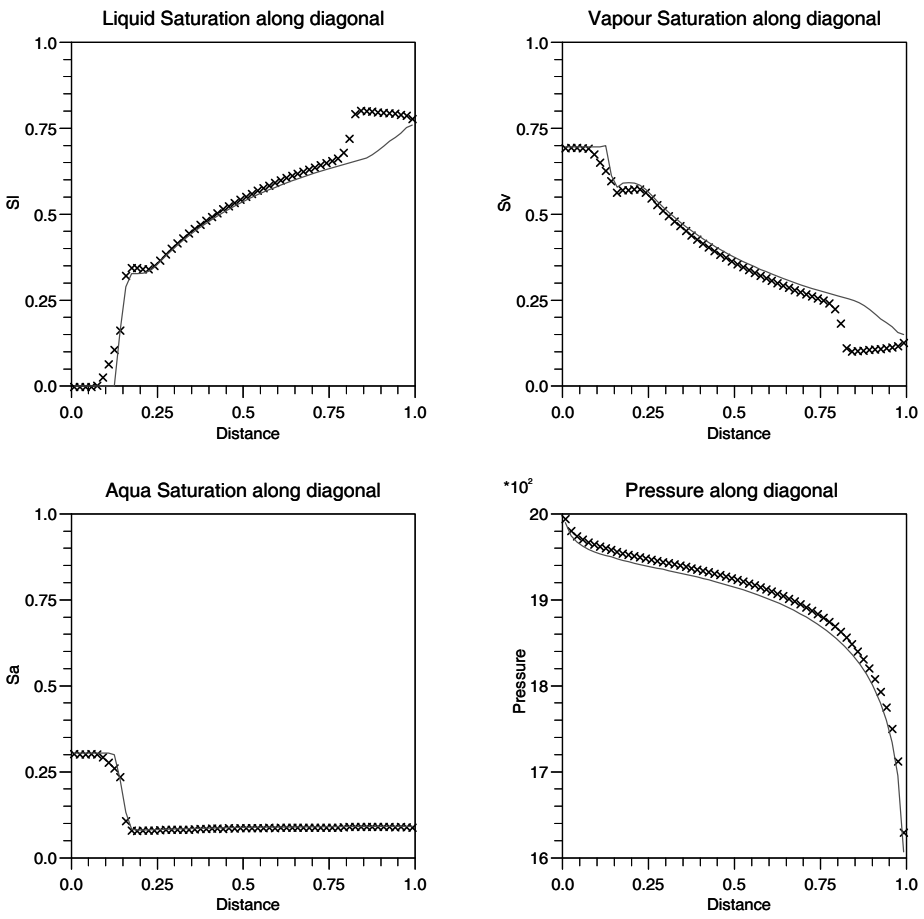

Figure 7.4: Solution values along the diagonal of the 2-D Areal problem from the VIP and Higher Order Godunov codes overlaid (VIP-solid line, HOG-crosses).

dunov code suggest that this first wave is actually a rarefaction-shock compound wave rather than a shock, which the VIP code predicts. Results from a fine grid simulation of the analogous 1-D problem using the Higher Order Godunov code, in particular the wavespeeds obtained, confirm that this first wave is in fact a rarefaction-shock compound wave. The VIP code again predicts a more advanced position for the second shock, just as in the 1-D comparison, although also indicating it has decayed due to the very high fluid velocity near the production well (as indicated by the pressure profile). The advanced second shock is again probably due to the different amount of mass injected early on in the simulation, as in the 1-D problem. The Higher Order Godunov code shows a pressure field of

larger magnitude, which is possibly due to the inherent volume error discrepancy. This will be investigated below by applying the volume error discrepancy reduction techniques to correct the pressure field. The simulation was also repeated using the Higher Order Godunov code at an increased CFL number of 0.9 to check the effect of the CFL number on the resolution of the results, but these results did not exhibit any noticeable increased (or decreased) resolution.

Since the IMPES equations do not have an associated volume error discrepancy we also simulate the Areal problem with the discrepancy reduction techniques. The maximum discrepancies in this problem were of the order 10^{-3} which also provides motivation for their reduction. The problem exhibits saturated flow throughout the computation, and so only the pressure field will be corrected in order to reduce the volume error discrepancy. The results of this simulation did not show any significant difference to the previous results. The maximum discrepancies were reduced from $\sim O(10^{-3})$ to $\sim O(10^{-7})$ using 3 iterations in each grid block, with the resulting maximum change in the pressure field being 0.2%.

We now describe the 2-D cross-sectional problem, which takes place in the $x-z$ plane with gravity acting in the negative z direction. The cross-section considered was 400 feet in length and 50 feet in height. Injection of fluid takes place along the entire left hand face of the reservoir at $x = 0$ and production of fluid along the entire right face of the reservoir at $x = 400$. Specification of the initial pressure distribution for cross-sectional problems is not straightforward as in the previous problems considered, since we need the condition of hydrostatic equilibrium of the fluids at t=0. This means that initially there is no fluid motion in the z-direction, the bottom of the reservoir being aligned with the horizontal so there will be no flow in the x-direction at t=0.

Hydrostatic equilibrium is achieved with the forces due to gravity balancing with the pressure gradient. The required pressure gradient in the injection fluid and reservoir fluid can be calculated using Darcy's law (3.3.1) for each phase. The phase velocity v_p will be zero when the pressure gradient balances with the gravitational potential, i.e.

$$\left(\frac{\partial p}{\partial z}\right)_p = \rho_p g,$$

the depth gradient $\frac{\partial d}{\partial z}$ is equal to 1.0 since the sides of the reservoir are aligned

with the vertical. When the fluid only contains 1 phase the required pressure gradient in the reservoir is the pressure gradient associated with that phase

$$\frac{\partial p}{\partial z} = \left(\frac{\partial p}{\partial z}\right)_p .$$

However when more than 1 phase exists we use a saturation weighted average of the individual pressure gradients associated with each phase, i.e.

$$\frac{\partial p}{\partial z} = s_l \left(\frac{\partial p}{\partial z}\right)_l + s_v \left(\frac{\partial p}{\partial z}\right)_v + s_a \left(\frac{\partial p}{\partial z}\right)_a .$$

The injected fluid had a composition of the following saturations,

$$\mathbf{s}_{inj} = \begin{bmatrix} 0.0 \\ 0.0 \\ 1.0 \end{bmatrix},$$

i.e. a waterflood, with a pressure at the top of the injection face of 2000 psi, the pressures were distributed down the the rest of the face using the pressure gradient $\frac{\partial p}{\partial z}$ associated with the injected fluid. The initial reservoir saturations were

$$\mathbf{s}_{res} = \begin{bmatrix} 1.0 \\ 0.0 \\ 0.0 \end{bmatrix},$$

with the pressure along the top of the reservoir being 1800 psi and the pressures below being distributed with a similar procedure to the injection face. Although there is no free gas initially in the reservoir, due to the vapour saturation being zero, there is an amount of gas dissolved in the oil as indicated by the 'solution gas ratio' R_l and hence the initial reservoir fluid is undersaturated. A production pressure of 1600 psi was assigned along the whole production face. The vector of phase densities, at standard conditions, used in this problem were

$$\boldsymbol{\rho} = \begin{bmatrix} 52.789 \\ 0.07655 \\ 62.382 \end{bmatrix}.$$

Numerical flux computation also simplifies to upwind determination in one of the coordinate directions for cross-sectional problems. The pressure boundary conditions used in the problem guarantee that the total velocities in the

x-direction are positive for all time. This leads to positive wavespeeds associated with the x coordinate direction and hence all x-directional flux calculations reduce to upwind determination. Counter-current flow only occurs in the vertical direction due to the effect of gravity on the fluid phases of differing densities, if the fluid phases had the same densities then no counter-current flow would occur. Hence the full phase space construction of the Riemann problem, used to calculate the numerical flux, is only needed for the calculation of the z-directional fluxes.

The cross-sectional problem was simulated using a 40×20 grid of blocks, a CFL number of 0.5 and with a tolerance on the calculated pressures of 0.1 psi. The numerical results from the VIP code are shown in Figure 7.5 at 15 days. The corresponding results from the Higher Order Godunov code, with the most accurate transverse fluxes, are shown in Figure 7.6.

From Figures 7.5 and 7.6 we see that the injected water, being more dense than the oil, is forced towards the bottom of the reservoir by the force of gravity. This results in a thin 'oil film' being left along the top of the reservoir by the injected fluid. The vapour saturation contour lines near the production face are due to the gas that was initially dissolved in the liquid phase bubbling out of solution due to the pressure dropping near the production well. The numerical results from the two codes show very good agreement, in fact closer agreement than the previous two problems studied, which is probably due to the fact we are injecting 1-phase (water) in this problem, and therefore the uncertainty associated with the well model is not so apparent.

We checked the resolution of the two sets of results by plotting the solution values along the length of the reservoir at $y = 25$ feet, i.e. along the middle of the reservoir, and is shown in Figure 7.7. The solid line indicates results from the VIP code and the crosses, results from the Higher Order Godunov code, and show very similar resolution.

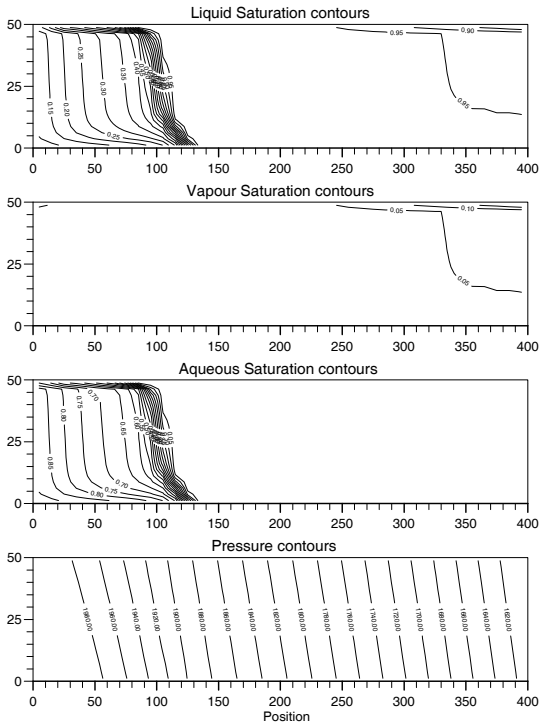

Figure 7.5: Numerical results of the 2-D cross-sectional problem from the VIP simulator at 15 days using a 40×20 grid and a CFL number of 0.5.

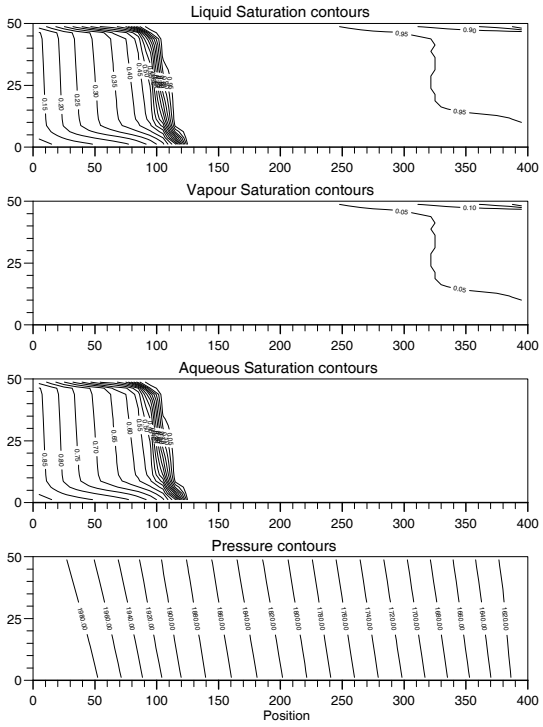

Figure 7.6: Numerical results of the 2-D cross-sectional problem from the Higher Order Godunov code at 15 days using a 40×20 grid and a CFL number of 0.5.

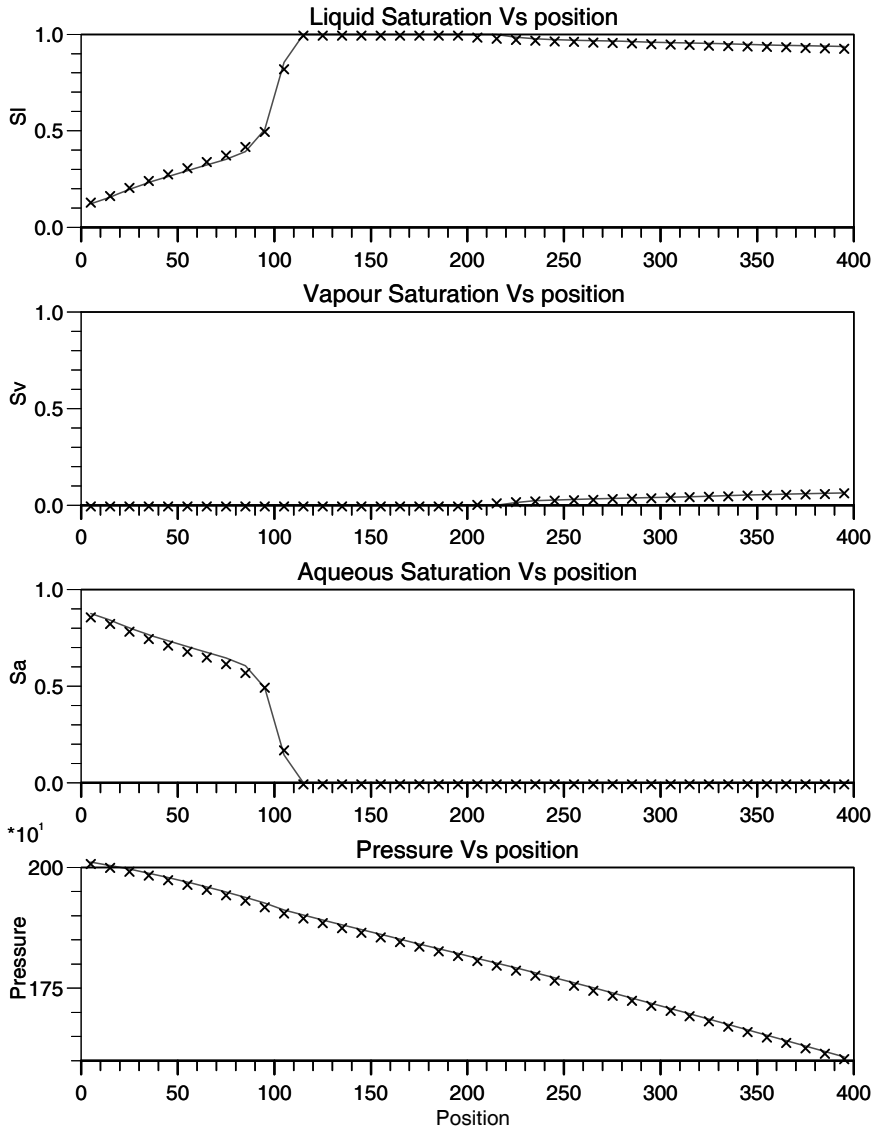

Figure 7.7: Numerical results of the 2-D cross-sectional problem from the VIP and Higher Order Godunov codes along the middle of the reservoir overlaid, taken at 15 days using a 40×20 grid and a CFL number of 0.5, solid line - VIP, crosses - Higher Order Godunov code.

Comparison of numerical results from the VIP and Higher Order Godunov codes in 1 and 2-dimensions has exhibited some notable differences. Firstly the VIP code predicted a more advanced position of the second shock front in the 1-D and 2-D Areal problems, compared to the Higher Order Godunov code. This means that 'breakthrough' times (the time at which the faster front reaches the production well) are underestimated compared to the Higher Order Godunov code. This is probably due to the different amounts of mass injected early on

in the computations, caused by the uncertainty about the injection well model used in the VIP code, and would seem to be confirmed by the results from the cross-sectional problem.

Secondly, the 2-D Areal results from the VIP code indicate that it has failed to resolve the prescence of a rarefaction wave in a rarefaction-shock compound wave near the injection well. The Higher Order Godunov code captures this compound wave, with an analogous 1-D problem confirming its existence. In general the two codes exhibit similar resolution of rarefaction waves and constant states, with improved shock resolution from the Higher Order Godunov code. Unfortunately we were unable to obtain results from VIP of the 2-D Areal problem at an earlier time to compare the resolution of the second shock front. With regard to efficiency, the VIP code consistently take significantly far more time steps to perform the simulations, hence indicating superior efficiency of the Higher Order Godunov code.

The three reservoir simulation problems all exhibit rarefaction-shock compound waves and hence local linear degeneracies in the characteristic wave fields of the conservation laws. These degeneracies do not appear to cause any problems to the TVD scheme in VIP, although VIP has difficulty in resolving the associated rarefaction-shock compound wave in the 2-D Areal problem. The 2-D cross-sectional problem also contains points of eigenvector deficiency which again do not cause any problems to the VIP code, the agreement of the results from VIP and the Higher Order Godunov code confirming this.

In summary, the comparison of the two codes has provided the following features. The main advantage of the VIP code is that the particular form of the TTLF TVD scheme is very straightforward to implement, component by component to the system of conservation laws, whereas the Higher Order Godunov code uses a full eigenvector decomposition. This implementation of the TVD flux-limiter scheme has a disadvantage in that, due to the ignoring of the coupling of the equations, the VIP code looses some resolution, which is shown up in the comparison of the first shock in the 1-D problem and the first rarefaction-shock compound wave in the 2-D problem. Another drawback of the VIP code is that a CFL number of 0.5 is needed due to the TVD scheme (0.66 if the Minmod limiter

is used), the Higher Order Godunov code has a theoretical stability limit of a CFL number of 1.0. The number of time steps used to perform the simulations has confirmed the Higher Order Godunov code is far more efficient in terms of overall computational time. Hence the superior resolution and overall efficiency of the Higher Order Godunov code compared to the VIP code, justify use of a full eigenvector decomposition in the algorithm.

Chapter 8

Summary and Further Work

In this thesis we have investigated the high resolution simulation of compressible fluid flow in oil reservoirs. In particular the Higher Order Godunov method has been applied to a variant of the industry standard Black-Oil model, in 1 and 2 dimensions. Computer codes were constructed to provide numerical results in order to perform the investigations. The following section contains a summary of the contents of the thesis and the findings from the work undertaken. Finally in the last section we outline ideas for further work.

8.1 Summary

In Chapter 2 we gave an overview of some of the theory and nomenclature associated with hyperbolic conservation laws which we have used throughout this thesis. Chapter 3 contained a description of a variant of the industry standard Black-Oil model, which was introduced by Trangenstein and Bell [46], and which we have used to model compressible reservoir fluid flow. In Chapter 4 we described the Higher Order Godunov numerical method [2, 10] for systems of conservation laws, including the modifications necessary for degenerate systems. The system of conservation laws in the Black-Oil model possesses these degeneracies and hence the Higher Order Godunov scheme was used to numerically solve them, a Fortran code having been written for this purpose.

In Chapter 5 we described how we implemented the Higher Order Godunov method on the system of conservation laws arising from the Black-Oil model. We

also discussed the solution of the parabolic pressure equation. We showed results from our 1-D code and compared them with results in the literature thereby validating our code. The 2-D code was validated by comparison of results with those from a commercial reservoir simulator.

Also in Chapter 5 the accuracy of the Higher Order Godunov method was investigated by applying it to the degenerate system of conservation laws arising from the 3-phase incompressible Buckley-Leverett model, see [49], for which we also constructed analytic solutions, and thus were able to compare the analytic and numerical results. The agreement of the numerical results with the analytic constructions was found to be very good.

Finally in Chapter 5, source terms were incorporated to model injection and production of fluid in 1 and 2 dimensions. A locally implicit procedure was used to remove the numerical stability problem associated with their use. The approaches described were effective at modelling source terms in 1 and 2 dimensions, and exhibited improved results over an explicit treatment.

The work in Chapter 6 concerned the inherent volume error discrepancy associated with the 3-component 3-phase Black-Oil model [46]. A 2-component 2-phase Black-Oil model [5] also exists, being the forerunner to the Black-Oil model [46], which was developed by Bell et al. and does not have an associated volume error discrepancy. Therefore 2-component 2-phase reservoir simulations may be performed with and without the volume error discrepancy and hence the effect of the discrepancy on the numerical results was investigated. We found that the results of these reservoir simulations were in close agreement and hence conclude that the Black-Oil model with the inherent volume error discrepancy is a good approximation to the more physically accurate Black-Oil model [5], at least for 2-component 2-phase simulations.

Also in Chapter 6 we investigated the application of a Second Order Pressure Correction (SOPC) technique which had been suggested by Trangenstein in [48] as a possible method of reducing the volume error discrepancy. We found that application of the SOPC method, although raising the temporal accuracy of the pressure field to second order, introduced unphysical oscillation into the pressure fields. This oscillation was removed from the results by controlling the growth of

time steps early on in the computations. However the SOPC technique was not found to be effective at reducing the volume error discrepancy.

We then described an effective procedure for reducing the volume error discrepancy, which amounted to a local iterative solution of the volume balance equation. We solved the volume balance equation for pressure in each grid block at the end of each time step which resulted in a corrected pressure field and had the effect of substantially reducing the volume error discrepancy. However unphysical spikes in the pressure fields were introduced when phase changes occurred in the simulations. To circumvent this problem we iteratively solved the volume balance equation for component density instead of pressure either side of the phase changes, and solved for pressure in the rest of the flow field. This had the desired effect in that the unphysical spikes were removed from the pressure fields and the volume error discrepancy was also reduced. We applied this technique to some 2-component 2-phase problems and found the results were in closer agreement to the results obtained from simulating these problems with the no volume error discrepancy formulation of the Black-Oil model [5], compared to not using the discrepancy reduction techniques. Hence the methods described of reducing the volume error discrepancy, is effective at improving the physical accuracy of the numerical results of Black-Oil reservoir simulations using the model in [46].

The effect of the magnitude of fluid compressibility was thought to have an effect on the level of volume error discrepancy generated, see Trangenstein [48]. Simulations with a sequential thermal model, similar in general structure to the Black-Oil model, involving injection of highly compressible steam ran into difficulties due to high volume error discrepancies generated, see [48]. We investigated the effect of gas injections, with gas compressibility comparable to that of steam, using the Black-Oil model. We found that subject to providing extra dissipation at the shock connecting the region of high and low fluid compressibilities and controlling the growth of time steps early on in the simulation, no difficulties (described in [48]) arose, the computations proceeding smoothly with no unacceptably large discrepancies arising.

In Chapter 7 the numerical results from the TTLF TVD flux-limiter scheme

present in the commercial reservoir simulation code VIP were compared to those from the Higher Order Godunov scheme, when applied to the degenerate system of conservation laws arising from the Black-Oil model. We discussed the relative efficiencies of the two numerical schemes and compared the quality of the numerical results.

The VIP code has an advantage over the Higher Order Godunov code since the TVD scheme is easily implemented component by component to the system of conservation laws. However this leads to a disadvantage of the scheme in that the resolution obtained is not as high as that obtainable from the Higher Order Godunov code, which is due to the ignoring of the coupling of the equations, and was shown in the comparisons of the numerical results. Another disadvantage of the VIP code is that it must be used with a CFL number of 0.5, whereas the Higher Order Godunov scheme can theoretically be used with a CFL number of 1.0. Also in practice the Higher Order Godunov code takes far fewer time steps to perform the simulations and hence is far more computationally efficient. It is therefore felt that these points justify use of the full eigenvector decomposition in the Higher Order Godunov code.

8.2 Further Work

We now discuss some ideas for further work, the most obvious being the use of adaptive gridding techniques for solution of the partial differential equations. The main idea here is to concentrate the computational effort where the solution to the conservation laws is changing most rapidly, with a relatively course grid where the solution is not changing with time. Hence improved resolution is obtained at discontinuities and savings in computational effort result. However adaptive gridding techniques have been applied to 2-D polymer flooding and 2-D 2-phase incompressible flow, using the Higher Order Godunov method, by Edwards [16], but not to 3-phase compressible flow. In particular Edwards presents a formulation giving high quality results on large aspect ratio grids.

The ultimate goal here is the construction of a 3-D adaptive strategy, and hence a computer code, to solve the Black-Oil flow equations in the most efficient

way possible. Grid adaptivity introduces an interesting problem in that the rock properties need to be held on the finest computational grid, and hence some sort of averaging procedure of the properties is needed in order to be able to represent them on the coarser grids. One way of tackling this problem is known as 'renormalisation', see King [27]. Edwards and Christie [17] have shown how this renormalisation technique can be combined with an adaptive Higher Order Godunov scheme in 2-D.

Another area of further work involves the discretisation used in the parabolic pressure equation. The largest volume error discrepancies generated in the numerical results occur at phase changes and discontinuities in the component density field. The coefficients in the pressure equation at the cell edges are calculated by averaging the coefficients either side of the cell interface, which could be in between a phase change or part of a discontinuity. Therefore this averaging out of the coefficients could have a bearing on the relatively high volume error discrepancies generated at the phase changes and discontinuities. This could be investigated, as could modifications to the discretisation of the pressure equation to improve the situation, if it is found to be a cause. Hence this could represent a correction of the root cause of the high discrepancies at the said points, rather than the correction of the discrepancies once they have arisen.

References

[1] K.Aziz and A.Settari,"Petroleum Reservoir Simulation", Applied Science Publishers Ltd, 1979.

[2] J.Bell, P.Collela and J.Trangenstein, "Higher Order Godunov Methods for General Systems of Hyperbolic Conservation Laws", J. Comp. Phys. **82**, pp 362-397, 1989.

[3] J.Bell, C.Dawson and G.Shubin, "An Unsplit Higher Order Godunov Method for Scalar Conservation Laws in Multiple Dimensions ", J. Comp. Phys. **74**, pp 1-24, 1988.

[4] J.Bell and G.Shubin, "Higher Order Godunov Method for Reducing Numerical Dispersion in Reservoir Simulation", SPE 13514, pp 179-186, 1985.

[5] J.Bell, G.Shubin and J.Trangenstein, "A Method of Reducing Numerical Dispersion in Two-Phase Black-Oil Reservoir Simulation", J. Comp. Phys. **65**, pp 71-106, 1986.

[6] J.Bell, J.Trangenstein and G.Shubin, "Conservation laws of Mixed Type Describing Three-Phase flow in Porous Media", SIAM J. Appl. Math. **46**, pp 1000-1017, 1986.

[7] M.Blunt and B.Rubin, "Implicit Flux Limiting Schemes for Petroleum Reservoir Simulation", in proceedings of the second European Conference on the Mathematics of Oil Recovery, Editions Technip, Paris, pp 131-138, 1990.

[8] J.P.Boris and D.L.Book, "Flux Corrected Transport 1: SHASTA a Fluid Transport Algorithm That Works", J. Comp. Phys. **11**, pp 38-69, 1973.

[9] M.A.Christie and D.J.Bond, "Multidimensional Flux-Corrected Transport for Reservoir Simulation" in Eighth SPE Symposium on Reservoir Simulation, pp 81-90, Dallas, Texas, Feb 1985.

[10] P.Collela, "Multidimensional Upwind Methods for Hyperbolic Conservation Laws", J. Comp. Phys. **87**, pp 171-200, 1990.

[11] P.Collela and P.Woodward, "The Piecewise Parabolic Method (PPM) for Gas-Dynamical Simulations", J. Comp. Phys. **54**, pp 174-201, 1984.

[12] J.P.Collins, P.Collela and H.M.Glaz, "An Implicit-Explicit Eulerian Godunov Scheme for Compressible Flow", submittted to J. Comp. Phys. 1990.

[13] R.Courant, K.Friedrichs and H Lewy, Mathematische Annalen, **100**, p 32, 1928.

[14] E.C.Donaldson, G.V.Chilingarian and T.F.Yen, "Enhanced Oil Recovery, II Processes and Operations", Elsevier Science Publishers, Amsterdam, 1989.

[15] J.Douglas and T.Dupont, "Galerkin Methods for Parabolic Equations", SIAM J. Numer. Anal. **7**, pp 575-626, 1970.

[16] M.G.Edwards, "A Dynamically Adaptive Godunov Scheme for Reservoir Simulation on Large Aspect Ratio Grids", To Appear in the Proceedings of the ICFD Conference on Numerical Methods for Fluid Dynamics, University of Reading 1992.

[17] M.G.Edwards and M.A.Christie, "Dynamically Adaptive Godunov Schemes with Renormalization in Reservoir Simulation", SPE paper 25268, in Proceedings of the 12th SPE Symposium on Reservoir Simulation, New Orleans, 1993.

[18] B.Engquist and S.Osher, "Stable and Entropy Satisfying Approximations for Transonic Flow Calculations", Math. Comp. **34**, pp 45-75, 1980.

[19] B.Engquist and S.Osher, "One Sided Difference Approximations for Nonlinear Conservation Laws", Math. Comp. **36**, pp 321-351, 1981.

[20] S.K.Godunov, "A Finite Difference Method for the Numerical Computation of Discontinouous Solutions of the Equations of Fluid Dynamics", Mat. Sb. **47**, pp 271-290, 1959.

[21] G.H.Golub and C.F. van Loan, "Matrix Computations", John Hopkins University Press, 1983.

[22] J.Goodman and R.LeVeque, "A Geometric Approach to High Resolution TVD Schemes", SIAM J. Numer. Anal. **25**, pp 268-284, 1988.

[23] J.Goodman and R.LeVeque, "On the Accuracy of Stable Solutions for 2D Scalar Conservation Laws", Mathematics of Computation **45**, pp 15-21, 1985.

[24] A.Harten, "High Resolution Schemes for Hyperbolic Conservation Laws", J. Comp. Phys. **49**, pp 357-393, 1983.

[25] A.Harten, P.D.Lax and B. Van Leer, "On Upstream Differencing and Godunov Type Schemes for Hyperbolic Conservation Laws", SIAM Review, **25**, pp 35-67, 1983.

[26] K.Holing, J.Alvestad and J.Trangenstein, "The Use of Second Order Godunov Type Methods for Simulating EOR Processes in Realistic Reservoir Models", in proceedings of the second European Conference on the Mathematics of Oil Recovery, Editions Technip, Paris, pp 101-111, 1990.

[27] P.R.King, "The use of Renormalisation for Calculating Effective Permeability", Transport in Porous Media, **4**, pp 37-58, 1989.

[28] P.D.Lax, "Hyperbolic Systems of Conservation Laws and The Mathematical Theory of Shock Waves" SIAM Regional Conference Series in Applied Mathematics, 1973.

[29] P.D.Lax and B.Wendroff, "Systems of Conservation Laws", Comm. on Pure and Applied Math. **13**, pp 217-237, 1960.

[30] T.P.Liu, "The Riemann Problem for General Systems of Conservation Laws", J. Diff. Eqns. **18**, pp 218-234, 1975.

[31] O.A.Oleinik, "Discontiuous Solutions of Non-linear Differential Equations", Amer. Math. Soc. Transl. Ser. **2**,**26**, pp 95-171, 1957.

[32] S.Osher and F.Solomon, "Upwind Difference Schemes for Hyperbolic Systems of Conservation Laws", Math. Comp. **38**, pp 339-374, 1982.

[33] P.Roe, "Approximate Riemann Solvers, Parameter Vectors and Difference Schemes", J. Comp. Phys. **43**, pp 357-372, 1981.

[34] P.Roe, in proceedings of Large Scale Computations in Fluid Mechanics, "Some Contributions to the Modelling of Discontinuous Flows", Lecture Notes in Applied Maths., **22**, part 2 pp 163-193, AMS, 1985.

[35] P.Roe and D.Sidilkover, "Optimum Positive Linear Schemes for Advection in Two and Three Dimensions", SIAM J. Numer. Anal. **29**, pp 1542-1568, 1992.

[36] B.Rubin and M.Edwards , "Extension of the TVD Midpoint Scheme to Higher Order Accuracy", SPE paper 25265, in Proceedings of the 12th SPE Symposium on Reservoir Simulation, New Orleans, 1993.

[37] V.V.Rusanov, "Calculation of Interaction of Non-Steady Shock Waves With Obstacles", J. Comput. Math. Phys. USSR, **1** , pp 267-279, 1961.

[38] D.Schaeffer and M.Shearer "Riemann Problems for Nonstrictly Hyperbolic 2×2 Systems of Conservation Laws", Trans. Amer. Math. Soc. **304**, pp 267-306, 1987.

[39] J.W.Sheldon, B.Zondek and W.T.Cardwell, "One -Dimensional, Incompressible, Non-Capillary, Two-Phase Fluid Flow in a Porous Medium", Trans. Soc. Pet. Eng. AIME **216**, p 290-296, 1959.

[40] M.C.Smith, "Weak Solutions of the 2×2 Strictly Hyperbolic Systems of Conservation Laws", MSc. Thesis, University of Bristol, October 1991.

[41] J.Smoller, "Shock Waves and Reaction-Diffusion Equations", Springer-Verlag, 1983.

[42] H.L.Stone, "Probability Model for Estimating Three-Phase Relative Permeability", J. Pet. Tech. , pp 214-218, 1970.

[43] H.L.Stone and A.O.Garder, Jr., "Analysis of Gas-Cap or Dissolved Gas Reservoirs", Trans. Soc. Pet. Eng. AIME **222**, p 92-104, 1961.

[44] G.Strang, "On the Construction and Comparison of Difference Schemes", SIAM J. Numer. Anal. **5**, pp 506-517, 1968.

[45] P.K.Sweby, "High Resolution Schemes Using Flux Limiters for Hyperbolic Conservation Laws", SIAM J. Numer. Anal. **21**, pp 995-1000, 1984.

[46] J.Trangenstein and J.Bell, "Mathematical Structure of Black-Oil Reservoir Simulation", SIAM J. Appl. Math. **49**, pp 749-783, 1989.

[47] J.Trangenstein and J.Bell, "Mathematical Structure of Compositional Reservoir Simulation", SIAM J. Sci. Stat. Comput. **10**, pp 817-845, 1989.

[48] J.Trangenstein, "Analysis of a Model and Sequential Numerical Method for Thermal Reservoir Simulation", in the Mathematics of Oil Recovery, pp 359-380, Editor P.R.King, Clarendon Press, Oxford 1992.

[49] J.Trangenstein, "Multi-Phase Flow in Porous Media: Mechanics, Mathematics and Numerics", Volume **34** of Lecture notes in Engineering, Springer-Verlag, 1988.

[50] B.Van Leer, "Towards the Ultimate Conservative Difference Scheme. II. Monotonicity and Conservation Combined in a Second Order Scheme", J. Comp. Phys. **14**, pp 361-370, 1974.

[51] B.Van Leer, "Towards the Ultimate Conservative Difference Scheme. V. A Second Order Sequel to Godunov's Method", J. Comp. Phys. **32**, pp 101-136, 1979.

[52] R.S.Varga, "Matrix Iterative Analysis", Prentice Hall Publishers, 1962.

[53] H.A.Van Der Vorst, "BI-CGSTAB: A Fast and Smoothly Converging Variant of BI-CG for the Solution of Nonsymmetric Linear Systems", SIAM J. Sci. Stat. Comput. **13**, pp 631-644, 1992.

[54] R.F.Warming and R.M.Beam, "Upwind Second Order Difference Schemes and Applications in Aerodynamics", AIAA Journal, **14**, pp 1241-1249, 1976.

[55] R.F.Warming and B.J.Hyett, "The Modified Equation Approach to the Stability and Accuracy of Finite-Difference Methods", J. Comp. Phys. **14**, pp 159-179, 1974.

[56] S.Zalesak, "Fully Multidimensional Flux Corrected Transport Algorithms for Fluids", J. Comp. Phys. **31**, pp 335-362, 1979.